Université de Montréal

Comprendre l'imperméabilité cutanée : étude spectroscopique de mélanges modèles de la phase lipidique du stratum corneum

par Adrian Paz Ramos

Département de chimie
Faculté des arts et des sciences

Thèse présentée à la Faculté des études supérieures et postdoctorales
en vue de l'obtention du grade de *Philosophiae Doctor* (Ph.D.)
en chimie

Mars 2018

Résumé

Le stratum corneum (SC), la couche la plus externe de l'épiderme des mammifères, agit comme une barrière dictant le taux d'absorption des molécules exogènes à travers la peau et empêchant la perte d'eau du corps. Le SC est principalement composé de cellules mortes aplaties et entièrement kératinisées (cornéocytes), noyées dans une matrice lipidique constituée fondamentalement de céramides, d'acides gras libres et de cholestérol. La diffusion transdermique des molécules est principalement liée aux lipides intercellulaires qui forment des membranes multilamellaires en phase solide.

L'objectif principal de cette thèse est de mieux comprendre la relation entre la structure de la matrice lipidique et l'imperméabilité de la peau. La phase lipidique du SC comprend plus de 400 lipides différents. En raison de cette composition très complexe, des membranes modèles sont souvent utilisées pour l'étude des propriétés physico-chimiques des membranes, du comportement des lipides et de la perméabilité de différents produits chimiques.

Nous avons d'abord déterminé comment la longueur des chaînes acyles d'acides gras libres influence le comportement de phase d'une matrice lipidique composée de céramide NS24, d'acide lignocérique (FFA24) ou palmitique (FFA16) et de cholestérol. Les propriétés structurales des membranes ont été examinées par ^{2}H RMN et par spectroscopie infrarouge. Cette étude a montré que le comportement de phase de ces mélanges ternaires est fortement affecté par la longueur de l'acide gras. Nous avons trouvé que l'acide lignocérique avec le céramide NS24 et le cholestérol conduit à la formation d'un mélange plus homogène que celui qui inclut l'acide palmitique. De plus, le mélange ternaire contenant de l'acide lignocérique a montré une transition de la phase solide vers la phase gel lorsqu'il a été chauffé au-dessus de

37 °C, une caractéristique inhabituelle pour ce type de membranes modèles. La combinaison de lipides ordonnés et membranes homogènes est proposée comme un élément critique pour l'imperméabilité du SC.

Deuxièmement, nous avons étudié un mélange plus complexe contenant du cholestérol, une série d'acides gras libres variant de 16 à 24 atomes de carbone et deux types de céramides : le céramide NS24 et le céramide EOS. Ce dernier est considéré comme un composant clé pour la formation de la phase de périodicité longue dans les membranes du SC native et modèles. Les résultats de spectroscopie ^{2}H RMN, infrarouge, et Raman ont montré que l'acide gras libre et la chaîne acyle du céramide NS24 restent en phase solide à la température physiologique tandis que la chaîne oléate du céramide EOS entraîne la formation de domaines hautement désordonnés. Ces nanogouttelettes restent à l'état liquide jusqu'à -30 °C. La contrainte stérique imposée par la matrice lipidique cristalline est proposée être à l'origine de la difficulté de cristallisation des chaînes oléate des céramides EOS. Cette découverte modifie substantiellement la description structurale du SC et propose un nouveau rôle physiologique du céramide EOS, ce lipide étant un puissant modulateur de l'équilibre solide/liquide du SC. Ces travaux conduisent à réexaminer le mécanisme présentement proposé pour expliquer la perméabilité du SC, ainsi que l'effet d'agents transdermiques.

Finalement, nous avons étudié l'interaction d'acides gras à très longue chaîne avec des membranes de 1-palmitoyl-2-oléoyl-*sn*-glycéro-3-phosphocholine (POPC) afin de déterminer comment s'adaptent ces acides gras aux contraintes spatiales. Trois acides gras différents avec une chaîne acyle variant de 16 à 24 atomes de carbone ont été utilisés : l'acide palmitique (FFA16), arachidique (FFA20) et lignocérique (FFA24). L'épaisseur d'un feuillet d'une bicouche de POPC correspond à la longueur de la partie hydrophobe de FFA16, et donc

inférieure à la longueur de FFA20 et FFA24. La façon dont ces acides gras s'adaptent à la bicouche de POPC a été étudiée par ^{2}H RMN et par simulations de dynamique moléculaire. Nous avons trouvé que la partie inférieure de la chaîne acyle de FFA24 protoné est désordonnée d'une façon similaire à ce qui a été observé pour la chaîne oléate du céramide EOS, sa chaîne acyle interagit avec la partie la plus fluide du feuillet opposé. Cette interdigitation de la fin de la chaîne acyle provoque un deuxième plateau observé dans les profils d'ordre (S_{C-D}), une caractéristique qui est inhabituelle dans les systèmes lipidiques. Dans ce cas, le groupe carboxyle protoné de FFA24 était situé légèrement sous la tête polaire de la POPC. La déprotonation du FFA24 déplace la molécule vers l'interface aqueuse. Cette translation diminue la contrainte spatiale, augmente l'ordre de la chaîne acyle et entraîne la disparition du plateau correspondant au bout de la chaîne désordonnée.

Les résultats présentés dans cette thèse contribuent à mieux comprendre comment la structure de la matrice lipidique du SC dicte l'imperméabilité de la peau. Nous avons montré des preuves spectroscopiques du comportement de phase de certains lipides importants du SC et suggéré un nouveau mécanisme pour la régulation de la diffusion transdermique des molécules.

Mots-clés : stratum corneum, membranes modèles, comportement de phase, lipides, peau, acides gras à très longue chaîne, phospholipides.

Abstract

The stratum corneum (SC), the outermost layer of mammal epidermis, acts as a barrier dictating the rate of absorption of exogenous molecules through the skin and preventing water loss from the body. SC is mainly composed of flattened and fully keratinized dead cells (corneocytes), embedded in a lipid matrix, which is mostly constituted of ceramides, free fatty acids, and cholesterol. The transdermal diffusion of molecules is mainly related to the intercellular lipids, which form multilamellar membranes in the solid-crystalline phase.

The main goal of this thesis is to better understand the relationship between the structure of the lipid matrix and the skin impermeability. SC lipid phase includes more than 400 different lipid species. Due to this very complex composition, model membranes are often used for the study of the physicochemical properties of membranes, the lipid behavior, and of the permeability of different chemicals.

First, we determined how the length of the free fatty acid acyl chains influences the phase behavior of a lipid matrix composed of ceramide NS24, lignoceric (FFA24) or palmitic (FFA16) acid, and cholesterol. The structural properties of membranes were examined by ^{2}H NMR and infrared spectroscopy. This study revealed that the phase behavior of these ternary mixtures is strongly affected by the length of the FFA. We found that lignoceric acid led to the formation of a more homogeneous mixture with ceramide NS24 and cholesterol, than the palmitic acid/ceramide NS24/cholesterol mixture. Also, the tertiary mixture containing lignoceric acid showed a transition from solid to gel phase when heated above 37 ^{o}C, an unusual feature for this type of model membranes. The combination of ordered lipids and homogeneous membranes is proposed as a critical element for SC impermeability.

Second, we studied a more complex mixture containing cholesterol, a series of free fatty acids varying from 16 to 24 carbon atoms, and two types of ceramides: ceramide NS24 and EOS. The latter is considered a key component for the formation of the long periodicity phase in native and model SC membranes. The ^{2}H NMR, infrared and Raman spectroscopy results showed that both the free fatty acid and the ceramide NS24 acyl chain remained in the solid-crystalline phase at physiological temperature while the oleate chain in ceramide EOS led to the formation of highly disordered domains. These liquid nanodrops remained in the liquid state down to -30 °C. The steric constraint imposed by the crystalline lipid matrix is proposed to prevent the crystallization of ceramide EOS oleate chains. This finding modifies the structural description of the SC substantially and proposes a novel physiological role of ceramide EOS as this lipid is a strong modulator of SC solid/liquid balance. The work leads to a re-examination of the mechanism currently proposed to explain the permeability of SC, as well as the effect of transdermal agents.

Finally, we studied the interaction of very long-chain fatty acids with 1-palmitoyl-2-oleoyl-*sn*-glycero-3-phosphocholine (POPC) membranes to determine how these fatty acids adapt to spatial constraints. Three different FFAs with acyl chain varying from 16 to 24 carbon atoms were used: palmitic (FFA16), arachidic (FFA20) and lignoceric (FFA24) acid. The leaflet thickness of a POPC bilayer corresponds to the length of the hydrophobic part of FFA16, and therefore is smaller than the length of FFA20 and FFA24. The way in which these fatty acids structurally adapt in POPC bilayers was study by ^{2}H NMR and molecular dynamics simulations. We found that the lower part of the protonated FFA24 acyl chain was disordered in a manner similar to that observed for the oleate chain of the EOS ceramide, its acyl chain interacts with the more fluid part of the opposite leaflet. This interdigitation of the end of the

acyl chain caused a second plateau observed in the order profiles (S_{C-D}), an unusual feature in lipid systems. In this case, the protonated carboxyl group of FFA24 was located slightly below the polar head of the POPC. The deprotonation of the FFA24 shifted the molecule toward the aqueous interphase. This movement reduces the spatial constraints, increases the order of the acyl chain and causes the disappearance of the plateau at the end of the chain.

The results presented in this thesis contributed to better understand how the structure of the SC lipid matrix dictates the skin impermeability. We showed spectroscopic evidences of the distinct phase behavior of some of the most important SC lipids. Furthermore, we suggested a novel mechanism for the regulation of transdermal diffusion of molecules.

Keywords: stratum corneum, model membranes, phase behavior, lipids, skin, very-long chain fatty acids, phospholipids.

Table des matières

Liste des tableaux

Liste des figures

Liste des symboles et abréviations

^{2}H RMN : Résonance magnétique nucléaire du deutérium

AFM : Microscopie à force atomique (*Atomic force microscopy* en anglais)

BBCer III : Céramide III extrait de cerveau bovin (*Bovine brain ceramide III* en anglais)

BSA : Albumine de sérum bovin (*Bovine serum albumin* en anglais)

Cer : Céramide

Chol : Cholestérol

CholS : Sulfate de cholestérol

DMPC : 1,2-dimyristoyl-*sn*-glycéro-3-phosphocholine

DNPC : 1,2-dinervonyl-*sn*-glycéro-3-phosphocholine

DPPC : 1,2-dipalmitoyl-*sn*-glycéro-3-phosphocholine

EDTA : *Ethylenediaminetetraacetic acid*

E-PABA : Acide éthyle-*p*-aminobenzoïque

FFA : Acide gras libre (*Free fatty acid* en anglais)

HEPES : *4-(2-hydroxyethyl)-1-piperazineethanesulfonic acid*

IR : Infrarouge

k : Constante de ressort

l_α : Phase fluide

l_β: Phase gel

l_d : Phase liquide désordonnée

l_o : Phase liquide ordonnée

LPP : Phase de périodicité longue (*Long periodicity phase* en anglais)

PaLPC : 1-palmitoyl-*sn*-glycéro-3-phosphocholine

POPC : 1-palmitoyl-2-oléoyl-*sn*-glycéro-3-phosphocholine

SC : Stratum corneum

SM : Sphingomyéline

SPP : Phase de périodicité courte (*Short periodicity phase* en anglais)

VLCFAs : Acides gras à très longue chaîne (*Very long-chain saturated fatty acids* en anglais)

X-ALD : *X-linked adrenoleukodystrophy*

À ma famille

Remerciements

Je souhaite tout d'abord exprimer ma gratitude envers mon directeur de recherche, Prof. Michel Lafleur, pour son aide, sa présence au quotidien et pour m'avoir permis de m'initier au monde passionnant de la chimie des lipides.

Ce travail n'aurait pas pu être mené à bien sans l'aide des techniciens du LCM et du Département de chimie, spécialement Patricia Moraille, Samir Elouatik et Cédric Malveau. Un grand merci pour votre savoir-faire et vos suggestions toujours très utiles.

Il me semble également essentiel d'évoquer mes collègues du groupe de recherche : Mien Chien, Aysha, Alexandre, Robert, Benjamin et plus récemment Mahmoud, Oussama et Mehdi. Merci pour les bons moments passés ensemble!

De sincères remerciements à M. Peter Macdonald, professeur à l'Université de Toronto, de me faire l'honneur d'être le membre externe du jury de soutenance. Je tiens également à remercier M. Xiaoxia Zhu et M. Pierre Chaurand, professeurs de l'Université de Montréal, qui ont accepté d'évaluer ce travail de thèse.

Sur un point de vue plus personnel, je souhaiterais remercier toute ma famille à Cuba, qui m'a toujours poussé à aller plus loin dans mes études. Ma compagne, Dainelys, qui m'a soutenu dans les moments difficiles et qui m'a supporté tout au long de cette aventure. Je remercie également ma mère et ma grand-mère pour les encouragements durant toutes ces années. Un merci particulier à ma tante Sonia pour tout le soutien apporté dès le début de mes études. Enfin, un merci tout particulier à mon petit Josué qui m'accompagne depuis presque un an et qui a su me faire rire dans les moments les plus difficiles.

Finalement, je voudrais remercier les Fonds Québécois de la Recherche sur la Nature et les Technologies (FQRNT) pour leur contribution financière, qui m'a permis de réaliser cette thèse dans des meilleures conditions matérielles.

Chapitre 1: Introduction

1.1 La peau

1.1.1 Structure et fonction de la peau

La peau est le plus grand organe du corps humain, avec environ 2 m^2 de surface et 10 % de notre poids.[1-2] Elle forme une interface flexible entre notre corps et l'environnement externe, qui protège notre organisme des composés exogènes indésirables et des microorganismes, ainsi que de la perte excessive d'eau. De plus, elle offre un environnement contrôlé pour réaliser les fonctions corporelles vitales.[2]

La peau est constituée de trois couches différentes : l'hypoderme, le derme et l'épiderme (Figure 1.1).

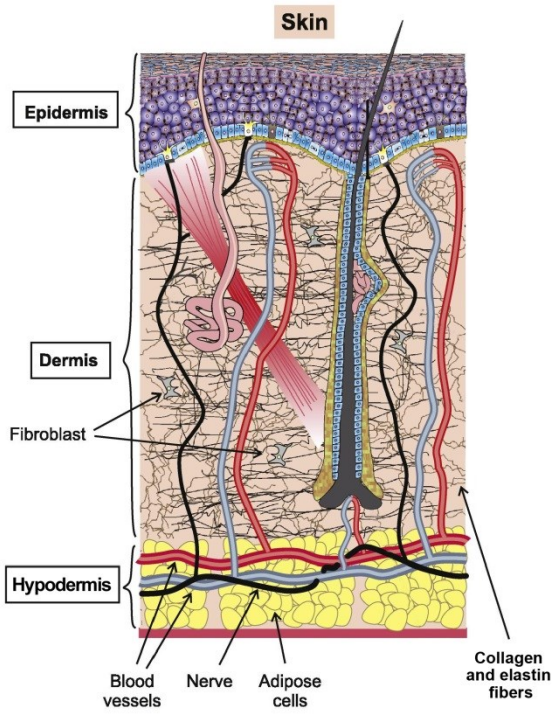

Figure 1.1. Représentation schématique de la section transversale de la peau humaine. Adaptée de la référence 3 avec la permission de Elsevier.

La couche la plus profonde, l'hypoderme, est constituée principalement par des adipocytes, des cellules spécialisées dans le stockage de la graisse, et par des vaisseaux sanguins.[2] Le tissu adipeux donne une grande élasticité à l'hypoderme et à la peau en général. Cette couche d'environ 0,8 mm joue un rôle très important dans la protection mécanique de la peau, la thermorégulation du corps et comme réserve d'énergie.[2,4]

Le derme, la couche intermédiaire de la peau, est constitué de tissu conjonctif enrichi en collagène, nerfs et vaisseaux sanguins, avec une épaisseur entre 0,6 mm et 4 mm. Le derme est considéré comme un réservoir d'eau, contenant environ 20 à 40 % de l'eau totale du corps. Il est le principal responsable de la thermorégulation de la peau.[5] À la frontière entre le derme et l'épiderme se trouve la jonction dermo-épidermique, qui est une zone d'ancrage et de soutien mécano-élastique entre les deux couches. Cette interface permet aussi la filtration sélective de substances entre le derme et l'épiderme.[5-6]

L'épiderme est un épithélium stratifié d'environ 0,1 mm d'épaisseur formé par cinq couches différentes : le stratum basale, le stratum spinosum, le stratum granulosum, le stratum lucidum et le stratum corneum (Figure 1.2).

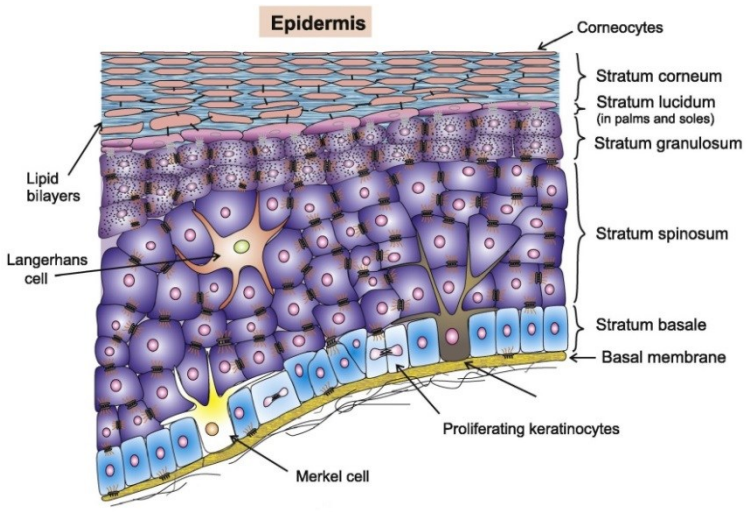

Figure 1.2. Représentation schématique de la section transversale de l'épiderme. Adaptée de la référence 3 avec la permission de Elsevier.

L'épiderme est principalement constitué par des kératinocytes (~95% du total des cellules dans l'épiderme), des cellules capables de synthétiser la kératine, une protéine insoluble dans l'eau.[7] Il est aussi possible de trouver d'autres cellules dans l'épiderme, telles que les mélanocytes et les cellules de Merkel et de Langerhans.[8] Chaque couche de l'épiderme peut être distinguée à partir de la morphologie des kératinocytes.

Le stratum basale, aussi appelé stratum germinativum est la couche la plus profonde de l'épiderme. Cette couche, d'environ 1-3 cellules d'épaisseur, est le lieu de naissance des kératinocytes.[8] C'est à partir de cet endroit que commence la migration cellulaire vers la surface de la peau, un processus continu qui dure environ 30 jours. Durant cette migration, les kératinocytes subissent diverses transformations biochimiques qui affectent leur morphologie ainsi que leur composition. Après cette couche, nous trouvons le stratum spinosum, appelé aussi couche épineuse. Cette couche est formée par des cellules polygonales avec une allure épineuse à l'origine de son nom. Le cytoplasme des kératinocytes qui se trouvent dans cette

couche contient des filaments intermédiaires de kératine en quantité plus importante que dans la couche basale.

Le stratum granulosum est la dernière couche vivante de l'épiderme. Il a une épaisseur entre 3 et 5 cellules qui sont d'apparence fusiforme.[9] La principale caractéristique de cette couche est la présence de granules amorphes de kératohyaline et de corps lamellaires d'Odland (kératinosomes) provenant de l'appareil de Golgi. Ces granules sont plus nombreux vers la partie la plus externe du stratum granulosum où ils fusionnent pour former des vésicules à l'extérieur des cellules. À la suite de cette mort cellulaire programmée, les vésicules versent leur contenu dans l'espace extracellulaire à frontière du stratum corneum; ce matériel agit en tant que précurseurs de la matrice lipidique.[10] Ces corps lamellaires sont constitués principalement de phospholipides, de glycosphingolipides et de stérols libres. Après leur extrusion des vésicules, ces espèces sont transformées par des enzymes telles que la phospholipase A, la glycosidase et la céramide synthase, en composants de la matrice lipidique du stratum corneum.[11] Dans les régions où la peau est plus épaisse, comme la paume des mains et la plante des pieds, on trouve le stratum lucidum. Cette couche est constituée fondamentalement par des kératinocytes morts et aplatis (cornéocytes), dans lesquels certains organelles sont encore trouvées.[6,9]

La dernière étape du processus de différentiation cellulaire dans l'épiderme est la formation d'une couche mince des cornéocytes immergés dans une matrice lipidique : le stratum corneum (SC). À ce point, les cornéocytes sont complètement kératinisés et les lipides provenant du stratum granulosum sont entièrement transformés en composants de la matrice lipidique. Il est possible d'affirmer que le rôle principal de l'épiderme est la formation du stratum corneum, le responsable de l'imperméabilité cutanée.

1.2 La barrière cutanée: le stratum corneum

Le stratum corneum est considéré le principal responsable de l'imperméabilité de la peau. Avec une épaisseur qui peut varier entre 5 et 20 µm selon la localisation, cette couche est constituée par des cellules complètement kératinisées virtuellement imperméables, noyées dans un mélange très particulier de lipides à l'état cristallin. Le modèle de «briques et mortier» a été souvent utilisé pour décrire la structure de ce biocomposite, où les briques représentent les cornéocytes et le mortier la matrice lipidique (Figure 1.3).[12]

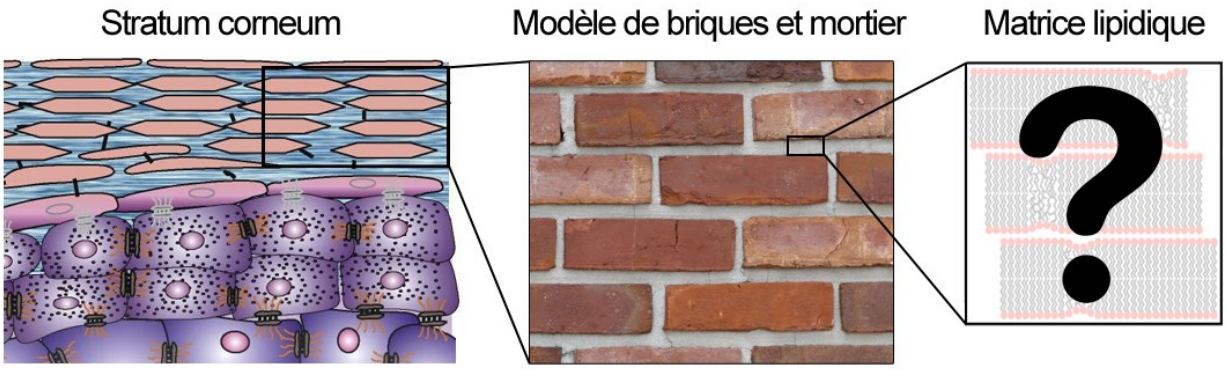

Figure 1.3. Modèle de briques et mortier du stratum corneum.

Étant donné l'imperméabilité des cornéocytes, c'est la matrice lipidique qui régule la diffusion des différents produits à travers le SC et de la peau en général. À cet effet, il a été démontré que la peau perd entre 20 et 50 % de son imperméabilité lorsque la fraction lipidique est extraite avec des solvants organiques.[13] Ce rôle fondamental motive l'importance d'étudier le comportement des lipides qui forment le SC, afin de déterminer son implication dans la formation de la barrière cutanée.

L'objectif principal de cette thèse est de mieux comprendre la relation entre la structure de la matrice lipidique et l'imperméabilité de la peau.

1.2.1 Composition lipidique du SC

Le stratum corneum a une composition lipidique très particulière. À différence de la plupart des membranes biologiques qui sont fluides et constituées de phospholipides, le SC est composé presque exclusivement de céramides, d'acides gras libres et de cholestérol, en quantités équimolaires - il y a aussi une petite quantité (environ 1 %) de sulfate de cholestérol (Figure 1.4).[14] Ce mélange ternaire se trouve à l'état cristallin à la température physiologique, ce qui empêche la libre diffusion des substances à travers la peau.[15-16]

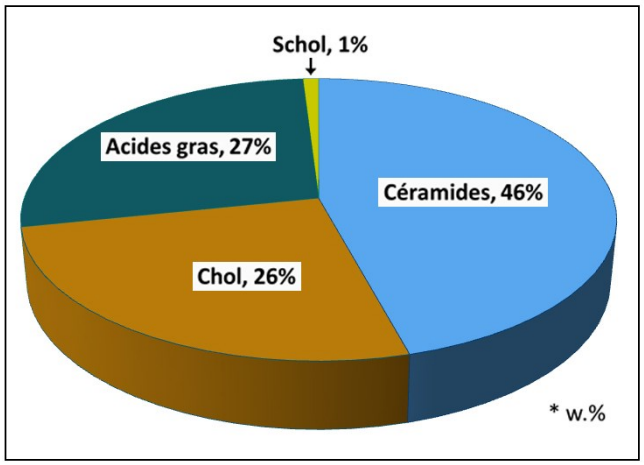

Figure 1.4. Composition lipidique du stratum corneum (% poids).[14]

Bien que les céramides soient des composants mineurs dans la plupart des tissus et des membranes biologiques, les céramides représentent environ la moitié de l'ensemble des espèces lipidiques en poids dans le SC. On trouve un minimum de 15 familles de céramides (Figure 1.5).[17]

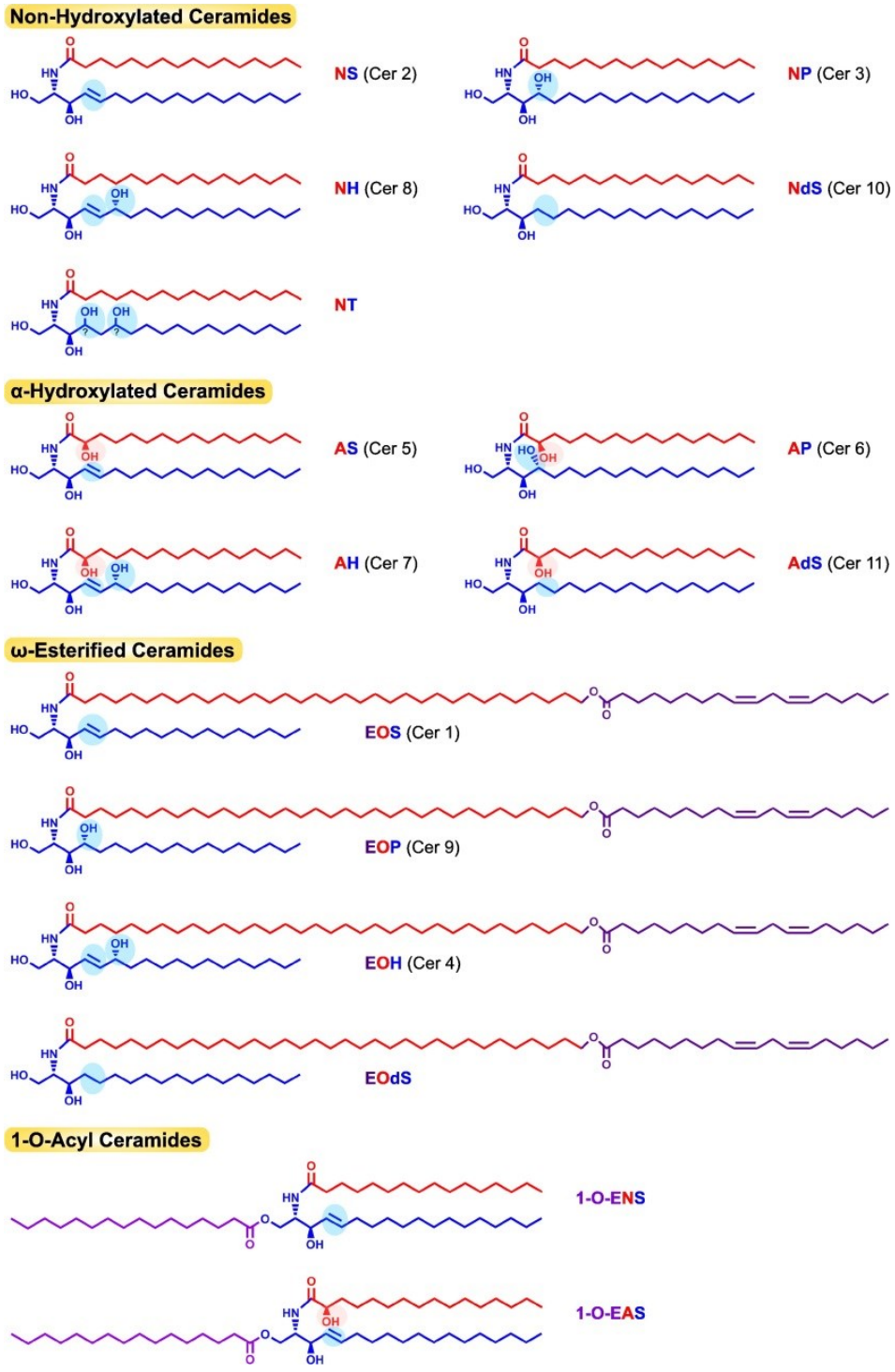

Figure 1.5. Structure des céramides du SC. La nomenclature proposée par Motta et coll. est indiquée - l'ancienne nomenclature est indiqué entre parenthèses. Adaptée de la référence 17 avec la permission de Elsevier.

D'un point de vue chimique, les céramides sont constitués par un acide gras attaché à une base sphingoïde par une liaison amide. Ces acides gras ont différentes longueurs de chaîne qui varient généralement entre 16 et 36 atomes de carbone. En combinant les différentes familles de céramides et les différentes longueurs de chaînes, un total de 342 espèces ont été identifiées dans le SC jusqu'à présent.[18]

La nomenclature établie par Motta et coll.[19] est habituellement utilisée pour nommer les céramides (Tableau 1.1).

Tableau 1.1 Nomenclature des céramides du SC.

Acide gras / Base sphingoïde	Non-hydroxy FA [N]	α-hydroxy FA [A]	ω-hydroxy-FA [EO]
Sphingosine [S]	CerNS	CerAS	CerEOS
Phytosphingosine [P]	CerNP	CerAP	CerEOP
6-hydroxy-sphingosine [H]	CerNH	CerAH	CerEOH
Dihydrosphingosine [dS]	CerNdS	CerAdS	CerEOdS
Dihydroxy-sphinganine [T]	CerNT	—	—

Dans ce système, chaque céramide est identifié par un minimum de 2 lettres. La première lettre désigne le type d'acide gras (*FA*) attaché à la base sphingoïde: N pour non-

hydroxy FA, A pour α-hydroxy FA et O pour ω-hydroxy-FA. La dernière lettre définit le type de base sphingoïde: S pour la sphingosine, P pour la phytosphingosine, H pour la 6-hydroxy-sphingosine, dS pour la dihydrosphingosine et T pour la dihydroxy-sphinganine. De plus, une troisième lettre s'ajoute au tout début pour les céramides estérifiés avec un autre FA (E) ou pour les céramides liés aux protéines (P).[19]

Le céramide non hydroxylé [NS] avec une chaîne saturée de 24 atomes de carbone est un des céramides les plus abondants dans le SC humain.[20] Parmi les autres céramides très importants pour l'imperméabilité de la peau, on retrouve l'acylcéramide (Cer EOS), constituée d'un acide gras ω-hydroxylé auquel un acide insaturé est lié par un ester. Ce type de céramides est inhabituellement long, avec l'acide ω-hydroxylé d'une longueur de chaîne entre 26 et 36 atomes de carbone, tandis que l'acide estérifié correspond généralement à l'acide linoléique ou oléique.

Il existe aussi une grande variété d'acides gras dans le SC, leur longueur de chaîne variant entre 12 et 36 atomes de carbone. Ces acides gras sont généralement saturés pour les chaînes jusqu'à 30 atomes de carbone. Des acides gras monoinsaturés ont été identifiés au niveau de traces pour les chaînes de 32-36 atomes de carbone. Les acides gras avec 22, 24 et 26 atomes de carbone sont les plus abondants dans le SC.[11] Le cholestérol est aussi une composante très importante des lipides du SC. On trouve aussi une quantité d'environ 1 % de sulfate de cholestérol (CholS) dans le SC. Son rôle est lié à la cohésion des cornéocytes, afin d'assurer une structure stable durant le processus naturel de desquamation de la peau. L'ichtyose récessive a été liée à une accumulation inhabituelle de sulfate de cholestérol dans le SC et conduit à une réduction importante de la desquamation.[21]

1.2.2 Structure de la phase lipidique du SC

Durant les années 80s, grâce à l'utilisation des techniques de diffraction des rayons X aux petits et aux grands angles, il a été déterminé que les lipides du SC humain forment deux types de structures lamellaires.[22-23] Ces structures, appelées « phase de périodicité courte » (*Short periodicity phase, SPP* en anglais) et « phase de périodicité longue » (*Long periodicity phase, LPP* en anglais) ont une distance de répétition d'environ 6 nm et 13 nm, respectivement.[22-23] La présence de cholestérol cristallin a été aussi constatée.[24] À la différence des humains, des études sur la structure du SC de souris et de cochon ont montré seulement la formation de la LPP, ce qui suggère que l'arrangement des lipides de cette structure est universel et crucial pour assurer l'imperméabilité de la peau.

L'organisation latérale des lipides est aussi très importante du point de vue de la perméabilité. Les lipides du SC adoptent principalement un empilement orthorhombique à la température physiologique (Figure 1.6).[16] Dans cet empilement, les molécules sont près les unes des autres, ce qui provoque une réduction de la perméabilité.[16] Par contre, dans la région la plus externe du SC, ils existent des régions où les lipides sont organisés dans un empilement hexagonal, ce qui entraîne une augmentation de la perméabilité.[25] Une augmentation de la température peut provoquer aussi une transition de l'empilement orthorhombique vers hexagonal (Figure 1.6).[25] De plus, il y a une petite fraction des lipides qui se trouvent dans un état plus désordonné dans le SC. Cette fraction est supposée être relativement perméable.

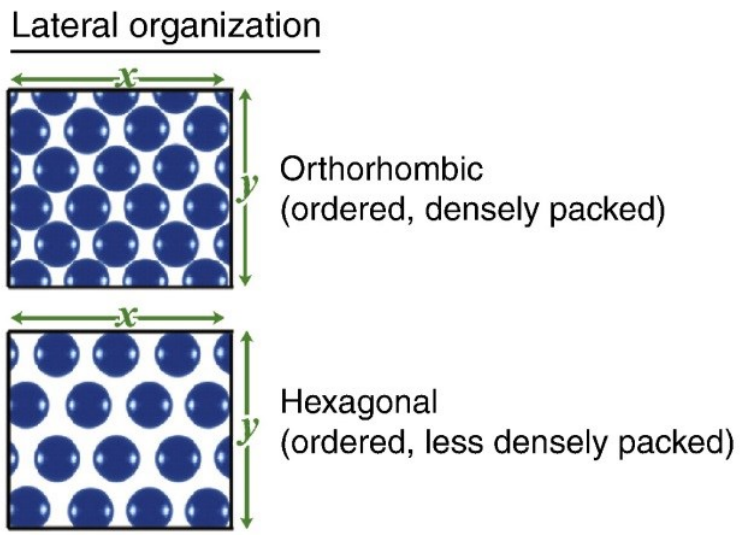

Figure 1.6. Représentation de l'organisation latérale des lipides du SC. Adaptée de la référence 16 avec la permission de Elsevier.

La façon précise dont les lipides du SC s'organisent pour former les structures lamellaires et latérales décrites précédemment est encore inconnue. À ce jour, plusieurs modèles ont été proposés afin de comprendre cette organisation.

En 1994, Bo Forslind introduit le modèle des domaines en mosaïque (*Domain mosaic model* en anglais) (Figure 1.7).[26] Dans ce modèle, les lipides s'agrègent pour former des domaines imperméables à l'état cristallin/gel qui sont unis les uns des autres par des joints de grain (*grain borders* en anglais). Ces joints de grain sont constitués de lipides en phase liquide ordonnée et sont plus perméables que la phase solide cristalline. C'est précisément à travers les joints que la diffusion des molécules est supposée se produire. Une telle organisation explique la diffusion limitée des molécules à travers le SC mais aussi les propriétés mécaniques de la surface de la peau.

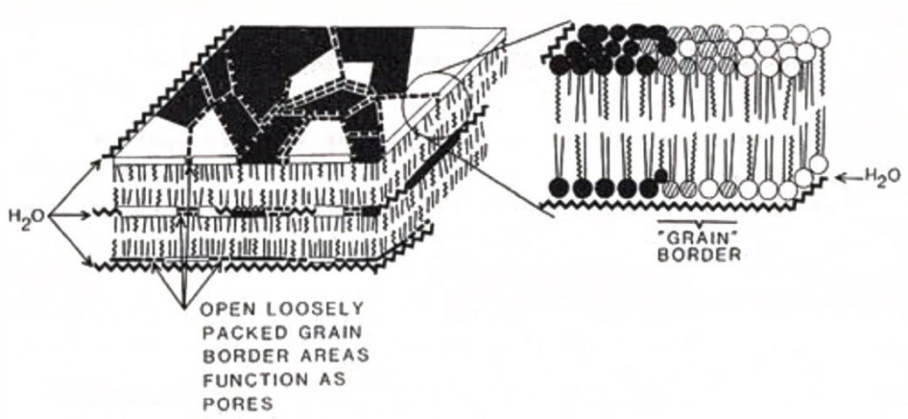

Figure 1.7. Le modèle des domaines en mosaïque.[26]

Ce modèle explique l'organisation latérale orthorhombique des lipides puisqu'il considère que les domaines à l'état solide cristallin adoptent cette symétrie. Par contre, il ne fournit aucune information sur l'organisation lamellaire des lipides.

En 2001, Norlén présentait le modèle de la « phase gel unique » (*Single gel phase model* en anglais) (Figure 1.8).[27] Ce modèle plutôt simpliste considérait que tous les lipides de la matrice du SC formaient une phase gel homogène.

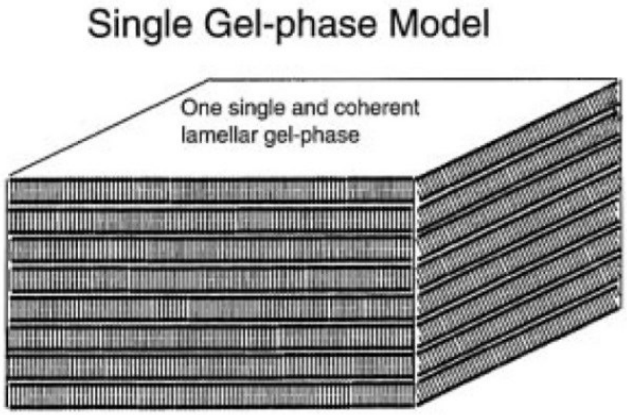

Figure 1.8. Le modèle de la phase gel unique. Adaptée de la référence 27 avec la permission de Elsevier.

À différence du modèle des domaines en mosaïque, il n'y avait pas des joints de grain, ni de lipides plus désordonnés. De plus, la présence des lipides exclusivement en phase gel expliquait l'empilement hexagonal, mais ignorait complètement les observations sur l'empilement orthorhombique. Ce modèle a également échoué à élucider la structure lamellaire des lipides du SC.

En 2008, Kessner et coll.[28] proposent un modèle pour expliquer l'organisation lamellaire des lipides, en mettant l'accent sur le rôle du céramide EOS (Figure 1.9). Le céramide EOS est considéré comme une composante essentielle pour la formation de la LPP.[29-30] Ils ont étudié, par diffraction de neutrons, un mélange modèle qui contenait le céramide EOS ainsi que le céramide AP, l'acide palmitique et le cholestérol. Cependant, malgré la présence du céramide EOS dans le mélange, la LPP n'était pas observée.[28] Dans ce modèle, le céramide EOS excédait de la bicouche pour s'étendre dans la bicouche adjacente, ce qui n'est pas favorable du point de vue énergétique.

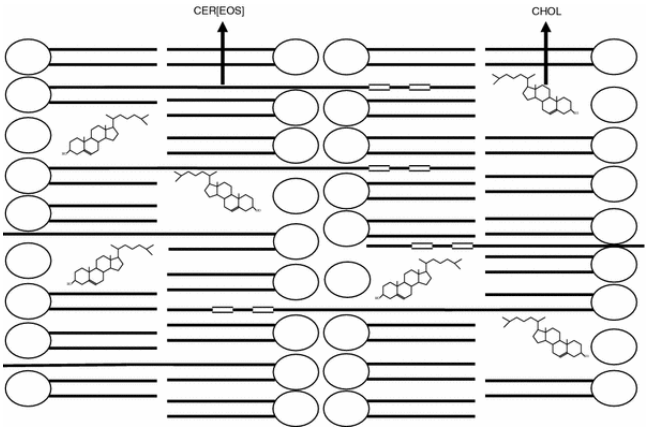

Figure 1.9. Modèle de Kessner et collaborateurs. Adaptée de la référence 28 avec la permission de Springer.

Un autre modèle moléculaire pour décrire la SPP du SC a été proposé par Skolova et coll. en 2014 (Figure 1.10).[31]

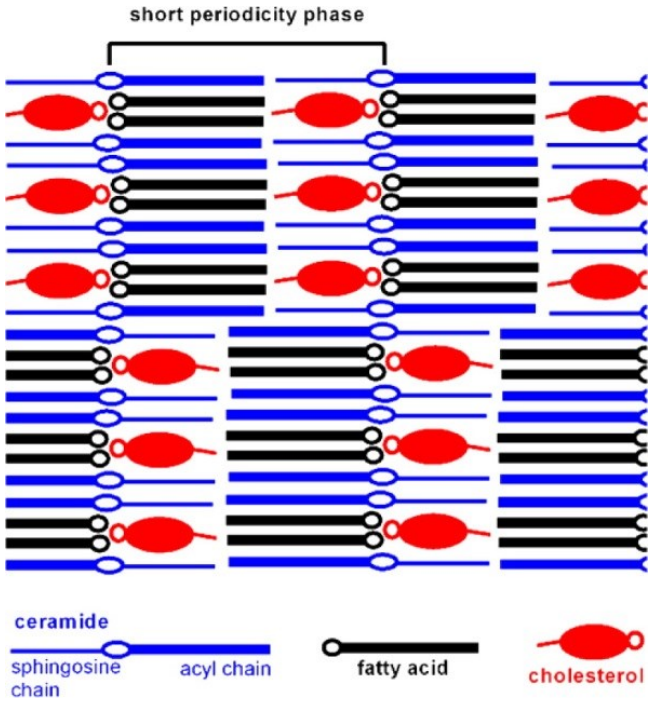

Figure 1.10. Modèle de Skolova et collaborateurs. Adaptée de la référence 31. Copyright (2014) American Chemical Society.

Ce modèle est obtenu à partir d'observations en spectroscopie infrarouge et en diffraction de neutrons avec des membranes modèles de céramide NS24, d'acide lignocérique et de cholestérol. Un trait novateur du modèle est que les molécules de céramide peuvent adopter une conformation complétement étirée (*splayed*), afin de favoriser les interactions de van der Waals entre sa chaîne de 24 atomes de carbone et l'acide lignocérique. Dans l'autre feuillet, la partie sphingosine serait en contact avec le cholestérol, qui a une longueur hydrophobe similaire. Du point de vue de l'organisation latérale, ce mélange a adopté l'empilement orthorhombique, ce qui est en concordance avec le SC natif.[31]

1.2.3 Mélanges modèles du SC

La matrice lipidique du SC est un système extrêmement complexe et pratiquement impossible de reproduire à l'échelle du laboratoire. De plus, sa composition n'est pas homogène mais varie selon l'endroit du corps.[32] La composition lipidique change aussi d'une personne à l'autre en fonction de certains paramètres comme l'âge, la race et même les conditions climatiques.[32] À cause de cela, la plupart des études se sont appuyées sur l'utilisation de modèles simplifiés pour élucider le rôle des lipides individuels dans la matrice et pour obtenir des informations sur leur organisation moléculaire.

L'une des premières membranes modèles utilisées est le mélange équimolaire de céramide NS avec une chaîne palmitoyl, l'acide palmitique et le cholestérol.[33-35] Ce mélange était considéré un modèle classique en raison de sa simplicité, du fait qu'il inclut les trois composants principaux du SC, de la disponibilité commerciale de ceux-ci et du fait que ce mélange fournit un couplage hydrophobe optimisé. De façon analogue au SC natif, les lipides dans ce mélange sont à l'état solide cristallin à la température physiologique et ils sont organisés dans un empilement orthorhombique.[36-37]

Par contre, malgré le fait du couplage hydrophobe optimal, les lipides de ce mélange forment principalement des phases séparées; le Cer NS16 et l'acide palmitique sont distribués dans des domaines cristallins différents.[35-36] La figure 1.11 montre la proportion relative de l'acide palmitique par rapport à la teneur totale en lipides sur une surface de 40 x 40 μm^2 dans ce mélange. Ici, les zones rouges correspondent à des régions enrichies en acide palmitique tandis que les zones bleues correspondent aux régions appauvris en ce lipide.

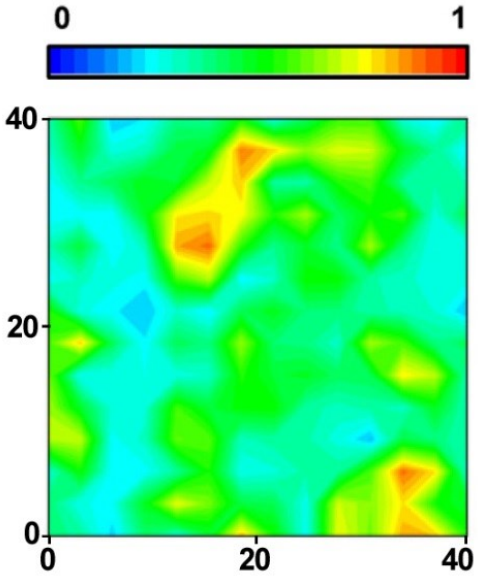

Figure 1.11. Carte obtenue par imagerie Raman du mélange CerNS16/FFA16/Chol à 35 ^{o}C. Les valeurs/couleurs représentent la proportion relative locale de FFA16: les zones rouges correspondent à des régions enrichies en FFA16 par rapport à la proportion moyenne de FFA16 dans le mélange tandis que les zones bleues correspondent à des zones appauvries. Adaptée de la référence 35 avec la permission de Elsevier.

Une des carences de cette membrane modèle est la faible représentativité des lipides qui la composent par rapport au SC natif. En fait, même si la famille des céramides NS est abondante dans le SC, c'est l'espèce avec une chaîne acyle de 24 atomes de carbone qui est la plus abondante (~26%), tandis que le Cer NS16 représente seulement 3 % en poids du total des céramides NS dans le SC.[38] Une observation similaire peut être faite avec l'acide palmitique, puisque ce lipide ne représente que 1,3 % du total des acides gras présents dans le SC.[39]

Afin de reproduire la composition du SC natif plus fidèlement, des mélanges modèles qui utilisent des acides gras longs (20-24 atomes de carbone), le céramide NS24 ou des analogues, ainsi que du cholestérol, sont de plus en plus utilisées.[31,40-41] L'emploi de mélanges

d'acides gras entre 16 et 26 atomes de carbone, dans des proportions similaires à celles du SC natif commencent à devenir la norme.[42-43] Du point de vue de l'organisation latérale des lipides, ces nouveaux mélanges modèles permettent l'obtention de l'état solide cristallin, avec un empilement orthorhombique de façon analogue au SC. De plus, une augmentation de la miscibilité des lipides qui forment ces mélanges a été constatée; on obtient des mélanges plus homogènes que ce qu'était obtenu précédemment avec le mélange CerNS16/FFA16/Chol (Figure 1.12).[43]

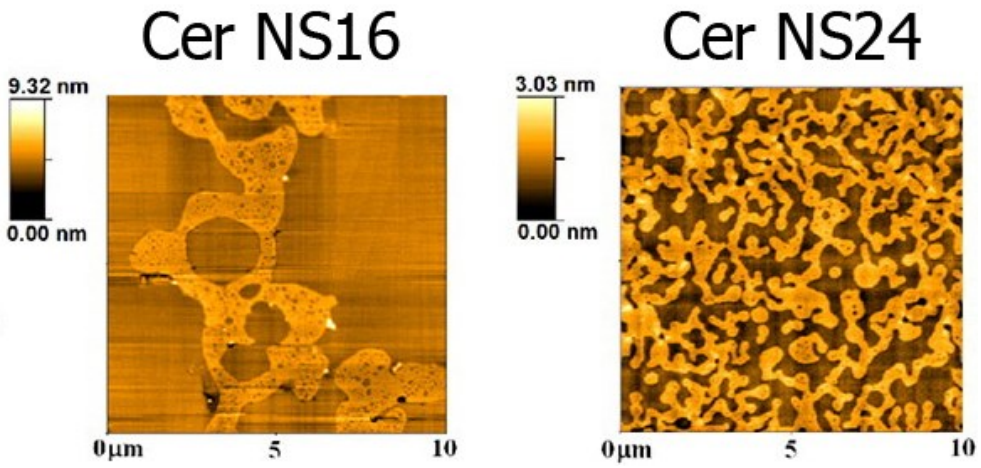

Figure 1.12. Image de microscopie à force atomique d'une monocouche d'un mélange contenant le céramide NS16 (gauche) et NS24 (droite). Adaptée de la référence 43 avec la permission de Elsevier.

Reproduire l'organisation lamellaire des lipides du SC en utilisant des membranes modèles est un processus complexe. Actuellement, pour plusieurs des membranes modèles, le but ultime est d'obtenir la LPP, car elle est supposée être grandement responsable de l'imperméabilité du SC. Certaines études montrent que la présence de céramide EOS est essentielle pour préparer des membranes modèles capables de reproduire la LPP, à condition que l'acide estérifié soit insaturé.[29-30] Par contre, même si la présence du céramide EOS dans

les mélanges lipidiques est indispensable pour obtenir la LPP, ce n'est pas la seule condition. En fait, le modèle de Kessner et coll. décrit précédemment, combinant le céramide EOS avec le céramide AP, l'acide palmitique et le cholestérol, n'a pas reproduit la LPP.[28] Jusqu'à maintenant, la combinaison du céramide EOS, du céramide NS24, des acides gras longs et du cholestérol semble celle qui reproduit l'organisation latérale et lamellaire du SC. C'est ce type de mélanges modèles qui a été étudié dans le cadre de cette thèse. Dans un premier temps, nous avons déterminé l'influence de la longueur de chaîne des acides gras sur les propriétés physico-chimiques des mélanges constitués de céramide NS24, d'acide palmitique ou lignocérique, ainsi que de cholestérol. Ensuite, nous avons étudié un mélange plus complexe constitué d'acides gras qui possédaient entre 16 et 24 atomes de carbone, des céramides EOS et NS24 et de cholestérol, afin d'établir le comportement de chaque type de lipide dans la formation de la LPP.

1.3 Techniques de caractérisation des membranes modèles

1.3.1 ^{2}H RMN[44-47]

La résonance magnétique nucléaire du deutérium (^{2}H RMN) est une technique spectroscopique très puissante dans la caractérisation des membranes lipidiques; elle a été la principale technique utilisée dans le cadre des travaux de cette thèse. Elle nous permet d'identifier, entre autres, les différentes phases lipidiques et l'ordre conformationnel des chaînes. La condition principale pour utiliser cette technique est que les lipides soient deutérés. Le spectre RMN des noyaux deutérium (D), avec un *spin* (I) égal à 1, est dominé par des interactions électroniques quadrupolaires, ce qui provoque la formation d'un doublet, appelé doublet Pake (Figure 1.13).[46]

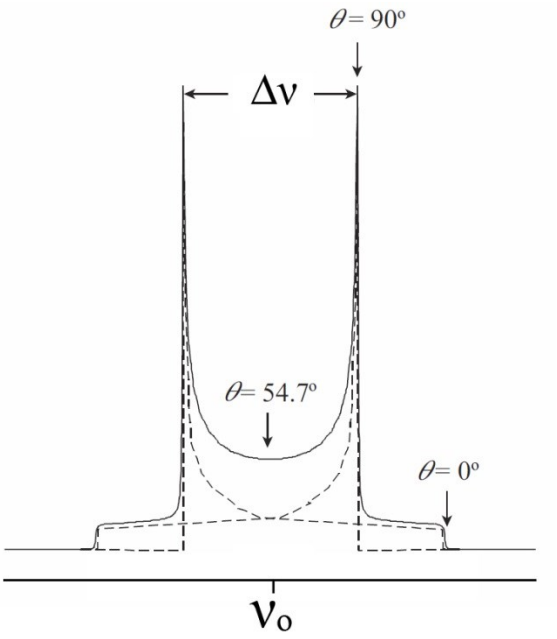

Figure 1.13. Doublet Pake.[46]

L'éclatement quadrupolaire (Δν) de ce doublet est déterminé par l'orientation moyenne de la liaison C-D par rapport à l'angle du champ magnétique appliqué selon :

$$\Delta\nu = \frac{3}{2} A_Q \left\langle \frac{3\cos^2\theta - 1}{2} \right\rangle \quad \text{Eq. 1.1}$$

où A_Q est la constante statique quadrupolaire (égale à 167 kHz pour les chaînes acyles saturées) et θ est l'angle entre le champ magnétique et la liaison C-D. Dans une poudre, l'orientation des molécules est aléatoire, ce qui donne un spectre caractéristique – le spectre de poudre.

La différence de dynamique des chaînes lipidiques produit des spectres caractéristiques pour chaque phase (Figure 1.14). Les lipides dont les chaînes deutérées sont immobiles sur l'échelle de temps ^{2}H RMN (10^{-5} s), donnent des valeurs maximales de Δν. C'est le cas pour les lipides à l'état solide (Figure 1.14A).

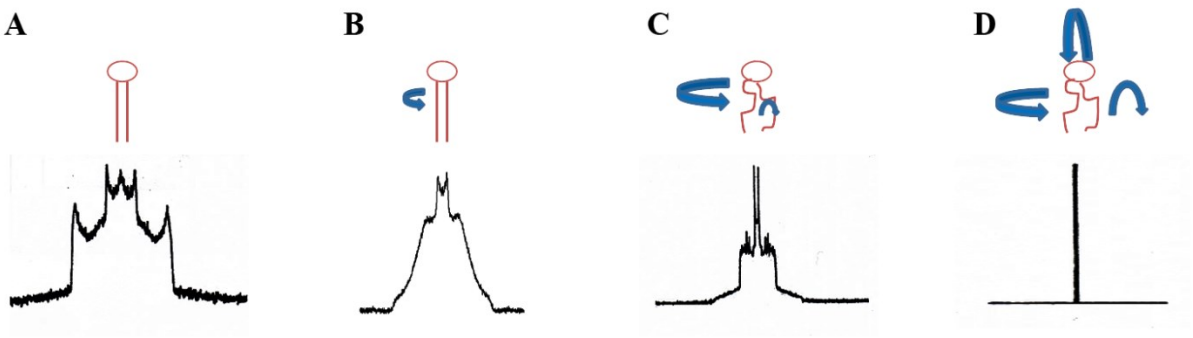

Figure 1.14. Spectres ^{2}H RMN des différentes phases lipidiques : A – Solide, B – Gel, C – Liquide ordonnée, D – Isotrope.

Le spectre typique de la phase solide montre un signal très large avec des valeurs d'éclatement quadripolaire maximales d'environ 120 kHz, ce qui correspond aux groupes méthylènes immobiles de conformations *trans* équivalents. La contribution centrale plus étroite est attribuée au groupe méthyle terminal (CD_3) mobile même en phase solide. Les chaînes dans la phase gel subissent un mouvement de rotation à des vitesses de l'ordre de l'échelle de temps ^{2}H RMN, menant à un paramètre d'asymétrie significatif. Le résultat est un spectre où les pics ne sont pas bien résolus. Seulement le doublet central, qui correspond au groupe CD_3 terminal plus mobile, est bien résolu (Figure 1.14B).

La diffusion rotationnelle des lipides autour de leur axe long dans les phases liquide ordonnée (l_o) et fluide (l_α) (Figure 1.14C) est rapide sur l'échelle de temps RMN et ceci amène un axe de symétrie supplémentaire dans le système. Cette rotation le long de l'axe long du lipide donne lieu à des pics beaucoup plus nets par rapport à la phase gel. Les chaînes lipidiques dans la phase l_o sont plus ordonnées par rapport à la phase fluide (l_α), donc elles montrent des valeurs de $\Delta\nu$ légèrement plus élevées. Les interactions quadrupolaires se moyennent à zéro pour les chaînes dans la phase isotrope. Cela entraîne la présence d'un seul

pic fin dans le spectre ^{2}H RMN (Figure 1.14D). Une coexistence de deux phases (ex. les phases gel et l_o) peut souvent être observée par la superposition des profils typiques de chacune des phases.

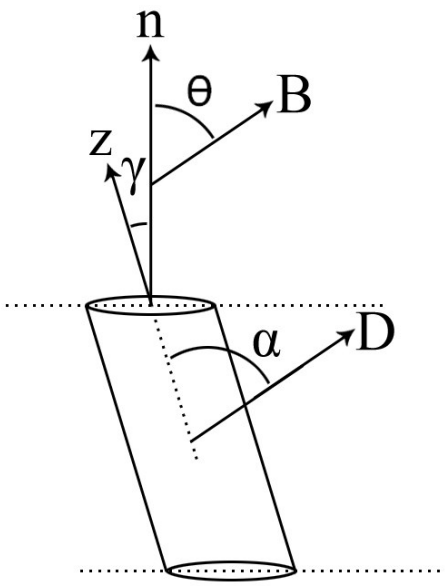

Figure 1.15. Représentation schématique d'une molécule de lipide dans une bicouche. La lettre n représente la normale de la bicouche, z, l'axe de rotation du lipide tandis que B représente la direction du champ magnétique.

Une autre manière de décrire l'ordre des chaînes lipidiques est à l'aide du paramètre d'ordre conformationnel (S_{C-D}). Dans une bicouche fluide, il faut tenir compte la rotation des molécules au long de l'axe z, l'orientation de la molécule par rapport à la normale de la bicouche et l'isomérisation *trans-gauche* de la chaîne acyle. En tenant compte de ces facteurs, l'équation 1.2 de l'éclatement quadrupolaire adopte la forme suivante :

$$\Delta\nu = \frac{3}{2} A_Q \left\langle \frac{3\cos^2\theta - 1}{2} \right\rangle \left\langle \frac{3\cos^2\gamma - 1}{2} \right\rangle \left\langle \frac{3\cos^2\alpha - 1}{2} \right\rangle = \frac{3}{2} A_Q \left(\frac{3\cos^2\theta - 1}{2} \right) S_{mol} S_{C-D} \quad \text{Eq. 1.2}$$

où γ est l'angle entre la normale de la bicouche et l'axe z de la molécule et α est l'angle entre la liaison C-D et l'axe z de la molécule (Figure 1.15). Les termes S_{mol} et S_{C-D} décrivent respectivement le paramètre d'ordre moléculaire et d'ordre conformationnel. Généralement, pour une bicouche fluide, on considère que l'axe de rotation du lipide coïncide avec la normale de la bicouche; en conséquence, $S_{mol} = 1$.

La distribution des valeurs de S_{C-D} le long de chaîne acyle perdeutérée peut être obtenue à partir de la distribution des Δν dans le spectre. Pour ce faire, il est utile de traiter mathématiquement le spectre par une méthode appelée *dePaking*; ce traitement permet d'éliminer du spectre la dépendance orientationnelle, en supposant qu'elle soit décrite par le spectre de poudre dont la forme est connue. Ainsi, on élimine du spectre les contributions de l'angle θ de la figure 1.15. Le procédé de *dePaking* transforme donc un spectre de poudre en spectre caractéristique d'un échantillon orienté, soit un simple doublet dont l'éclatement est essentiellement représentatif du terme dépendant de l'angle α, et donc, donne accès à S_{C-D}. Dans le cas d'une chaîne contentant x groupements perdeutérés, la procédure transforme un spectre composé de x spectres de poudre en x doublets. La figure 1.16 montre le spectre de la 1-palmitoyl-2-oléoyl-*sn*-glycéro-3-phosphocholine deutérée (POPC-d_{31}) avant et après le processus de *dePaking*.

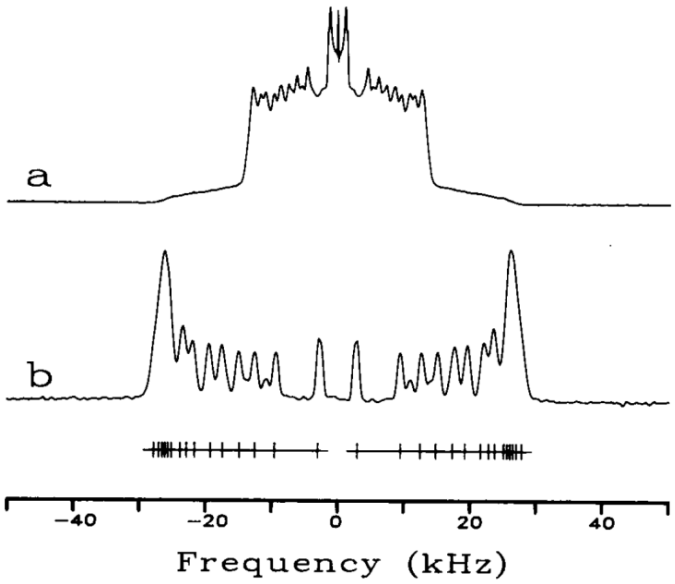

Figure 1.16. Spectre ^{2}H RMN de la POPC-d_{31} (a) et le correspondant spectre d*ePaké* (b). Adaptée de la référence 47 avec la permission de Elsevier.

Généralement, les doublets les plus larges, situés aux extrémités du spectre, sont produits par la superposition de plusieurs doublets correspondant à la région la plus ordonnée de la chaîne acyle (Figure 1.16B). Il est possible de tracer une courbe de S_{C-D} en fonction de la position des carbones de la chaîne acyle (Figure 1.17B)[47] Au cours de cette thèse nous avons utilisé la méthode décrite par Lafleur et coll.[47] pour déterminer le profil d'ordre conformationnel lissé des chaînes (*smoothed order profile*). Dans cette approche, on identifie le doublet le plus interne (plus mobile) dans le spectre dePaké, et son $\Delta\nu$ est associé au CD_3. Ensuite, on intègre l'aire correspondant aux doublets restants. Cette aire est divisée en tranches correspondant au nombre de groupes CD_2 qui contribuent au signal. La fréquence correspondant au centre de chaque tranche est utilisée pour définir la valeur de S_{C-D} de chacun des méthylènes pour chaque position de la chaîne acyle. Le profil d'ordre est obtenu en

supposant qu'il y a une décroissance monotone de l'ordre le long de la chaîne, de la tête polaire au méthyl terminal.

Le profil d'ordre montre généralement une région où il y a moins de variation dans les valeurs de S_{C-D} (le plateau) et qui correspond à la partie supérieure de la chaîne qui est près de la tête polaire. Dans cette région, la pression latérale subie par les têtes polaires provoque une limitation du désordre conformationnel dans le segment supérieur de la chaîne. En allant vers le méthyl terminal, on constate une diminution progressive des valeurs de S_{C-D}, associée à une augmentation de l'isomérisation *trans-gauche*.

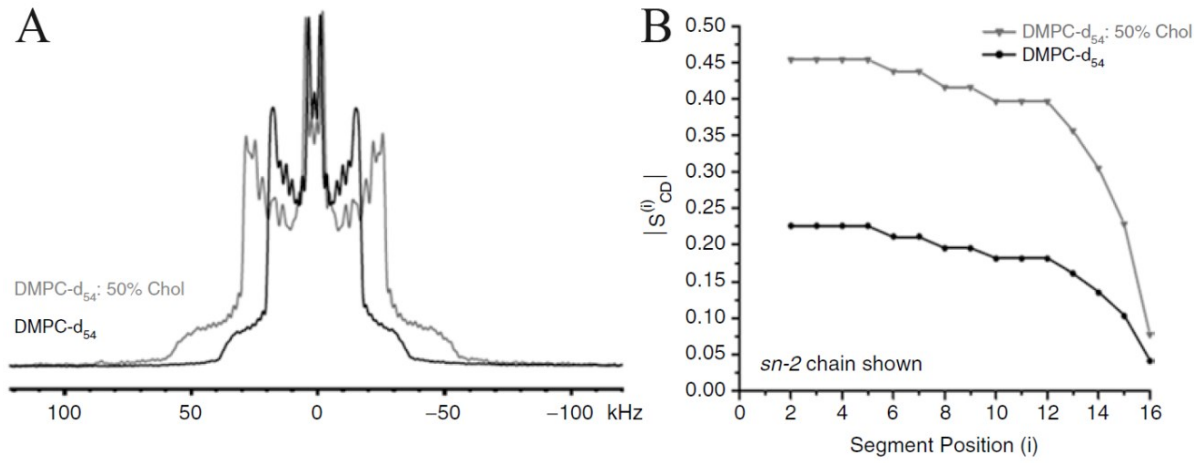

Figure 1.17. A : Spectre ^{2}H RMN de la 1,2-dimyristoyl-*sn*-glycéro-3-phosphocholine deutérée (DMPC-d_{54}) (trait foncé) et d'un mélange DMPC-d_{54}/Chol 50:50 (trait pâle). B : Profils d'ordre obtenus à partir de A. Adaptée de la référence 48 avec la permission de Springer.

Les lipides qui se trouvent dans la phase l_o sont plus ordonnés que ceux dans la phase l_α (Figure 1.17). Le plateau des lipides dans la phase l_α se trouve généralement entre S_{C-D} = 0,20 - 0,25, tandis que le plateau des lipides dans la phase l_o se trouve à des valeurs supérieures. Il faut mentionner que la valeur maximale de S_{C-D} est de 0,5.

L'utilisation de mélanges miroir nous permet d'étudier le comportement d'un lipide en particulier dans un système plus complexe. La ^{2}H RMN nous permet de suivre la structure et la dynamique d'un lipide en particulier lorsque l'échantillon est préparé avec un lipide deutéré et le reste des lipides hydrogénés On peut préparer des échantillons avec la même composition mais pour lesquels la composante deutérée est différente; c'est ce que nous appelons des mélanges miroir. Dans le cadre de cette thèse, nous avons préparé des mélanges du SC composés de CerNS24/FFA/Chol, où nous avons utilisé comme FFA l'acide lignocérique deutéré ou l'acide palmitique deutéré, afin d'étudier l'influence de la longueur de chaîne de l'acide gras sur les propriétés physico-chimique de ces mélanges modèles (Chapitre 2). Nous avons utilisé trois mélanges miroir du type CerEOS/CerNS/FFAs/Chol (Chapitre 3). Ces mélanges incluaient l'acide lignocérique deutéré, le céramide NS24 avec sa chaîne C24 deutérée, ou le céramide EOS avec sa chaîne oléate deutérée afin d'étudier le comportement individuel de ces lipides dans le mélange. Finalement, lors de notre étude de l'interaction des acides gras à très longue chaîne sur les membranes de phospholipides, nous avons préparé de mélanges miroir avec l'acide gras deutéré ou la POPC deutérée (Chapitre 4). Cela nous a permis de connaître la façon dont les acides sont organisés dans la bicouche de POPC.

1.3.2 Spectroscopie infrarouge[49-51]

La spectroscopie infrarouge est une des techniques de caractérisation les plus importantes et polyvalentes de nos jours. Elle sert à analyser des produits en phase gazeuse, liquide et solide de manière simple et avec une bonne sensibilité. Cette technique fournit de l'information relative aux énergies vibrationnelles des molécules, sert à identifier les groupes fonctionnels mais aussi certaines conformations de ces groupements.

La spectroscopie infrarouge est largement utilisée dans l'étude des lipides. Une des applications les plus courantes est l'analyse du thermotropisme des lipides, c'est-à-dire le changement de phase en fonction de la température. Dans ce cas, nous utilisons la vibration d'élongation C-H symétrique (ν_sC-H) ou asymétrique des chaînes aliphatiques, qui sont des signaux intenses pour les molécules organiques (Figure 1.18).

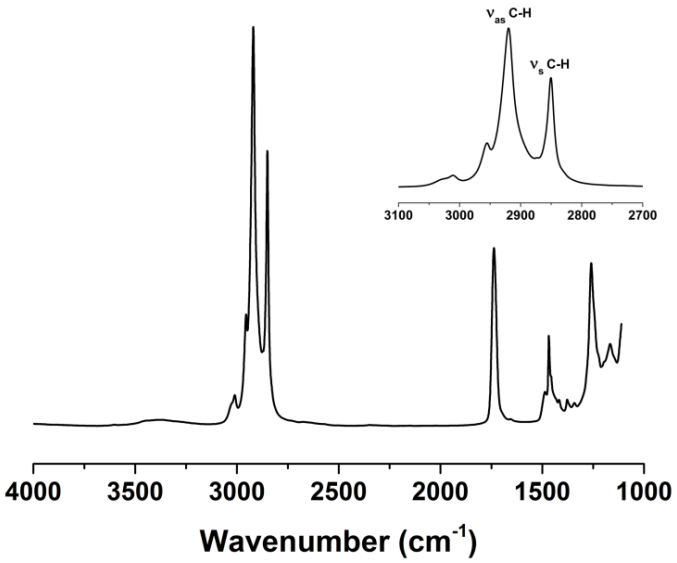

Figure 1.18. Spectre infrarouge de la POPC.

Ces signaux se trouvent généralement entre les 2800 et 3100 cm^{-1} et la position et la largeur de ces bandes sont sensibles à l'ordre conformationnel des chaînes hydrocarbonées; donc elles peuvent être utilisées pour suivre les transitions de phase des lipides.[52] Pour la plupart des lipides, il y a une ou plusieurs transitions de phase lors d'une augmentation de la température. Donc, les chaînes aliphatiques passent d'un état plus ordonné, où chaque groupe CH_2 tout au long de la chaîne est en conformation *trans*, vers un état plus désordonné, pour lequel il y a une augmentation des conformations *gauches*. La fréquence d'absorption d'une liaison est décrite par:

$$\nu = \frac{1}{2\pi}\sqrt{\frac{k}{\mu}} \qquad \text{Eq. 1.3}$$

où *k* est la constante de force de la liaison, et μ est la masse réduite du groupe méthylène. Les conformères *gauches* changent légèrement la constante de ressort *k*, et provoquent ainsi une augmentation de la fréquence **ν**. Le changement de la fréquence en fonction de la température est donc utilisé pour décrire les transitions de phases lipidiques (Figure 1.19).

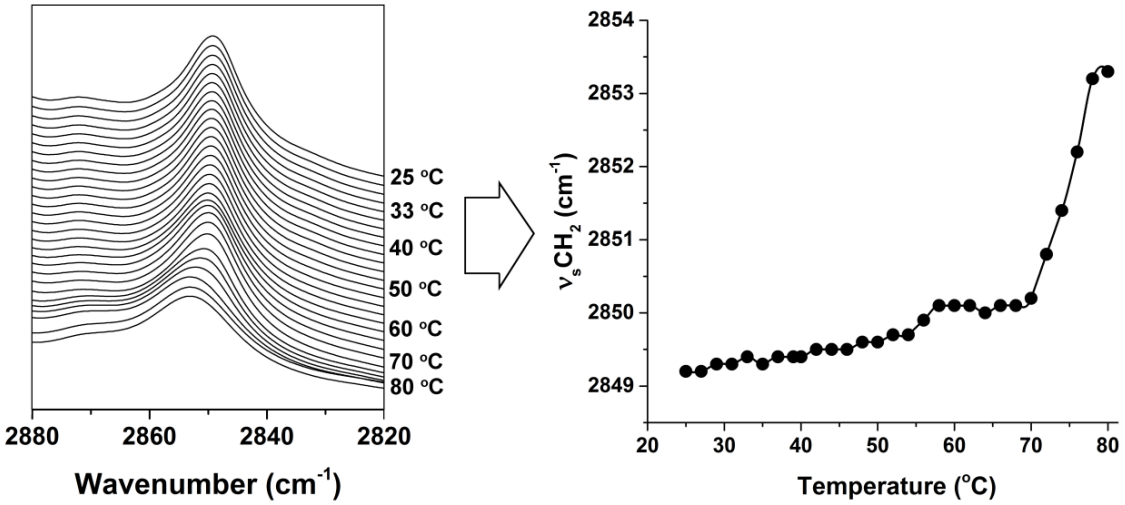

Figure 1.19. Variation de la position de la bande d'élongation symétrique ν_sC-H du céramide NS16 en fonction de la température.

Il est généralement accepté que les lipides se trouvent en phase solide si la valeur de ν_sC-H est inférieure à 2850 cm^{-1}. La transition vers une phase gel n'affecte pas de façon significative la position de la bande, étant donné que les chaînes restent tout *trans*, la transition entraînant principalement une augmentation de la vitesse de rotation. Une transition vers la phase l_o déplace légèrement la position de la bande autour de 2851-2852 cm^{-1}, tandis qu'une transition vers la phase l_d déplace la bande autour de 2853 cm^{-1}. Des valeurs de fréquence

supérieures à 2853 cm^{-1} sont généralement indicatives de la phase désordonnée, comme la phase liquide.[33,53-54]

Un grand avantage de cette technique est de décrire d'une façon simultanée le comportement de deux composants différents dans les mélanges en utilisant des espèces deutérées. Dans ce cas, une augmentation de la masse réduite provoquée par la substitution des protons (H) par des deutériums (D) déplace la position de la bande d'élongation des méthylènes et méthyls vers les basses fréquences, entre 2000 et 2300 cm^{-1} (Figure 1.20).

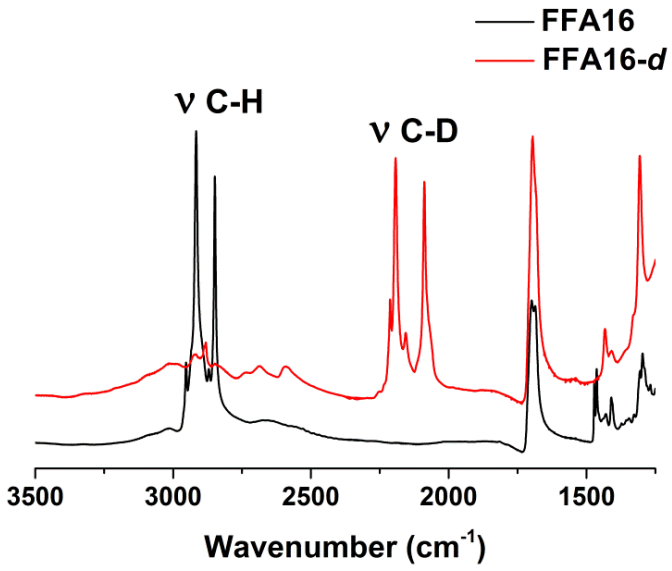

Figure 1.20. Spectre infrarouge de l'acide palmitique (FFA16) hydrogéné (noir) et deutéré (rouge).

La bande d'élongation symétrique des méthylènes (ν_sC-D) est aussi sensible à l'ordre conformationnel de chaînes. Au cours de cette thèse, nous avons préparé des mélanges avec des lipides deutérés et hydrogénés afin de décrire le comportement de ces composés de façon simultanée, dans le même échantillon.

La spectroscopie infrarouge permet aussi de décrire la symétrie de l'empilement des chaînes lipidiques en phase solide, grâce au signal de déformation des méthylènes (δCH_2). Ce signal se trouve vers 1468 cm^{-1} pour le CH_2 et 1088 cm^{-1} pour le CD_2. Un dédoublement de cette bande est indicatif d'un couplage vibrationnel entre les chaînes dans une symétrie orthorhombique (Figure 1.21).

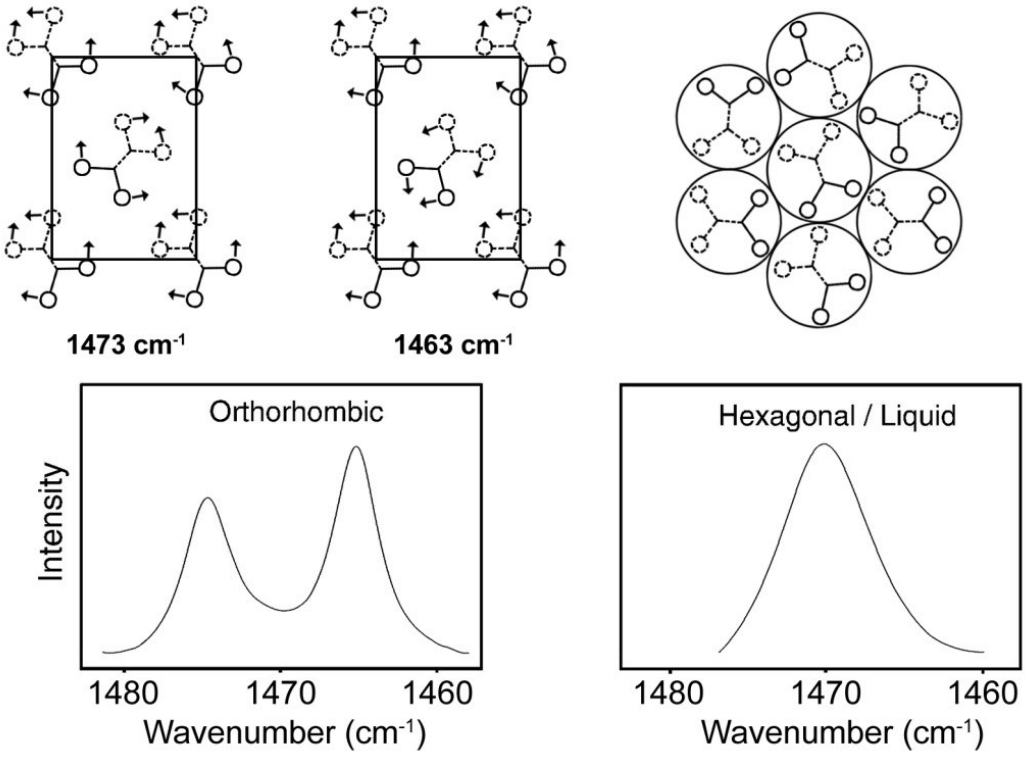

Figure 1.21. Dépendance entre l'empilement des chaînes lipidiques et le dédoublement de la bande de déformation (δCH_2).[16]

Ce couplage est seulement possible si les modes de déformation des chaînes adjacentes ont approximativement la même fréquence de vibration et une orientation spatiale correcte. Cet éclatement disparaît pour un empilement hexagonal ou pour un empilement sans symétrie. Cette région permet d'identifier la transition de la phase solide orthorhombique vers la phase

gel (hexagonal). La présence du dédoublement de la bande de déformation est très importante dans l'étude de membranes modèles du SC; l'empilement orthorhombique se trouve dans la matrice lipidique du SC natif et sa présence semble être associée à l'imperméabilité du SC.[55-56]

En plus de caractériser la formation de la phase orthorhombique, la région de déformation permet d'analyser l'homogénéité du mélange en utilisant simultanément des lipides deutérés et hydrogénés. Le couplage vibrationnel n'est possible que si les groupes possèdent à peu près la même fréquence de vibration; ainsi le couplage est réduit si les chaînes deutérées et hydrogénées sont voisines les unes des autres.

Le dédoublement de la bande de déformation peut indiquer la présence des domaines enrichis dans une espèce en particulier. La largeur de l'éclatement de la bande de déformation est associée à la taille des domaines lipidiques. Une largeur maximal indique des domaines de 100 molécules ou plus[57], tandis que l'éclatement diminue pour la formation de plus petits domaines ou des domaines moins purs. Dans le cadre des travaux de cette thèse, nous avons utilisé l'information provenant du dédoublement de la bande de déformation de la région C-D et C-H pour établir l'homogénéité des mélanges contenant l'acide lignocérique ou l'acide palmitique (Chapitre 2).

1.3.3 Spectroscopie Raman[50,58-59]

La spectroscopie Raman est une technique très utile pour la caractérisation des systèmes lipidiques. De façon analogue à la spectroscopie infrarouge, cette technique fournit de l'information relative aux énergies vibrationnelles des groupes fonctionnels, ce qui permet l'identification de différentes molécules. En fait, ces deux techniques sont considérées comme complémentaires. Dans l'analyse des systèmes lipidiques, où la présence de l'eau est une

condition indispensable, la spectroscopie Raman présente l'avantage d'une faible diffusion Raman des molécules d'eau (Figure 1.22).

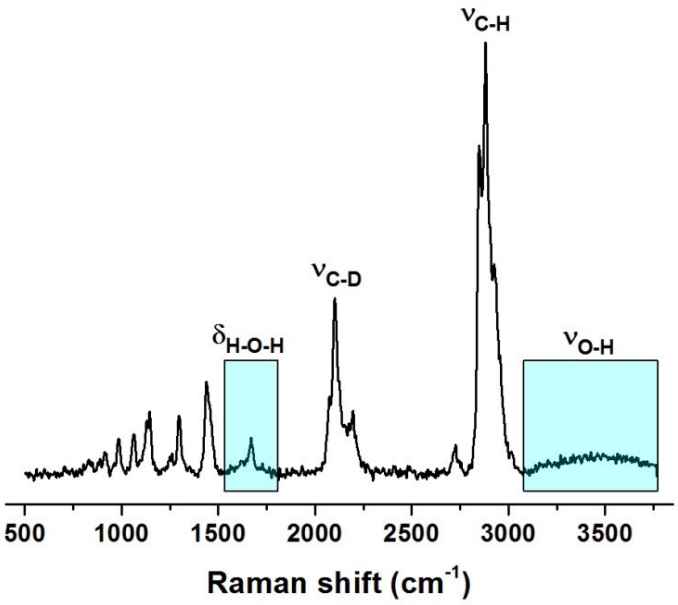

Figure 1.22. Spectre Raman d'un mélange de CerNS24/FFA24-d_{47}/Chol obtenu en immersion dans l'eau.

La spectroscopie Raman nous permet de décrire l'ordre conformationnel de chaînes lipidiques en analysant la largeur à la mi-hauteur de la bande d'élongation symétrique du lien C-D.[60] Une augmentation du nombre de conformères *gauche* provoque une augmentation de la largeur de cette bande; donc il est possible de caractériser l'ordre conformationnel des chaînes lipidiques à partir de cette largeur.[60]

1.4 Plan de la thèse

À l'heure actuelle, la relation entre la structure de la matrice lipidique du SC et l'imperméabilité de la peau n'est pas bien établie. Il est connu que la matrice lipidique constituant le SC est le principal responsable de la diffusion limitée des molécules vers

l'intérieur de l'organisme. Cette matrice est principalement formée par des lipides à l'état cristallin, qui s'organisent dans un empilement orthorhombique à la température physiologique. Les lipides du SC montrent aussi une organisation lamellaire caractérisée par la présence d'une phase de périodicité longue et une phase de périodicité courte. Par contre, la façon dont les lipides s'organisent pour former ces deux phases est encore inconnue. Le rôle de certains lipides tels que les acides et céramides à longue chaînes acyles, ainsi que le céramide EOS n'est aussi pas bien établi.

Certaines maladies de la peau comme l'eczéma ou la dermatite atopique se caractérisent par une diminution de la proportion d'acides et de céramides à longue chaînes et une augmentation de la proportion de lipides à chaînes courtes dans la matrice lipidique du SC.[61] Pour ces maladies, une réduction marquée du contenu d'acide lignocérique (FFA24) et cérotique (FFA26), accompagnée d'une augmentation de l'acide palmitique (FFA16) a été observée. La quantité de céramides NS16 et AS16 a montré aussi une augmentation importante chez les patients. Comme résultat de cette variation, le SC devient plus perméable, ce qui provoque la perte d'eau à travers la peau.

Connaissant ce phénomène, nous avons proposé comme première tâche d'étudier l'influence de la longueur de la chaîne des acides gras sur les propriétés physico-chimiques des membranes modèles du SC, ce qui sera décrit au chapitre 2 de la thèse. À cet effet, nous avons utilisé deux membranes modèles composées par le N-lignocéroyl-D-érythro-sphingosine (Cer NS24), le cholestérol, et l'acide palmitique ou lignocérique. Au cours de cette étude, nous avons constaté une séparation de phase et la formation de domaines lipidiques cristallins lorsque le mélange incluait de l'acide palmitique. Cependant, l'acide lignocérique conduisait à un mélange plus homogène. De plus, cet acide favorisait la formation d'une phase gel, ce qui

est une caractéristique inhabituel pour la plupart des mélanges modèles du SC étudiés. Ces travaux montrent donc que la présence des acides gras très longs, combinés avec un céramide à chaîne très longue (Cer NS24) et le cholestérol, permet de reproduire d'une meilleure façon les caractéristiques du SC natif par rapport aux membranes modèles précédentes.

Le chapitre 3 vise sur la compréhension du rôle de certains lipides très importants dans la matrice lipidique du SC : l'acide lignocérique, le céramide NS24 ainsi que le céramide EOS. Ce dernier est considéré comme un composant clé pour la formation de la phase de périodicité longue dans le SC. Cette étude présente le résultat de la caractérisation spectroscopique d'un mélange modèle du SC plus complexe, permettant de bien reproduire la LPP. Il était composé d'une série d'acides gras saturés dont la longueur variait entre 16 et 24 atomes de carbone, des céramides NS24 et EOS et du cholestérol. Les données obtenues par ^{2}H-NMR, spectroscopie infrarouge et Raman ont révélé que le céramide EOS conduit à la formation de domaines liquides de taille nanométrique hautement désordonnés dans la matrice solide cristalline. Il a été proposé que l'organisation lipidique impose une contrainte stérique sur les chaînes oléates du Cer EOS qui empêche leur cristallisation. De manière surprenante, ces nanogouttelettes restaient à l'état liquide jusqu'à -30 °C. Ces découvertes modifient substantiellement la description structurale du SC que nous avons jusqu'au présent et conduit à reconsidérer la relation structure/fonction de ce matériau biologique.

Le chapitre 4 a pour but de déterminer comment les acides gras saturés à très longue chaîne (*Very-long chain fatty acids*, VLCFAs) s'adaptent dans des membranes modèles constituées avec un lipide possédant des chaînes plus courtes, spécifiquement la POPC. Nous avons utilisé les acides palmitique (FFA16), arachidique (FFA20) et lignocérique (FFA24). L'organisation des membranes a été décrite par des mesures de ^{2}H RMN et des simulations de

dynamique moléculaire. Nous avons aussi examiné l'impact de l'état de protonation de l'acide sur la position et l'ordre des chaînes de ces acides gras dans les membranes de phospholipides. Nous avons montré que le groupe carboxylique des acides se situe légèrement sous la tête polaire de la POPC et sa très longue chaîne acyle interagit avec les lipides du feuillet opposé lorsque le groupement est déprotoné. Cette interdigitation provoque un deuxième plateau observé au centre de la bicouche dans les profils d'ordre (S_{C-D}); ce profil est inhabituel pour les systèmes lipidiques.

Finalement, le chapitre 5 montre les conclusions générales de cette thèse, permettant de faire un bilan global sur les objectifs principaux proposés. De plus, nous présentons les perspectives futures de ce travail.

1.5 Situation des articles à la date du dépôt

Chapitre 2 : Paz Ramos, A.; Lafleur, M. Chain length of free fatty acids influences the phase behavior of stratum corneum model membranes. *Langmuir* **2015**, *31*, 11621–11629.

Les expériences ont été effectuées par Adrian Paz Ramos. La rédaction a été effectuée par Adrian Paz Ramos et Michel Lafleur.

Chapitre 3 : Paz Ramos, A.; Gooris, G.; Bouwstra, J.; Lafleur, M. Evidence of hydrocarbon nanodrops in highly ordered Stratum Corneum model membranes. *J. Lipid Res*. **2018**, 59, 137–143.

Les expériences ont été effectuées par Adrian Paz Ramos. La caractérisation par diffraction des rayons X aux petits angles était effectuée par Gert Gooris. La rédaction a été effectuée par Adrian Paz Ramos et Michel Lafleur, avec la participation de Joke Bouwstra. Gert Gooris et Joke Bouwstra ont fourni les échantillons.

Chapitre 4 : Paz Ramos, A.; Lagüe, P.; Lamoureux, G.; Lafleur, M. Effect of saturated very long-chain fatty acids on the organization of lipid membranes: A study combining ^{2}H NMR spectroscopy and molecular dynamics simulations. *J. Phys. Chem. B*, **2016**, 120, 6951–6960.

Les expériences ont été effectuées par Adrian Paz Ramos. Les simulations de dynamique moléculaire ont été effectuées par Patrick Lagüe et Guillaume Lamoureux. La rédaction a été effectuée par Adrian Paz Ramos, Michel Lafleur, avec la collaboration de Patrick Lagüe et Guillaume Lamoureux.

1.6 Références

(1) Leider, M. On the weight of the skin. *J. Invest. Dermatol.* **1949**, *12*, 187-191.

(2) Agache, P.; Lihoreau, T.; Mac-Mary, S.; Fanian, F.; Humbert, P. The human skin: an overview. In *Agache's Measuring the Skin*, Humbert, P.; Maibach, H.; Fanian, F.; Agache, P., Eds.; Springer International Publishing, **2016**, 1-4.

(3) Benítez, J. M.; Montáns, F. J. The mechanical behavior of skin: Structures and models for the finite element analysis. *Comput. Struct.* **2017**, *190*, 75-107.

(4) Nachman, M.; Franklin, S. E. Artificial skin model simulating dry and moist in vivo human skin friction and deformation behaviour. *Tribol. Int.* **2016**, *97*, 431-439.

(5) Walling, R. E. Dermis: structure, composition and role in thermoregulation. Nova Biomedical, **2014**, 121.

(6) R. K. Freinkel, D. T. W. The biology of skin. Parthenon Publishing, **2001**, 432.

(7) McGrath, J. A.; Uitto, J. Anatomy and organization of human skin. In *Rook's Textbook of Dermatology*; Wiley-Blackwell, **2010**, 1-53.

(8) Rook's Textbook of Dermatology 9th edition ed., **2016**.

(9) Krause, W. J.; Krause, W. J. Krause's essential human histology for medical students. Universal Publishers, **2005**, 320.

(10) Landmann, L. Epidermal permeability barrier: transformation of lamellar granule-disks into intercellular sheets by a membrane-fusion process, a freeze-fracture study. *J Invest. Dermatol.* **1986**, *87*, 202-209.

(11) Norlén, L.; Nicander, I.; Lundsjö, A.; Cronholm, T.; Forslind, B. A new HPLC-based method for the quantitative analysis of inner stratum corneum lipids with special reference to the free fatty acid fraction. *Arch. Dermatol. Res.* **1998**, *290*, 508-516.

(12) Nemes, Z.; Steinert, P. M. Bricks and mortar of the epidermal barrier. *Exp. Mol. Med.* **1999**, *31*, 5-19.

(13) Blank, I. H. Factors which influence the water content of the stratum corneum. *J. Invest. Dermatol.* **1952**, *18*, 433-440.

(14) Weerheim, A.; Ponec, M. Determination of stratum corneum lipid profile by tape stripping in combination with high-performance thin-layer chromatography. *Arch. Dermatol. Res.* **2001**, *293*, 191-199.

(15) Menon, G. K.; Cleary, G. W.; Lane, M. E. The structure and function of the stratum corneum. *Int. J. Pharm.* **2012**, *435*, 3-9.

(16) van Smeden, J.; Janssens, M.; Gooris, G. S.; Bouwstra, J. A. The important role of stratum corneum lipids for the cutaneous barrier function. *Biochim. Biophys. Acta* **2014**, *1841*, 295-313.

(17) Rabionet, M.; Gorgas, K.; Sandhoff, R. Ceramide synthesis in the epidermis. *Biochim. Biophys. Acta* **2014**, *1841*, 422-434.

(18) Masukawa, Y.; Narita, H.; Shimizu, E.; Kondo, N.; Sugai, Y.; Oba, T.; Homma, R.; Ishikawa, J.; Takagi, Y.; Kitahara, T., et al. Characterization of overall ceramide species in human stratum corneum. *Journal of Lipid Research* **2008**, *49*, 1466-1476.

(19) Motta, S.; Monti, M.; Sesana, S.; Caputo, R.; Carelli, S.; Ghidoni, R. Ceramide composition of the psoriatic scale. *Biochim. Biophys. Acta* **1993**, *1182*, 147-151.

(20) t'Kindt, R.; Jorge, L.; Dumont, E.; Couturon, P.; David, F.; Sandra, P.; Sandra, K. Profiling and characterizing skin ceramides using reversed-phase liquid chromatography–quadrupole time-of-flight mass spectrometry. *Anal. Chem.* **2012**, *84*, 403-411.

(21) Elias, P. M.; Williams, M. L.; Maloney, M. E.; Bonifas, J. A.; Brown, B. E.; Grayson, S.; Epstein, E. H., Jr. Stratum corneum lipids in disorders of cornification. Steroid sulfatase and cholesterol sulfate in normal desquamation and the pathogenesis of recessive X-linked ichthyosis. *J. Clin. Invest.* **1984**, *74*, 1414-1421.

(22) Friberq, S. E.; Osborne, D. W. Small Angle X-Ray diffraction patterns of stratum corneum and a model structure for its lipids. *J. Dispersion Sci. Technol.* **1985**, *6*, 485-495.

(23) White, S. H.; Mirejovsky, D.; King, G. I. Structure of lamellar lipid domains and corneocyte envelopes of murine stratum corneum. An x-ray diffraction study. *Biochemistry* **1988**, *27*, 3725-3732.

(24) Bouwstra, J. A.; Gooris, G. S.; van der Spek, J. A.; Bras, W. Structural investigations of human stratum corneum by small-angle X-ray scattering. *J. Invest. Dermatol.* **1991**, *97*, 1005-1012.

(25) Pilgram, G. S. K.; Marjolein Engelsma-van Pelt, A.; Koerten, H. K.; Bouwstra, J. A. Electron diffraction provides new information on human stratum corneum lipid organization studied in relation to depth and temperature. *J. Invest. Dermatol.* **1999**, *113*, 403-409.

(26) Forslind, B. O. A domain mosaic model of the skin barrier. *Acta Derm-Venereol.* **1994**, *74*, 1-6.

(27) Norlén, L. Skin barrier structure and function: the Single Gel Phase model. *J. Invest. Dermatol.* **2001**, *117*, 830-836.

(28) Kessner, D.; Kiselev, M.; Dante, S.; Hauß, T.; Lersch, P.; Wartewig, S.; Neubert, R. H. H. Arrangement of ceramide [EOS] in a stratum corneum lipid model matrix: new aspects revealed by neutron diffraction studies. *Eur. Biophys. J.* **2008**, *37*, 989-999.

(29) de Jager, M. W.; Gooris, G. S.; Dolbnya, I. P.; Bras, W.; Ponec, M.; Bouwstra, J. A. Novel lipid mixtures based on synthetic ceramides reproduce the unique stratum corneum lipid organization. *J. Lipid Res.* **2004**, *45*, 923-932.

(30) Bouwstra, J. A.; Gooris, G. S.; Dubbelaar, F. E. R.; Ponec, M. Phase behavior of stratum corneum lipid mixtures based on human ceramides: the role of natural and synthetic ceramide 1. *J. Invest. Dermatol.* **2002**, *118*, 606-617.

(31) Školová, B.; Hudská, K.; Pullmannová, P.; Kováčik, A.; Palát, K.; Roh, J.; Fleddermann, J.; Estrela-Lopis, I.; Vávrová, K. Different phase behavior and packing of ceramides with long (C16) and very long (C24) acyls in model membranes: infrared spectroscopy using deuterated lipids. *J. Phys. Chem. B* **2014**, *118*, 10460-10470.

(32) Bo Forslind, M. L. Skin, hair, and nails: structure and function. CRC Press, **2003**.

(33) Kodati, V. R.; Lafleur, M. Comparison between orientational and conformational orders in fluid lipid bilayers. *Biophys. J. 64*, 163-170.

(34) Souza, S. L.; Valério, J.; Funari, S. S.; Melo, E. The thermotropism and prototropism of ternary mixtures of ceramide C16, cholesterol and palmitic acid. An exploratory study. *Chem. Phys. Lipids* **2011**, *164*, 643-653.

(35) Kwak, S.; Lafleur, M. Effect of dimethyl sulfoxide on the phase behavior of model stratum corneum lipid mixtures. *Chem. Phys. Lipids* **2009**, *161*, 11-21.

(36) Brief, E.; Kwak, S.; Cheng, J. T. J.; Kitson, N.; Thewalt, J.; Lafleur, M. Phase behavior of an equimolar mixture of N-palmitoyl-D-*erythro*-sphingosine, cholesterol, and palmitic acid, a mixture with optimized hydrophobic matching. *Langmuir* **2009**, *25*, 7523-7532.

(37) Lafleur, M. Phase behaviour of model stratum corneum lipid mixtures: an infrared spectroscopy investigation. *Can. J. Chem.* **1998**, *76*, 1501-1511.

(38) Bouwstra, J. A.; Gooris, G. S.; Cheng, K.; Weerheim, A.; Bras, W.; Ponec, M. Phase behavior of isolated skin lipids. *J. Lipid Res.* **1996**, *37*, 999-1011.

(39) de Sousa Neto, D.; Gooris, G.; Bouwstra, J. Effect of the ω-acylceramides on the lipid organization of stratum corneum model membranes evaluated by X-ray diffraction and FTIR studies (Part I). *Chem. Phys. Lipids* **2011**, *164*, 184-195.

(40) Schmitt, T.; Lange, S.; Sonnenberger, S.; Dobner, B.; Demé, B.; Neubert, R. H. H.; Gooris, G.; Bouwstra, J. A. Determination of the influence of C24 D/(2R)- and L/(2S)-isomers of the CER[AP] on the lamellar structure of stratum corneum model systems using neutron diffraction. *Chem. Phys. Lipids* **2017**, *209*, 29-36.

(41) Oguri, M.; Gooris, G. S.; Bito, K.; Bouwstra, J. A. The effect of the chain length distribution of free fatty acids on the mixing properties of stratum corneum model membranes. *Biochim. Biophys. Acta* **2014**, *1838*, 1851-1861.

(42) Mojumdar, Enamul H.; Gooris, Gert S.; Barlow, David J.; Lawrence, M. J.; Deme, B.; Bouwstra, Joke A. Skin lipids: localization of ceramide and fatty acid in the unit cell of the long periodicity phase. *Biophys. J.* **2015**, *108*, 2670-2679.

(43) Pullmannová, P.; Pavlíková, L.; Kováčik, A.; Sochorová, M.; Školová, B.; Slepička, P.; Maixner, J.; Zbytovská, J.; Vávrová, K. Permeability and microstructure of model stratum corneum lipid membranes containing ceramides with long (C16) and very long (C24) acyl chains. *Biophys. Chem.* **2017**, *224*, 20-31.

(44) Molugu, T. R.; Lee, S.; Brown, M. F. Concepts and methods of solid-state NMR spectroscopy applied to biomembranes. *Chem. Rev.* **2017**, *117*, 12087-12132.

(45) Leung, S. S. W.; Thewalt, J. Deuterium NMR of mixed lipid membranes. In *Advances in biological solid-state NMR: proteins and membrane-active peptides*; The Royal Society of Chemistry, **2014**, 180-199.

(46) Bryce, D. L.; Bernard, G. M.; Gee, M.; Lumsden, M. D.; Eichele, K.; Wasylishen, R. E. Practical aspects of modern routine solid-state multinuclear magnetic resonance spectroscopy: one-dimensional experiments. *Can. J. Spectrosc.* **2001**, *46*, 46-82.

(47) Lafleur, M.; Fine, B.; Sternin, E.; Cullis, P. R.; Bloom, M. Smoothed orientational order profile of lipid bilayers by 2H-nuclear magnetic resonance. *Biophys. J.* **1989**, *56*, 1037-1041.

(48) Tyler, A. I.; Clarke, J. A.; Seddon, J. M.; Law, R. V. Solid state NMR of lipid model membranes. In *Methods in Membrane Lipids*; Vol. 1232, 227-253.

(49) Stuart, B. H. Infrared Spectroscopy: fundamentals and applications. Wiley, **2005**.

(50) Larkin, P. Infrared and Raman spectroscopy. Elsevier, **2011**, 228.

(51) Ferraro, J. R. Practical Fourier transform infrared spectroscopy. Academic Press, **1990**, 534.

(52) Mendelsohn, R.; Moore, D. J. Vibrational spectroscopic studies of lipid domains in biomembranes and model systems. *Chem. Phys. Lipids* **1998**, *96*, 141-157.

(53) Gooris, G. S.; Bouwstra, J. A. Infrared spectroscopic study of stratum corneum model membranes prepared from human ceramides, cholesterol, and fatty acids. *Biophys. J.* **2007**, *92*, 2785-2795.

(54) Moore, D. J.; Rerek, M. E.; Mendelsohn, R. Lipid domains and orthorhombic phases in model stratum corneum: evidence from Fourier transform infrared spectroscopy studies. *Biochem. Biophys. Res. Commun.* **1997**, *231*, 797-801.

(55) Bouwstra, J. A.; Honeywell-Nguyen, P. L. Skin structure and mode of action of vesicles. *Advanced Drug Delivery Reviews* **2002**, *54*, S41-S55.

(56) Bouwstra, J. A.; Ponec, M. The skin barrier in healthy and diseased state. *Biochim. Biophys. Acta* **2006**, *1758*, 2080-2095.

(57) Snyder, R. G.; Goh, M. C.; Srivatsavoy, V. J. P.; Strauss, H. L.; Dorset, D. L. Measurement of the growth kinetics of microdomains in binary n-alkane solid solutions by infrared spectroscopy. *J. Phys. Chem.* **1992**, *96*, 10008-10019.

(58) Ferraro, J. R.; Nakamoto, K. Introductory Raman spectroscopy. Academic Press, **1994**, 370.

(59) Le Ru, E. C.; Etchegoin, P. G. Principles of surface-enhanced Raman spectroscopy. Elsevier, **2009**, 663.

(60) Mendelsohn, R.; Koch, C. C. Deuterated phospholipids as raman spectroscopic probes of membrane structure: Phase diagrams for the dipalmitoyl phosphatidylcholine(and its d62

derivative)-dipalmitoyl phosphatidylethanolamine system. *Biochim. Biophys. Acta* **1980**, *598*, 260-271.

(61) van Smeden, J.; Janssens, M.; Kaye, E. C. J.; Caspers, P. J.; Lavrijsen, A. P.; Vreeken, R. J.; Bouwstra, J. A. The importance of free fatty acid chain length for the skin barrier function in atopic eczema patients. *Exp. Dermatol.* **2014**, *23*, 45-52.

Chapitre 2: Chain length of free fatty acids influences the phase behavior of stratum corneum model membranes

Adrian Paz Ramos, Michel Lafleur.

Langmuir, **2015**, 31, 11621–11629.

2.1 Abstract

The skin, the largest organ of the human body, forms a flexible interface between our internal and external environment that protects our organism from exogenous compounds as well as excessive water loss. The stratum corneum (SC), the outermost layer of mammal epidermis, is mainly responsible for the skin impermeability. The SC is formed by corneocytes embedded in a lipid matrix, which is mostly constituted of ceramides (Cer), free fatty acids (FFA), and cholesterol (Chol), organized in two coexisting crystalline lamellar phases. This arrangement of lipids is crucial to skin barrier function. The aim of this paper is to determine the impact of FFA chain length on the phase behavior of SC model lipid membranes using solid-state deuterium NMR and IR spectroscopy. We studied ternary mixtures of N-lignoceroyl-D-*erythro*-sphingosine (Cer24), cholesterol, and palmitic (FFA16) or lignoceric (FFA24) acid in an equimolar ratio. This proportion replicates the lipid composition found in the SC lipid matrix. Our studies revealed that the phase behavior of Cer24/FFA/Chol ternary mixtures is strongly affected by the length of the FFA. We found the formation of phase-separated crystalline lipid domains when using palmitic acid whereas the use of lignoceric acid results in a more homogeneous mixture. In addition, it was observed that mixtures with lignoceric acid form a gel phase, a very unusual feature for SC model mixtures.

2.2 Introduction

The stratum corneum (SC), the outermost layer of the epidermis, is known as the main contributor to the permeability properties of skin.[1] It is formed by dead cells (corneocytes), embedded in a highly ordered lipid matrix mainly composed of ceramides (Cer), free fatty acids (FFA), and cholesterol (Chol) in an approximately equimolar ratio and a small quantity of cholesterol sulfate (CholS).[2] The diffusion of substances across the SC is proposed to proceed mainly via the intercellular lipid matrix since it is the continuous phase and the keratin-filled corneocytes are virtually impenetrable.[3,4] Because the lipid fraction is intimately related to the skin barrier property, the understanding of the lipid matrix structure and of the molecular interactions dictating it is crucial to comprehending and controlling the penetration of substances through the skin.

The lipid-phase behavior is intimately linked to the lipid composition that, therefore, dictates skin impermeability. The penetration of molecules through the SC depends on the order and packing of the lipid hydrocarbon chains,[5,6] a highly ordered phase offering a higher resistance to molecule diffusion than a disordered phase. It has been proposed that the SC is a composite material formed by the coexistence of both solid and fluid phases composing a domain mosaic.[7] The majority of the lipids in the SC are arranged in a crystalline phase, which is highly impermeable. It is proposed that these crystalline domains are glued one to another by regions of lipids in a liquid crystalline state. Such organization would explain the limited diffusion through the SC but also the mechanical properties of the skin surface.

Human SC displays an elaborate lipid composition. At least 15 ceramide subclasses are identified, one of the most abundant being Cer NS, a ceramide bearing a sphingosine group

with a nonhydroxy fatty acid.[8,9] A variety of fatty acid chains can be found in Cer NS, the most abundant being the linear and saturated chain containing 24 carbon atoms (26% of the total content of Cer NS in SC).[10] The SC free fatty acids are essentially linear and saturated, with the acyl chain length varying from C14 to C30; the most abundant species is C24 (37% of the FFA fraction in SC).[11] Because the SC lipid matrix is a complex system, several studies have relied on the use of simplified models to elucidate the role of individual lipid within the matrix and to gain information about their molecular organization. The equimolar mixture of nonhydroxylated palmitoyl ceramide (Cer16, *i.e.*, ceramide NS bearing a C16 fatty acid chain, 3% of the total content of Cer NS in SC[10]), a free fatty acid with a C16 acyl chain (FFA16, 1.3% of the FFA fraction in SC[11]), and cholesterol has been a classic model mixture due to its simplicity, the commercial availability of the three components, and the fact that this mixture provides an optimized hydrophobic matching. In this mixture, the lipids are, despite the hydrophobic matching, mainly phase-separated at physiological temperature, with Cer16 and FFA16 existing in distinct crystalline-phase domains with orthorhombic chain packing.[12−14] The miscibility of Cer16 with FFA16 and cholesterol was found to be more limited than that previously observed for bovine brain ceramide III (BBCer III).[15] This observation was associated with the BBCer III chain heterogeneity, the main ones being stearic (18:0), nervonic (24:1), and lignoceric (24:0) chains.

Recently, comparison between SC model mixtures containing Cer24 has shown that the lipid organization and the mixing behavior strongly depend on the free fatty acid chain length. It was shown that hydrated mixtures containing Cer24, FFA24, and Chol form mixed crystals, as determined by infrared and Raman spectroscopy, whereas a considerable phase separation between the lipid components was observed when the mixtures were formed by

Cer16, FFA16, and Chol.[16] In a similar fashion, two recent papers showed that the thermal behavior of ternary model mixtures is influenced by the length of the nonhydroxy fatty acid of ceramide.[17,18] It is shown that the equimolar Cer24/FFA24/Chol system forms a more homogeneous mixture than the Cer16/FFA24/Chol mixture, which is mostly phase-separated. It is also shown that the Cer24/FFA24/Chol mixture has a stronger propensity to be disordered upon heating than the Cer16/FFA24/Chol system, despite a longer ceramide chain.

In this paper, we examined the impact of FFA chain length on the phase behavior of equimolar mixtures of Cer24/FFA/Chol, comparing FFA16 and FFA24 using solid-state deuterium NMR (^{2}H NMR) and IR spectroscopy. The FFA chain length was shown to impact the lipid mixing properties,[16] but at this point, there is no detailed description of the phases adopted by the components of the mixtures. ^{2}H NMR is a powerful technique used to identify and quantify lipid phases in an SC model membrane as different profiles are obtained for different phases.[6,19,20] IR spectroscopy is also a useful technique for studying the structure and organization of lipid mixtures. Besides, the use of perdeuterated lipids allows the identification of the packing and miscibility of different lipids in a more complex mixture.[21–23] Using these techniques, we determined that the phase behavior of Cer24/FFA/Chol ternary mixtures is strongly affected by the length of the FFA and that mixtures with FFA24 form a gel phase, a feature that is not observed for analogous mixtures that include a component with a 16-carbon acyl chain (Cer16 or FFA16).

2.3 Materials and Methods

2.3.1 Materials

N-Lignoceroyl-D-*erythro*-sphingosine (Cer24) and cholesterol (Chol, 99%) were purchased from Avanti Polar Lipids (Birmingham, AL, USA). Palmitic acid (FFA16, >99%), lignoceric acid (FFA24, >99%), citric acid monohydrate (>98%), ethylenediaminetetraacetic acid (EDTA, 99%) and deuterium-depleted water (>99%) were obtained from Sigma Chemical Co. (St. Louis, MO, USA). Perdeuterated FFA16-d_{31} (99.3%) and FFA24-d_{47} (98.8%) were obtained from CDN Isotopes (Pointe-Claire, QC, Canada). Sodium chloride (>99%) was purchased from Amresco (Solon, OH, USA). Methanol (spectrograde) and benzene (high purity) were obtained from American Chemicals Ltd. (Montreal, QC, Canada) and BDH Inc. (Toronto, ON, Canada), respectively.

2.3.2 Mixture preparation

In this study, two different lipid mixtures were prepared: Cer24/FFA16-d_{31}/Chol and Cer24/FFA24-d_{47}/Chol. The lipids were individually dissolved in a benzene/methanol (7:3 v/v) solution, and then aliquots of an appropriate volume were mixed to obtain a 1:1:1 molar ratio. The samples were freeze-dried, and the resulting lipid powder was hydrated with excess citrate buffer (100 mM) containing NaCl (150 mM) and EDTA (0.4 mM) at pH 5.2. The buffer was prepared in deuterium-depleted water. Five freeze-and-thaw cycles, from 0 to 80 °C, were carried out, and the samples were incubated at 33 °C for at least 4 weeks to ensure that the samples had reached a thermodynamically stable state.

2.3.3 ^{2}H NMR Analysis

^{2}H NMR measurements were performed on a Bruker Avance II 400 WB spectrometer equipped with a 9.4 T magnet (^{2}H frequency = 61.4 MHz) using a Bruker static probe with a 5-mm coil. The spectra were acquired using a quadrupolar echo pulse sequence with a 90° pulse of 1.80 μs, an interpulse delay of 40 μs, and a recycle time of 50 s. Two thousand scans were collected for each ^{2}H NMR spectrum. The spectra were recorded as a function of increasing temperature, varying from 25 to 70 °C. The precision was evaluated to ±2 °C. T_1 (spin−lattice relaxation time) was determined for each sample using the inversion-recovery method.[24]

2.3.4 IR Analysis

IR analyses were carried out in a Thermo Nicolet 4700 spectrometer. An aliquot of hydrated lipid mixture was put on a CaF_2 window. Around 25 μL of citrate buffer was added to maintain complete hydration during the measurements. A second CaF_2 window, separated by a 5-μm-thick Teflon spacer from the first one, was deposited on the sample, and this assembly was inserted into a temperature-controlled brass sample holder. The spectra were recorded using 32 scans with a nominal spectral resolution of 1 cm^{-1}. The spectra were acquired as a function of increasing temperature, varying from 25 to 80 °C, with an equilibration period of 5 min for each temperature. The reported band positions correspond to the band maximum.

2.4 Results

Solid-state ^{2}H NMR was used to study the dynamics of the acyl chains of free fatty acids in the lipid membranes (Figure 2.1).

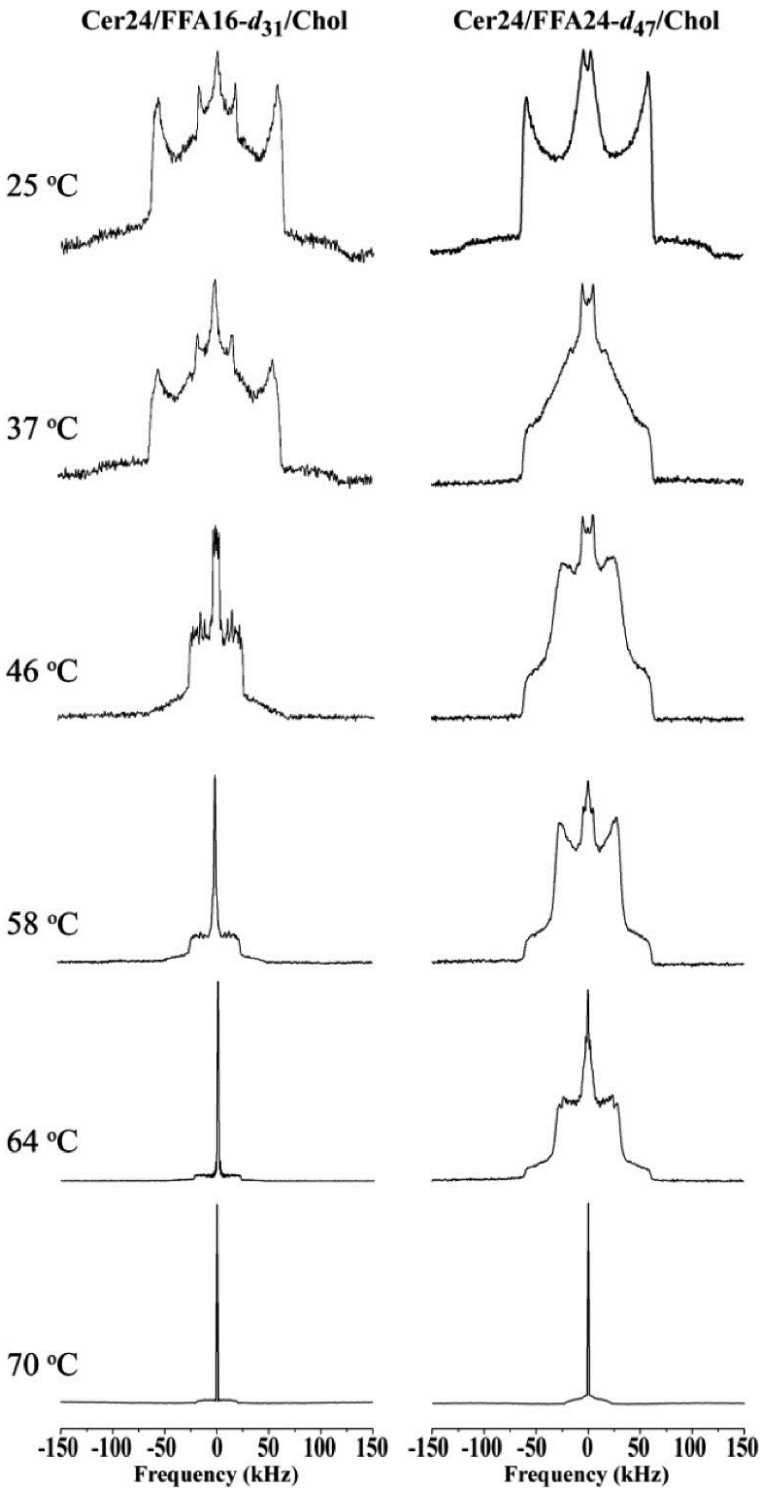

Figure 2.1. ^{2}H NMR spectra of Cer24/FFA16-d_{31}/Chol (left) and Cer24/FFA24-d_{47}/Chol (right) mixtures as a function of temperature.

At low temperature, the spectra of both samples exhibited powder patterns typical of solid-phase alkyl chains; the broad pattern with a quadrupolar splitting of ~120 kHz corresponds to the equivalent methylene groups (CD_2) along the all-*trans* chain that does not experience rotation (on the NMR time scale), and the narrow central contribution is assigned to the terminal methyl group (CD_3). It should be noted that the terminal methyl appeared to be more mobile in the Cer24/FFA24-d_{47}/Chol than in the Cer24/FFA16-d_{31}/Chol mixture as the measured quadrupolar splitting was 9 kHz for FFA24-d_{47} and 35 kHz for FFA16-d_{31}. Upon heating, the sample containing FFA16 showed a transition toward a liquid-ordered phase (l_o).[25,26] This phase is characterized by both (i) fast rotational motion along the lipid long axis (on the NMR time scale) giving rise to overlapped powder patterns typical of a system with axial symmetry and (ii) high orientational order of the lipid chains; the width of the outmost quadrupolar splitting was about 50 kHz. The spectrum recorded at 46 °C was typical of this phase. Upon further heating, a narrow central peak grew progressively, and this component represented 71% of the signal at 70 °C. Such a phase evolution for FFA (solid-to-l_o-to-isotropic phase transitions) was reported for FFA14 (myristic acid), FFA16, and FFA18 (stearic acid) mixed in equimolar proportions with BBCer III and cholesterol,[27,28] and for the Cer16/FFA16/Chol system.[12]

The mixture containing FFA24 exhibited different phase behavior. From the solid phase existing at low temperature, there was a phase transition toward a gel phase at ~30 °C. Between 30 and 60 °C, the spectrum showed an evolution that was consistent with almost all-*trans* chains that experienced increasing rotational diffusion. The width at the base of the spectra was 128 kHz, indicative of highly ordered chains undergoing rotation. However, the spectra at 37 and 46 °C did not show a pattern typical of axial symmetry, indicating that the

rotation along the long FFA axis was not in the fast NMR regime. This limited rotational diffusion was reminiscent of that observed from the spectrum of gel-phase DPPC-d_{62} bilayers.[29] At 58 °C, the spectrum of the Cer24/FFA24-d_{47}/Chol system was, if one excluded the central signal associated with the terminal methyl, reminiscent of a powder pattern with quadrupolar splitting between the two maxima of 62 kHz, *i.e.*, typical of an all-*trans* chain with fast rotation along its long axis. Therefore, upon heating, FFA24 remained highly ordered from a conformational point of view, and its rotational diffusion increased. The spectrum was dominated by an l_o-phase component when the temperature reached 64 °C. Subsequent heating led to the coexistence of a narrow line with the l_o-phase component; the area of the narrow signal corresponded to 58% at 70 °C. These spectra were very similar to those recently published.[18]

The variations of first moment (M1) of the ^{2}H NMR spectra recorded from the Cer24/FFA-*d*/Chol mixtures with temperature illustrated the overall changes in the spectral width, reflecting the phase changes experienced by the fatty acid in the lipid mixtures (Figure 2.2).

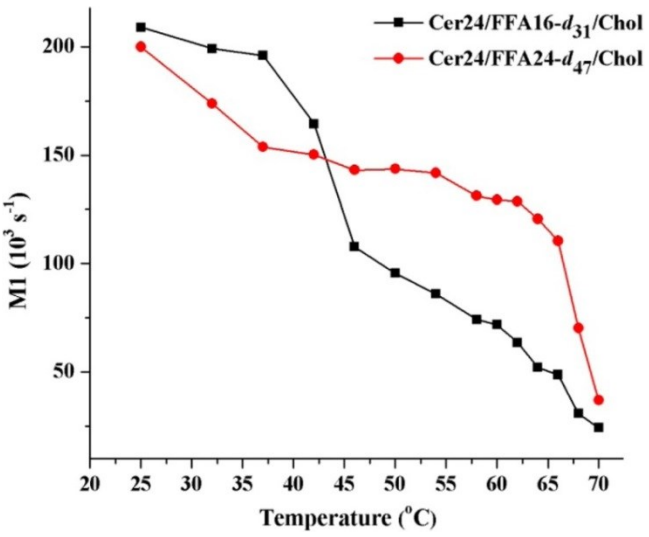

Figure 2.2. Variations of the first moment (M1) of the ^{2}H NMR spectra recorded from the Cer24/FFA-*d*/Chol mixtures as a function of temperature. The precision on these values was better than $\pm 4 \times 10^3$ s^{-1}.

The FFA16 in the Cer24/FFA16-d_{31}/Chol mixture was highly ordered (solid) up to 37 °C. It then underwent a transition from solid to the l_o phase, as illustrated by the drop in M1 values between 37 and 46 °C. From 46 °C, there was a more progressive decrease in M1 values, associated with the increase in the narrow line intensity. The Cer24/FFA24-d_{47}/Chol sample exhibited a distinct behavior. FFA24 was in a solid phase at 25 °C, corresponding to a high M1 value. A limited and rather monotonous reduction of M1 values was observed between 25 and 65 °C and was associated with increased rotational freedom without the introduction of significant conformational disorder. Subsequently, an abrupt decrease in M1 values observed at 68 °C could be associated with the transition toward the isotropic phase.

In order to determine whether the free fatty acids experienced different dynamics in the lamellar fluid phase, the ^{2}H NMR spectra of the fatty acids in the two lipid mixtures were

compared at 64 °C, a temperature for which both mixtures existed mainly in a fluid phase (Figure 2.3).

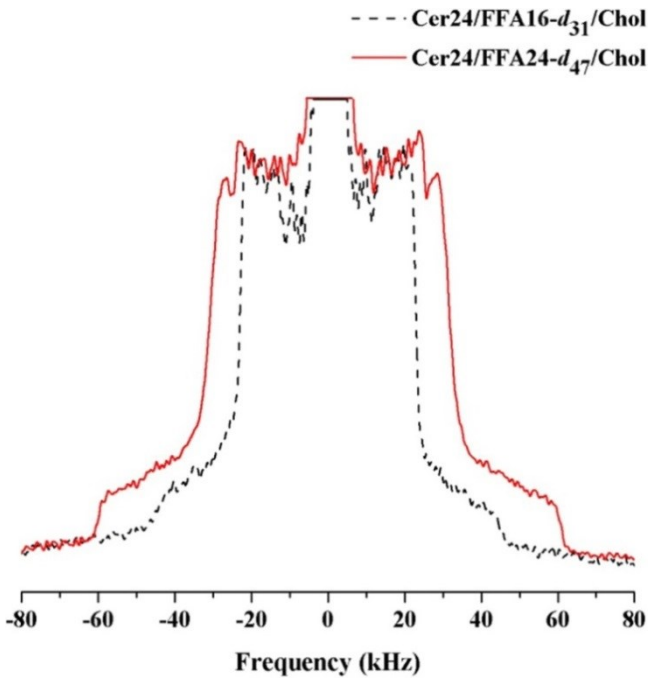

Figure 2.3. ^{2}H NMR spectra of Cer24/FFA-*d*/Chol mixtures at 64 °C.

Both spectra were typical of liquid-ordered phases. The widths at the base of the spectra were 90 and 120 kHz for the Cer24/FFA16-d_{31}/Chol and Cer24/FFA24-d_{47}/Chol systems, respectively. The very broad component in the Cer24/FFA24-d_{47}/Chol spectrum suggested that FFA24 had a very high orientational order. In fact, the spectrum appeared to be representative of two fluid phases because there were two resolved peaks that could be associated with the alkyl chain segment near the headgroup; the measured quadrupolar splittings (for the 90° orientation) were 55 kHz (related to the 120 kHz splitting, measured at the base, corresponding to a 0° orientation) and 47 kHz. The 90°-orientation quadrupolar splitting for the sample containing FFA16 was 42 kHz, a value similar to the one previously reported for FFA16/Chol.[25] It was concluded that the chain packing was tighter in

Cer24/FFA24-d_{47}/Chol than in Cer24/FFA16-d_{31}/Chol bilayers, with even possibly two distinct highly ordered fluid phases in the sample containing FFA24.

The spin-lattice nuclear relaxation time (T_1) was also determined for both samples at 25 °C. It was possible to distinguish the spin−lattice relaxation between the CD_2 and the CD_3 groups in the Cer24/FFA16-d_{31}/Chol samples (Supporting Information). T_1 values were estimated to be 5.8 and 0.96 s for the methylene groups and the terminal methyl, respectively. These values are comparable to those obtained for FFA16-d_{31} in BBCerIII/FFA16-d_{31}/Chol[28] and FFA16-d_{31}/Chol[25] systems at low temperatures. These long T_1 values are indicative of solid domains where limited motion prevents efficient spin−lattice relaxation. Conversely, the Cer24/FFA24-d_{47}/Chol sample exhibited a T_1 value of 0.44 s, indicating that this system followed a distinct relaxation process as discussed below.

The thermotropism of the Cer24/FFA16-d_{31}/Chol and Cer24/FFA24-d_{47}/Chol mixtures was also studied using infrared spectroscopy (Figure 2.4). This technique provided a simultaneous description of the behavior of both Cer and FFA in the mixtures because of the use of deuterated FFA. The methylene stretching mode is sensitive to the conformational order of hydrocarbon chains and can be used to probe phase transitions.[30,31] The evolution of the position of the methylene symmetric stretching band ($\nu_s CH_2$) described the changes in hydrogenated ceramide chains while the deuterated methylene symmetric stretching band ($\nu_s CD_2$) was associated with FFA chain order.

Figure 2.4 reports the changes in these two parameters as a function of temperature for the SC models. The derived thermal profiles are similar to those previously reported on equivalent mixtures.[16]

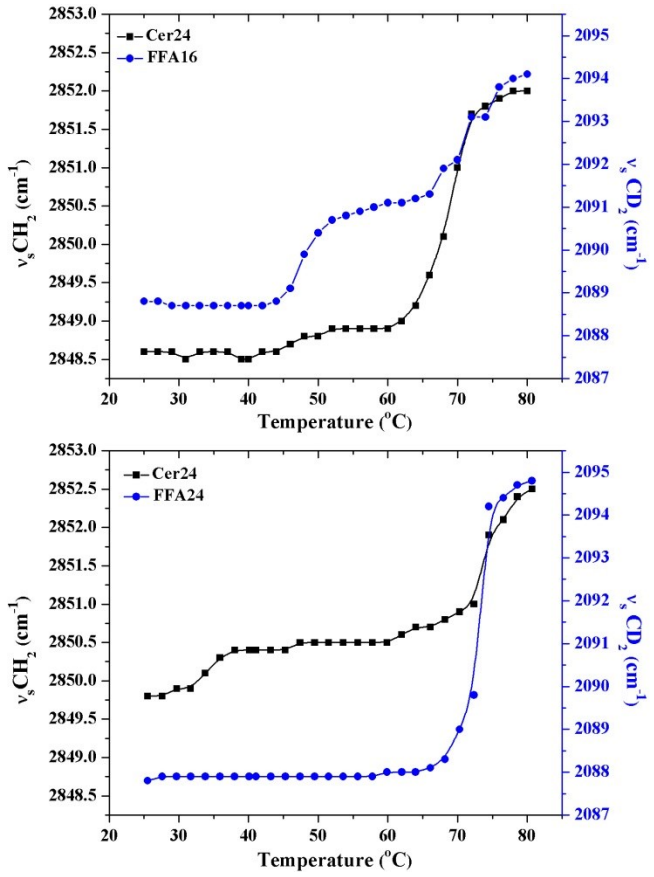

Figure 2.4. Thermotropic behavior of Cer24/FFA16-d_{31}/Chol and Cer24/FFA24-d_{47}/Chol mixtures as probed by the νCHs (■) for Cer24 and νCDs (blue ●) for deuterated FFA. The precision of these values was better than ±0.5 cm^{-1}.

In the Cer24/FFA16-d_{31}/Chol mixture, the $\nu_s CD_2$ band position at 2088.5 cm^{-1} showed that, below 45 °C, FFA16 was highly ordered, in a solid phase, in agreement with the ^2H NMR results. Upon further heating, the band progressively shifted toward high wavenumbers, reaching 2094 cm^{-1} at 80 °C. This behavior was associated with the disordering of FFA chains during the transition toward an l_o phase and then to an isotropic phase. This thermal profile is similar to that obtained for the BBCerIII/FFA16-d_{31}/Chol mixture.[32]

The ceramide acyl chains were highly ordered in an all-*trans* conformation under 60 °C, as indicated by the $\upsilon_s CH_2$ band wavenumber of <2850 cm^{-1}.[30,33] Further heating caused an abrupt increase in its position by ~3 cm^{-1}. This behavior could be related to the phase transformation toward the isotropic phase, causing significant disorder in the acyl chains.

The thermal behavior of the lipid species, as inferred from the IR spectroscopy, in the Cer24/FFA24-d_{47}/Chol mixture was different. The position of the $\nu_s CD_2$ band was fairly constant, at 2088 cm^{-1}, between 25 and 65 °C. The ^2H NMR analysis indicated that FFA24 experienced transitions from solid-to-gel-to-l_o phases over this temperature range. It appears that these phases were difficult to distinguish using this IR feature, likely because of their shared high conformational order. Subsequent heating to 70 °C led to an abrupt increase by more than 7 cm^{-1} in the $\nu_s CD_2$-mode wavenumber. This increase was related to the transition toward the highly disordered isotropic phase seen by ^2H NMR spectroscopy. The ceramide behavior, as inferred by IR spectroscopy, was characterized by a very ordered phase below 30 °C with a $\nu_s CH_2$ band position below 2850 cm^{-1}. A small shift in $\nu_s CH_2$ band position was observed between 30 and 35 °C. This temperature range corresponds to that where FFA24 was found to undergo a transition to a gel phase by ^2H NMR. In addition, the study of Stahlberg *et al*.,[18] where they used deuterated Cer24, revealed that ceramide would be involved in the solid-to-gel phase transition. Therefore, the shift of the $\nu_s CH_2$ band position was likely attributed to this phase change. It was shown that the $\nu_s CH_2$ mode was more sensitive to intermolecular coupling and librotorsional mobility than the $\nu_s CD_2$ mode.[34] These two contributions are likely considerably affected during the solid-to-gel phase, and the different sensitivity of the symmetric methylene stretching mode to these phenomena may explain why this transition was detected by the $\nu_s CH_2$ mode but not by the $\nu_s CD_2$ mode. There was a small

and progressive shift of the $\nu_s CH_2$ mode upon heating, and at 70 °C, an abrupt upshift was observed, corresponding to the formation of the isotropic phase.

Figure 2.5 shows the CD_2 deformation (δCD_2) region for the investigated ternary mixtures (Cer24/FFA16-d_{31}/Chol and Cer24/FFA24-d_{47}/Chol).

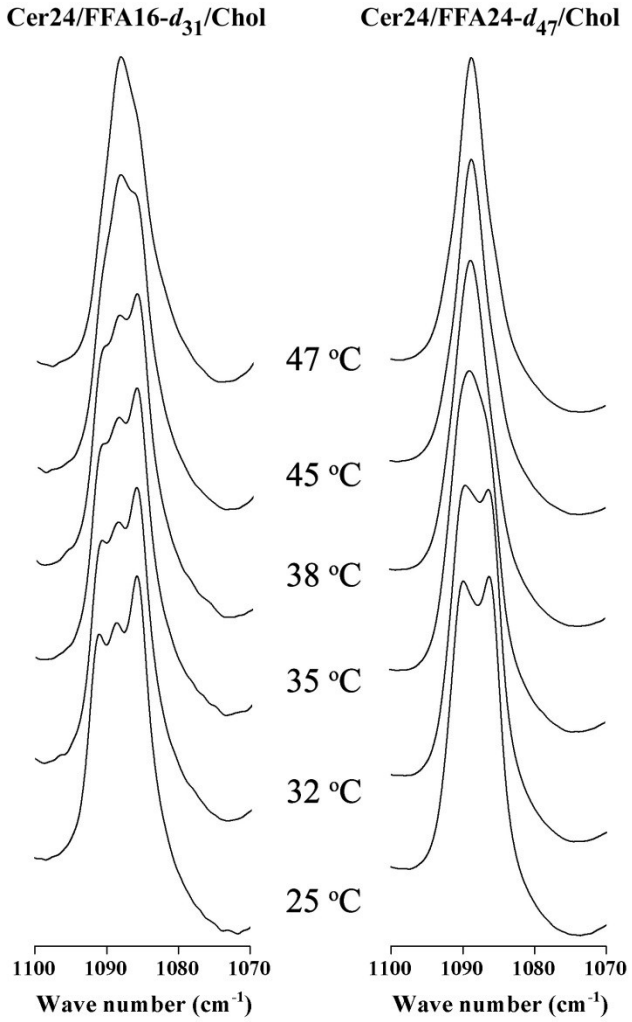

Figure 2.5. δCD_2 bands of Cer24/FFA16-d_{31}/Chol (left) and Cer24/ FFA24-d_{47}/Chol (right) mixtures as a function of temperature.

This region is a valuable probe for describing the symmetry of chain packing in the solid phase. A splitting of this mode is indicative of interchain vibrational coupling between

chains in an orthorhombic packing.[23,35,36] In addition, this coupling occurs only if the methylene deformation modes of adjacent chains have approximately the same frequency; therefore, the presence of a splitting can be related to the presence of phase-separated domains because deuterated FFA was used. The extent of the splitting is sensitive to the size of the domains;[35] a larger band splitting corresponds to larger and/or more phase-separated domains, up to a limiting value corresponding to pure domains including about 100 molecules.

Both investigated mixtures displayed a splitting of the δCD_2 band at low temperatures, indicating the existence of phase-separated domains of FFAs in a crystalline form with orthorhombic chain packing. In the sample with FFA16-d_{31}, three components were observed at 1085.8, 1088.5, and 1091.0 cm^{-1}, while in the mixture containing FFA24-d_{47} two components were found at 1086.3 and 1089.1 cm^{-1}. These profiles are similar to those previously obtained for equivalent mixtures.[16,31] The δCD_2 band splitting observed for the Cer24/FFA24-d_{47}/Chol mixture was smaller than that of the Cer24/FFA16-d_{31}/Chol system; this finding showed that the FFA domains were smaller and/or FFA domains displayed a limited FFA enrichment in the Cer24/FFA24-d_{47}/Chol model compared to in the Cer24/FFA16-d_{31}/Chol system.

The thermal evolution of the δCD_2 band splitting was also different for the two mixtures; the variations of the bandwidth as a function of temperature are reproduced in Figure 2.6.

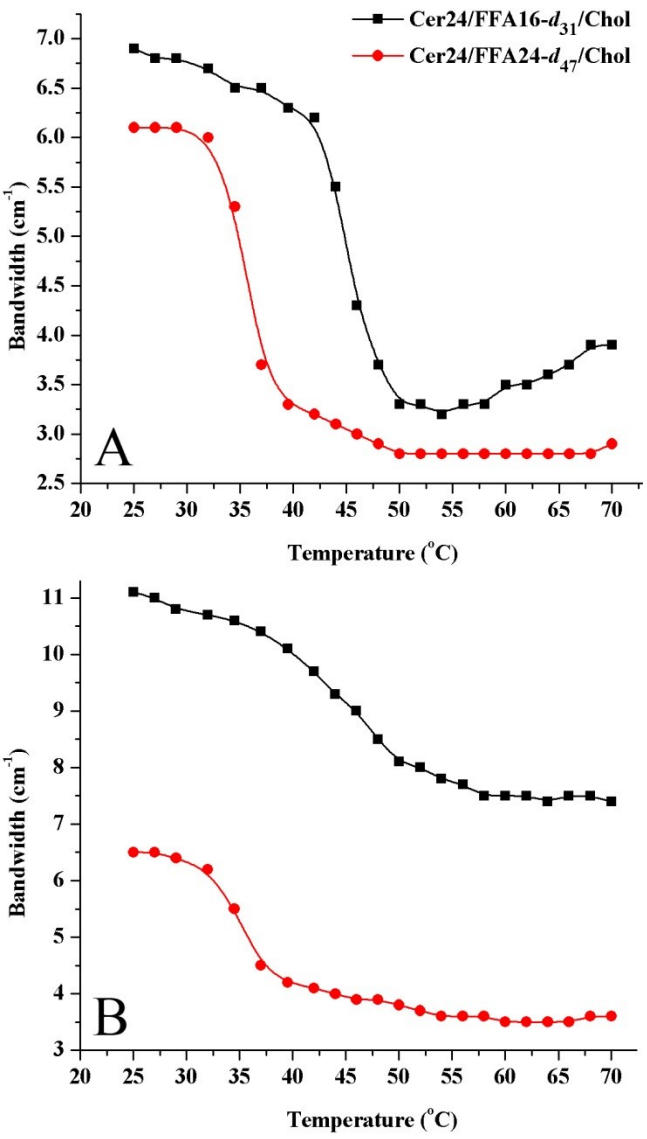

Figure 2.6. Variations of the width of the δCD_2 mode (A) and the δCH_2 mode (B), measured at 75 and 80% of the peak intensity, respectively. The precision of these values was better than ±0.2 cm^{-1}.

The δCD_2 splitting remained visible and roughly constant up to 47 °C for the Cer24/FFA16-d_{31}/Chol mixture, even though there was an increase in the central component intensity upon heating. This observation is consistent with the presence of the solid phase up to around 45 °C as inferred from the ^{2}H NMR analysis. The phase separation was replaced by

subsequent lipid mixing to form an l_o phase. In this mixture, FFA16 underwent a transformation from the solid to a more disordered phase at 45 °C while Cer24 showed only a main transition at 60 °C, toward a more disordered phase.

In the case of the Cer24/FFA24-d_{47}/Chol mixture, the δCD_2 splitting disappeared at a lower temperature, at ∼34 °C. The collapse of the splitting is consistent with the solid-gel phase transition determined from ^2H NMR spectroscopy. The splittings in the δCH_2 band at 1468 cm^{-1} were not as well resolved as for the deuterated analogue mode (Supporting Information). They convey information similar to that of splitting associated with orthorhombic chain packing in hydrogenated-species domains. The monitoring of the δCH_2 bandwidth can provide information about the evolution of the orthorhombic solid phase (Figure 2.6B). Two observations can be highlighted from this graph. First, at low temperature, the sample containing FFA16 exhibited a higher bandwidth than that with FFA24, suggesting the formation by ceramide of crystalline domains with orthorhombic chain packing that are larger and/or are more depleted of deuterated FFA than those formed with FFA24. Second, the collapse of the δCH_2 band splitting was observed at a higher temperature for the Cer24/ FFA16-d_{31}/Chol system than for the Cer24/FFA24-d_{47}/Chol mixture; the temperature at which half the bandwidth reduction was observed was 46 °C for the SC model mixture containing FFA16 and 35 °C for that with FFA24.

2.5 Discussion

The aim of this work was to detail the influence of the free fatty acid chain length on the phase behavior of model SC lipid mixtures that include Cer24, one of the most abundant nonhydroxy ceramides in SC. We believe that the ^2H NMR and FT-IR analyses allowed us to

highlight three features regarding the Cer24/FFA24-d_{47}/Chol system. First, its components display a greater miscibility than that observed for analogous mixtures. Second, the FFA24 solid phase, which is observed in the mixture at low temperature, gains motional freedom (essentially rotational) at a temperature lower than expected for such a long-chain FFA. Third, the Cer24/FFA24-d_{47}/Chol system forms a gel phase, a behavior that is unusual for SC model mixtures.

The Cer24/FFA24-d_{47}/Chol system displays a greater miscibility than analogous SC mixtures. In the present work, the analysis of δCD_2 and δCH_2 vibrations (Figures 2.5 and 2.6) shows a band splitting that indicates the formation of phase-separated domains of Cer24 and FFA24 with orthorhombic lateral packing. This orthorhombic lattice has already been reported for human SC[37,38] as well as for several SC lipid model mixtures. A striking difference between the mixtures with FFA16 and FFA24 is the magnitude of the vibrational splitting associated with the interchain coupling. The splittings of δCD_2 and δCH_2 bands showed that the mixture containing FFA24 forms smaller and/or more mixed crystalline domains. Other results obtained for similar SC mixtures corroborate this finding. Oguri *et al.*[16] showed that model mixtures formed from Cer24/FFAs/Chol (containing 47.8% FFA22 and 38.8% FFA24) exhibited smaller δCD_2 and δCH_2 band splittings (5.3 and 7.4 cm^{-1}, respectively) than those measured on the spectra of a mixture where the FFA mixture was substituted by FFA16-d_{31} (7.1 cm^{-1} for δCD_2 and 9.1 cm^{-1} for δCH_2). As reference values (measured the same way as the values presented in Figure 2.6), the splitting of pure Cer20 was found to be 9.8 cm^{-1},[41] whereas that of deuterated solid FFA was 8.5 cm^{-1}.[16] Therefore, the Cer24/FFA16-d_{31}/Chol mixture appears to be forming extensive phase-separated domains, according to its δCD_2 and δCH_2 splitting values. These values are similar to those previously reported for an equimolar

mixture of Cer16/FFA16-d_{31}/Chol,[14] where δCD_2 and δCH_2 band splittings were found to be 6 and 9.5 cm^{-1}, respectively, indicating that Cer16 and FFA16 formed phase-separated crystalline domains with orthorhombic chain packing. The mixture containing BBCer III, FFA16-d_{31}, and cholesterol[32] exhibited a splitting of the δCD_2 band of 6.7 cm^{-1} and of the δCH_2 band of 9.1 cm^{-1}, showing also an extensive phase separation. Interestingly, a binary equimolar mixture of FFA16-d_{31}/Chol, pH 6.1, showed a δCD_2 splitting of 7.3 cm^{-1}, indicating that cholesterol was practically excluded from the FFA16-d_{31} domains when the acid was protonated.[40] These comparisons establish that the Cer24/FFA24-d_{47}/Chol system displays a crystalline-phase separation that is not as extensive as those previously reported for analogous systems.

A greater miscibility of the components at low temperatures in Cer24/FFA24-d_{47}/Chol systems has also been reported by Raman spectroscopy.[16] It was shown that, after hydration, the phase separation was clearly enhanced for the sample containing FFA16 in comparison with the Cer24/FFA24-d_{47}/Chol sample. Skolova *et al*.[17] also found similar behavior when using a mixture of FFAs (C16-C24) in a Cer24/FFAs/Chol/CholS system. In this mixture, the high content of very-long-chain FFA22 (47.8%) and FFA24 (38.8%) seemed to favor the lipid miscibility analogously to the sample containing only FFA24.

The FFA24 solid phase that was observed at low temperature in the Cer24/FFA24-d_{47}/Chol system displayed more motional freedom (essentially rotational) than expected for such a long-chain FFA. This finding was supported by the T_1 values obtained for the mixtures that included deuterated FFA. T_1 obtained for Cer24/FFA16-d_{31}/Chol was typical of FFA solid domains, *i.e.*, with no or little motion.[25,28] The shorter T_1 obtained for the Cer24/FFA24-d_{47}/Chol mixture indicates the existence of relaxation mechanisms that are not generally

observed in other solid SC lipid models. In addition, the CD_3 signal showed considerable mobility of the end of the FFA chain. Therefore, these features observed in the Cer24/FFA24-d_{47}/Chol mixture suggest a molecular organization allowing unusual motional freedom.

The increased rotational diffusion inferred from the ^2H NMR spectra led to the formation a gel phase, a behavior that is unusual for SC model mixtures. The series of spectra of Cer24/FFA24-d_{47}/Chol recorded between 37 and 58 °C (Figure 2.2) showed that the FFA chain remained in an all-*trans* conformation (as assessed by the width of the signal) and acquired rotational mobility along the lipid long axis upon heating. The spectrum recorded at 46 °C was similar to that of pure DPPC-d_{62} at 25 °C whereas that at 58 °C resembled that of DPPC-d_{62} in the presence of lysopalmitoyl PC (PaLPC) (in a 3:l molar ratio) reported in a previous study.[29] In that study, these spectra could be nicely reproduced using as a model all-*trans* acyl chains undergoing axial rotation at 2.8×10^6 rad/s (440 kHz) for DPPC-d_{62} and at 6.8×10^8 rad/s (108 MHz) for DPPC with PaLPC. At 58 °C, the spectrum of the Cer24/ FFA24/Chol system appeared to be characteristic of the fast NMR regime. Therefore, FFA24 underwent a progressive solid-to-gel-to-l_o phase transition above 37 °C where temperature mainly affected the rotational diffusion and had a very limited effect on the conformational/orientational order of FFA24; this was shown by practically no change in the $\nu_s CD_2$ band position (Figure 2.4) and the relatively high M1 (Figure 2.2). Actually, the recent work by Stahlberg *et al.*[18] reported very similar behavior. In addition, using deuterated ceramides, they showed that the thermal evolution of ceramide was similar to that of FFA24. This behavior contrasts with most of those previously reported for SC model mixtures. The influence of FFAs with different chain lengths (ranging from C14 to C22) on the solid-phase formation in mixtures containing BBCer III, FFA, and cholesterol has also been

investigated.[27,32] It was shown that all of these BBCer III/FFA/Chol mixtures exhibited a coexistence of two crystalline phases at low temperature, one enriched in FFA and another enriched in BBCer III. Heating caused a solid-to-l_o phase transition in all of these investigated mixtures, regardless of the FFA chain length. It was observed that the mixing between FFA and cholesterol in the l_o phase decreases with increasing FFA chain length (>C20), an observation associated with their hydrophobic mismatch.[27] For the mixtures containing long-chain FFA, the solid-to-l_o phase transition was observed at higher temperature and involved a large fraction of BBCer III, but it must be pointed out that it was always a solid-to-l_o phase transition. Therefore, the behavior of the Cer24/FFA24-d_{47}/Chol system appears to be rather unusual.

The presence of Cer24 does not seem to be responsible for this phase behavior as Cer24 mixed with FFA16 and cholesterol displayed a thermotropism similar to that of the Cer16/FFA24/Chol system. In that mixture, Cer16 showed an extensive phase separation and solid phase at physiological temperature.[17] The distinct phase behavior of the Cer24/FFA24/Chol mixture also cannot be associated with FFA24 because the Cer16/FFA24/ Chol system displayed the common solid-to-l_o phase transition.[18] Therefore, it is concluded that the synergistic effect of both Cer24 and FFA24 is responsible for the distinctive phase behavior of Cer24/FFA24-d_{47}/Chol.

The origin of the phase behavior of the Cer24/FFA24-d_{47}/Chol system has been associated with the optimized hydrophobic match between FFA24 with Cer24.[17] However, it should be pointed out that the Cer16/FFA16/Chol mixture, which also provided hydrophobic matching, even at a superior level as Cer and FFA also matched the cholesterol hydrophobic length, led to extensive phase-separated domains at low temperatures, and did not exhibit a

gel-phase transition but a solid-to-l_o phase transition. The improved lipid miscibility at low temperature and the gel-phase formation may be related to a change in the thermodynamics and/or a change in the kinetics of solidification. First, the long chain length of FFA24 and Cer24 leads to strong van der Waals interchain interactions that are relatively more significant compared to interheadgroup interactions than those for shorter-chain systems. This contribution would, from a thermodynamic point of view, promote lipid mixing and could lead to the formation of mixed solid phases. The coexistence of different molecules in the mixed solid phase may promote gel-phase formation and the observed lowering of the transition temperature. In addition, the Cer24 sphingoid base includes a C18 acyl chain that provides an asymmetric hydrophobic moiety. This shorter chain could match more closely with cholesterol. The details of the molecular organization compensating for the hydrophobic mismatch are still unknown. Skolova *et al*.[17] recently presented a model in which Cer24 adopts an extended conformation, with its chains inserted in different bilayers. In this model, the long-chain free fatty acid could be associated with the very long ceramide chain (C24) while cholesterol is associated with the sphingoid chain, which promotes the mixture of the three components. Alternatively, Mojumdar *et al*.[42] proposed that the chain-length mismatch in mixtures of ceramides, FFA24, and cholesterol led to a partial interdigitation of FFA24 and ceramide acyl chains, with Cer24 being in a hairpin configuration. At this point, it is not possible to assess what lipid organization would lead to increased motions and would favor the propensity to form a gel phase, as observed here for the Cer24/FFA24-d_{47}/Chol system.

Second, the limited phase separation observed in the Cer24/FFA24-d_{47}/Chol mixture and the related gel-phase formation may be associated with kinetics effects. The lipid model systems were hydrated from randomly distributed lipid solids (obtained by freeze-drying from

organic solution). Therefore, the phase-separation process takes place upon hydration. This association is supported by recent work that recorded the broadening of the δCD_2 and δCH_2 bands during the hydration of Cer24/FFAs/Chol mixtures.[16] The domain formation is directly related to the diffusion of the molecules, and it is possible that, due to the long acyl chains, the lipids have restricted mobility that limits the growth rate of the solid domains and consequently their size. The dynamics of SC lipid-phase separations has not been extensively studied, and the exact mechanism is still not identified. It has been shown that the phase-separation kinetics in SC model lipid systems is temperature-dependent[32] and has been proposed to proceed via a spinodal decomposition.[43] The lipid diffusion in the matrix is likely associated with the available free volume. In a mechanism similar to that proposed for long-chain alkanes in solid matrices,[35] the diffusion could be suggested to be intermediate between simple exchange, observed for small molecules, and reptation, observed for polymers. Actually, for these alkanes in solid matrices it has been shown that the rate of demixing decreased as a function of increasing alkane chain length. Moreover, the normalized splittings of δCD_2 and δCH_2 bands in the IR spectra were smaller for the mixtures with longer-chain alkanes ($C_{30}H_{62}$ mixed with $C_{36}D_{74}$) than for mixtures with shorter-chain alkanes ($C_{28}H_{58}$ mixed with $C_{36}D_{74}$), indicating a more limited phase separation. In that work, an activation energy associated with the demixing process was estimated to be 2.0 kcal/mol of methylene groups. Therefore, the limited diffusion of the species with long alkyl chains could also be at the origin of the distinct phase behavior of the Cer24/FFA24-d_{47}/Chol mixture that displays a more homogeneous lipid distribution in the solid phase and a likely related formation of the gel phase.

The studies investigating the phase behavior of SC model systems, including the present work, indicate that the lipid chain length composition for both Cer and FFAs is a critical parameter in the phase behavior and mixing properties of model SC lipid membranes. In particular, the Cer24/FFA24/Chol SC model mixture, involving the most abundant species from a chain-length point of view, appears to behave in a distinct manner, exhibiting enhanced lipid mixing in the solid phase and forming a gel phase where the chains remain highly ordered and respond to heating by progressively increasing their rotational mobility. Until now, little consideration has been devoted to gel phases in SC systems; it should be attentively taken into account to determine whether it has relevance from physiological and functional points of view. For example, the reduction of the FFA and ceramide chain lengths is reported in lesional and nonlesional atopic eczema and atopic dermatitis patients.[44] These patients exhibit a considerable reduction in the SC content of very-long-chain FFAs with 24 or more carbon atoms while its content of shorter-chain FFAs (C16 and C18) is increased. Meanwhile, a reduction in ceramide subclasses containing very long chains is reported along with an increase in the Cer16 content. Patients with atopic eczema and atopic dermatitis exhibit skin barrier dysfunction, including increased trans-epidermal water loss.[45,46] Coupling the reduction in lipid chain length with altered phase behavior such as less homogeneous lipid mixing would constitute a major step forward in our understanding of the skin barrier.

2.6 Supporting Information

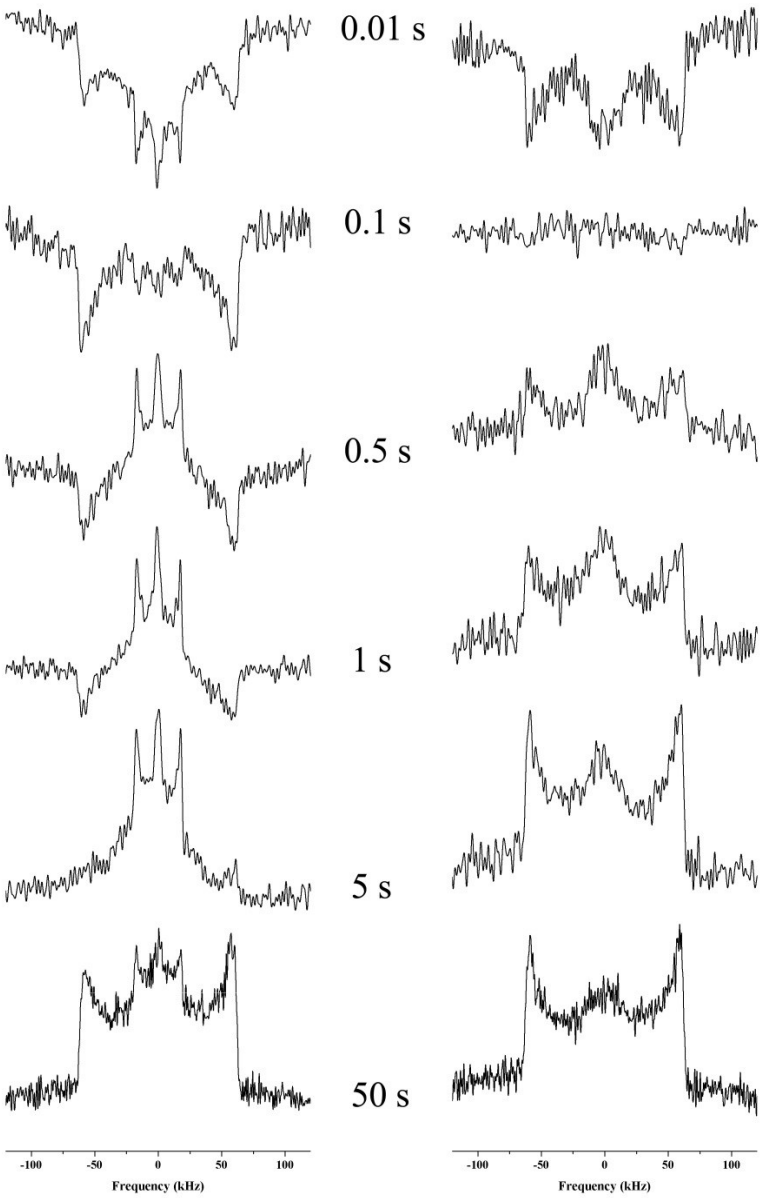

Figure 2.S1. Determination of spin-lattice relaxation time (T_1) using the inversion-recovery method. Cer24/FFA16-d_{31}/Chol (left) and Cer24/FFA24-d_{47}/Chol (right).

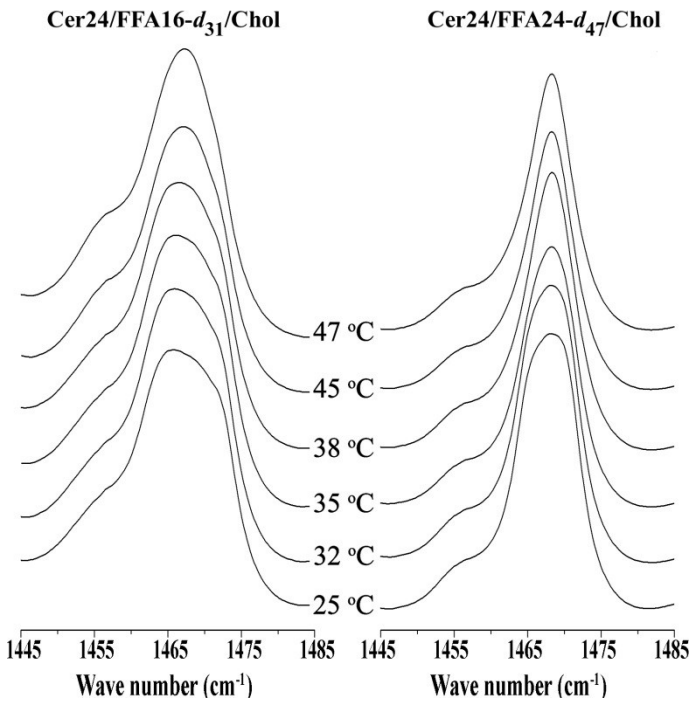

Figure 2.S2. δCH_2 bands of Cer24/FFA16-d_{31}/Chol (left) and Cer24/FFA24-d_{47}/Chol (right) mixtures as a function of temperature.

2.7 Acknowledgments

We thank the Natural Sciences and Engineering Research Council (NSERC) of Canada for financial support. A.P.R. thanks the Fonds de Recherche du Quebeć-Nature et Technologies (FRQNT) for his doctoral research scholarship for foreign students. This work was also funded by the FQRNT through its financial support of the Center for Self-Assembled Chemical Structures (CSACS).

2.8 References

(1) Feingold, K. R.; Elias, P. M. Role of lipids in the formation and maintenance of the cutaneous permeability barrier. *Biochim. Biophys. Acta* **2014**, *1841*, 280-294.

(2) Harding, C. R. The stratum corneum: structure and function in health and disease. *Dermatol. Ther.* **2004**, *17*, 6-15.

(3) Johnson, M. E.; Blankschtein, D.; Langer, R. Evaluation of solute permeation through the stratum corneum: Lateral bilayer diffusion as the primary transport mechanism. *J. Pharm. Sci.* **1997**, *86*, 1162-1172.

(4) Talreja, P. S.; Kasting, G. B.; Kleene, N. K.; Pickens, W. L.; Wang, T.-F. Visualization of the lipid barrier and measurement of lipid pathlength in human stratum corneum. *AAPS PharmSci.* **2001**, *3*, 48-56.

(5) Boncheva, M. The physical chemistry of the stratum corneum lipids. *Int. J. Cosmetic Sci.* **2014**, *36*, 505-515.

(6) Kwak, S.; Brief, E.; Langlais, D.; Kitson, N.; Lafleur, M.; Thewalt, J. Ethanol perturbs lipid organization in models of stratum corneum membranes: An investigation combining differential scanning calorimetry, infrared and 2H NMR spectroscopy. *Biochim. Biophys. Acta* **2012**, *1818*, 1410-1419.

(7) Forslind, B. O. A domain mosaic model of the skin barrier. *Acta Derm-Venereol.* **1994**, *74*, 1-6.

(8) Masukawa, Y.; Narita, H.; Shimizu, E.; Kondo, N.; Sugai, Y.; Oba, T.; Homma, R.; Ishikawa, J.; Takagi, Y.; Kitahara, T., *et al*. Characterization of overall ceramide species in human stratum corneum. *J. Lipid Res.* **2008**, *49*, 1466-1476.

(9) t'Kindt, R.; Jorge, L.; Dumont, E.; Couturon, P.; David, F.; Sandra, P.; Sandra, K. Profiling and Characterizing Skin Ceramides Using Reversed-Phase Liquid Chromatography–Quadrupole Time-of-Flight Mass Spectrometry. *Anal. Chem.* **2012**, *84*, 403-411.

(10) Bouwstra, J. A.; Gooris, G. S.; Cheng, K.; Weerheim, A.; Bras, W.; Ponec, M. Phase behavior of isolated skin lipids. *J. Lipid Res.* **1996**, *37*, 999-1011.

(11) de Sousa Neto, D.; Gooris, G.; Bouwstra, J. Effect of the ω-acylceramides on the lipid organization of stratum corneum model membranes evaluated by X-ray diffraction and FTIR studies (Part I). *Chem. Phys. Lipids* **2011**, *164*, 184-195.

(12) Brief, E.; Kwak, S.; Cheng, J. T. J.; Kitson, N.; Thewalt, J.; Lafleur, M. Phase Behavior of an Equimolar Mixture of N-Palmitoyl-D-*erythro*-sphingosine, Cholesterol, and Palmitic Acid, a Mixture with Optimized Hydrophobic Matching. *Langmuir* **2009**, *25*, 7523-7532.

(13) Souza, S. L.; Valério, J.; Funari, S. S.; Melo, E. The thermotropism and prototropism of ternary mixtures of ceramide C16, cholesterol and palmitic acid. An exploratory study. *Chem. Phys. Lipids* **2011**, *164*, 643-653.

(14) Kwak, S.; Lafleur, M. Effect of dimethyl sulfoxide on the phase behavior of model stratum corneum lipid mixtures. *Chem. Phys. Lipids* **2009**, *161*, 11-21.

(15) Velkova, V.; Lafleur, M. Influence of the lipid composition on the organization of skin lipid model mixtures: An infrared spectroscopy investigation. *Chem. Phys. Lipids* **2002**, *117*, 63-74.

(16) Oguri, M.; Gooris, G. S.; Bito, K.; Bouwstra, J. A. The effect of the chain length distribution of free fatty acids on the mixing properties of stratum corneum model membranes. *Biochim. Biophys. Acta* **2014**, *1838*, 1851-1861.

(17) Školová, B.; Hudská, K.; Pullmannová, P.; Kováčik, A.; Palát, K.; Roh, J.; Fleddermann, J.; Estrela-Lopis, I.; Vávrová, K. Different Phase Behavior and Packing of Ceramides with Long (C16) and Very Long (C24) Acyls in Model Membranes: Infrared Spectroscopy Using Deuterated Lipids. *J. Phys. Chem. B* **2014**, *118*, 10460-10470.

(18) Stahlberg, S.; Školová, B.; Madhu, P. K.; Vogel, A.; Vávrová, K.; Huster, D. Probing the Role of the Ceramide Acyl Chain Length and Sphingosine Unsaturation in Model Skin Barrier Lipid Mixtures by 2H Solid-State NMR Spectroscopy. *Langmuir* **2015**, *31*, 4906-4915.

(19) Rowat, A. C.; Kitson, N.; Thewalt, J. L. Interactions of oleic acid and model stratum corneum membranes as seen by 2H NMR. *Int. J. Pharm.* **2006**, *307*, 225-231.

(20) Fenske, D. B.; Thewalt, J. L.; Bloom, M.; Kitson, N. Models of stratum corneum intercellular membranes: 2H NMR of macroscopically oriented multilayers. *Biophys. J.* **1994**, *67*, 1562-1573.

(21) Garidel, P.; Fölting, B.; Schaller, I.; Kerth, A. The microstructure of the stratum corneum lipid barrier: Mid-infrared spectroscopic studies of hydrated ceramide:palmitic acid:cholesterol model systems. *Biophys. Chem.* **2010**, *150*, 144-156.

(22) Gorcea, M.; Hadgraft, J.; Moore, D. J.; Lane, M. E. Fourier transform infrared spectroscopy studies of lipid domain formation in normal and ceramide deficient stratum corneum lipid models. *Int. J. Pharm.* **2012**, *435*, 63-68.

(23) Moore, D. J.; Rerek, M. E.; Mendelsohn, R. Lipid Domains and Orthorhombic Phases in Model Stratum Corneum: Evidence from Fourier Transform Infrared Spectroscopy Studies. *Biochem. Biophys. Res. Commun.* **1997**, *231*, 797-801.

(24) Kingsley, P. B. Methods of measuring spin-lattice (T1) relaxation times: An annotated bibliography. *Concept Magnetic Res.* **1999**, *11*, 243-276.

(25) Paré, C.; Lafleur, M. Formation of liquid ordered lamellar phases in the palmitic acid/cholesterol system. *Langmuir* **2001**, *17*, 5587-5594.

(26) Vist, M. R.; Davis, J. H. Phase equilibria of cholesterol/dipalmitoylphosphatidylcholine mixtures: deuterium nuclear magnetic resonance and differential scanning calorimetry. *Biochemistry* **1990**, *29*, 451-464.

(27) Chen, X.; Kwak, S.; Lafleur, M.; Bloom, M.; Kitson, N.; Thewalt, J. Fatty Acids Influence “Solid” Phase Formation in Models of Stratum Corneum Intercellular Membranes. *Langmuir* **2007**, *23*, 5548-5556.

(28) Kitson, N.; Thewalt, J.; Lafleur, M.; Bloom, M. A Model Membrane Approach to the Epidermal Permeability Barrier. *Biochemistry* **1994**, *33*, 6707-6715.

(29) Jansson, M.; Thurmond, R. L.; Barry, J. A.; Brown, M. F. Deuterium NMR study of intermolecular interactions in lamellar phases containing palmitoyllysophosphatidylcholine. *J. Phys. Chem.* **1992**, *96*, 9532-9544.

(30) Mendelsohn, R.; Moore, D. J. Vibrational spectroscopic studies of lipid domains in biomembranes and model systems. *Chem. Phys. Lipids* **1998**, *96*, 141-157.

(31) Gooris, G. S.; Bouwstra, J. A. Infrared Spectroscopic Study of Stratum Corneum Model Membranes Prepared from Human Ceramides, Cholesterol, and Fatty Acids. *Biophys. J.* **2007**, *92*, 2785-2795.

(32) Lafleur, M. Phase behaviour of model stratum corneum lipid mixtures: an infrared spectroscopy investigation. *Can. J. Chem.* **1998**, *76*, 1501-1511.

(33) Mendelsohn, R.; Flach, C. R.; Moore, D. J. Determination of molecular conformation and permeation in skin via IR spectroscopy, microscopy, and imaging. *Biochim. Biophys. Acta* **2006**, *1758*, 923-933.

(34) Kodati, V. R.; El-Jastimi, R.; Lafleur, M. Contribution of the Intermolecular Coupling and Librotorsional Mobility in the Methylene Stretching Modes in the Infrared Spectra of Acyl Chains. *J. Phys. Chem.* **1994**, *98*, 12191-12197.

(35) Snyder, R. G.; Goh, M. C.; Srivatsavoy, V. J. P.; Strauss, H. L.; Dorset, D. L. Measurement of the growth kinetics of microdomains in binary n-alkane solid solutions by infrared spectroscopy. *J. Phys. Chem.* **1992**, *96*, 10008-10019.

(36) Moore, D. J.; Snyder, R. G.; Rerek, M. E.; Mendelsohn, R. Kinetics of Membrane Raft Formation: Fatty Acid Domains in Stratum Corneum Lipid Models. *J. Phys. Chem. B* **2006**, *110*, 2378-2386.

(37) Bouwstra, J. A.; Gooris, G. S.; Vries, M. A. S.-d.; van der Spek, J. A.; Bras, W. Structure of human stratum corneum as a function of temperature and hydration: A wide-angle X-ray diffraction study. *Int. J. Pharm.* **1992**, *84*, 205-216.

(38) Janssens, M.; Mulder, A. A.; van Smeden, J.; Pilgram, G. S. K.; Wolterbeek, R.; Lavrijsen, A. P. M.; Koning, R. I.; Koster, A. J.; Bouwstra, J. A. Electron diffraction study of lipids in non-lesional stratum corneum of atopic eczema patients. *Biochim. Biophys. Acta* **2013**, *1828*, 1814-1821.

(39) Basse, L. H.; Groen, D.; Bouwstra, J. A. Permeability and lipid organization of a novel psoriasis stratum corneum substitute. *Int. J. Pharm.* **2013**, *457*, 275-282.

(40) Ouimet, J.; Croft, S.; Paré, C.; Katsaras, J.; Lafleur, M. Modulation of the polymorphism of the palmitic acid/cholesterol system by the pH. *Langmuir* **2003**, *19*, 1089-1097.

(41) Chen, H.-C.; Mendelsohn, R.; Rerek, M. E.; Moore, D. J. Fourier transform infrared spectroscopy and differential scanning calorimetry studies of fatty acid homogeneous ceramide 2. *Biochim. Biophys. Acta* **2000**, *1468*, 293-303.

(42) Mojumdar, E. H.; Groen, D.; Gooris, G. S.; Barlow, D. J.; Lawrence, M. J.; Deme, B.; Bouwstra, J. A. Localization of Cholesterol and Fatty Acid in a Model Lipid Membrane: A Neutron Diffraction Approach. *Biophys. J.* **2013**, *105*, 911-918.

(43) Mendelsohn, R.; Selevany, I.; Moore, D. J.; Mack Correa, M. C.; Mao, G.; Walters, R. M.; Flach, C. R. Kinetic Evidence Suggests Spinodal Phase Separation in Stratum Corneum Models by IR Spectroscopy. *J. Phys. Chem. B* **2014**, *118*, 4378-4387.

(44) van Smeden, J.; Janssens, M.; Kaye, E. C. J.; Caspers, P. J.; Lavrijsen, A. P.; Vreeken, R. J.; Bouwstra, J. A. The importance of free fatty acid chain length for the skin barrier function in atopic eczema patients. *Exp. Dermatol.* **2014**, *23*, 45-52.

(45) Joo, K.-M.; Hwang, J.-H.; Bae, S.; Nahm, D.-H.; Park, H.-S.; Ye, Y.-M.; Lim, K.-M. Relationship of ceramide–, and free fatty acid–cholesterol ratios in the stratum corneum with skin barrier function of normal, atopic dermatitis lesional and non-lesional skins. *J. Dermatol. Sci.* **2015**, *77*, 71-74.

(46) Holm, E. A.; Wulf, H. C.; Thomassen, L.; Jemec, G. B. E. Instrumental assessment of atopic eczema: Validation of transepidermal water loss, stratum corneum hydration, erythema, scaling, and edema. *J. Am. Acad. Dermatol.* **2006**, *55*, 772-780.

Chapitre 3: Evidence of hydrocarbon nanodrops in highly ordered stratum corneum model membranes

Adrian Paz Ramos, Gert Gooris, Joke Bouwstra, Michel Lafleur.

The Journal of Lipid Research, **2018**, 59, 137–143.

3.1 Abstract

The stratum corneum (SC), the top layer of skin, dictates both the rate of water loss through the skin, and absorption of exogenous molecules into the body. The crystalline organization of the lipids in the SC is believed to be a key feature associated with the very limited permeability of the skin. In this work, we characterized the organization of SC lipid models that include, as in native SC, cholesterol, a free fatty acid series (saturated with C16-C24 chains), as well as a ceramide bearing an oleate linked to a very long saturated acyl chain (Cer EOS). The latter is reported to be essential for the native SC lipid organization. Our ^{2}H - NMR, infrared and Raman spectroscopy data reveal that Cer EOS leads to the formation of highly-disordered liquid domains in the solid/crystalline matrix. The lipid organization imposes steric constraint on Cer EOS oleate chains in such a way that these hydrocarbon nanodroplets remain in the liquid state down to -30 °C. These findings modify the structural description of the SC substantially, and propose a novel role of Cer EOS as this lipid is a strong modulator of SC solid/liquid balance.

3.2 Introduction

The mammalian skin barrier is a vital component of our body, tightly regulating the loss of water, and the adsorption of exogenous molecules. The stratum corneum (SC), the top layer of skin, is the most important element ensuring skin impermeability. It is formed by hydrophobic protein blocs glued together with stacks of unusual lipids. The SC lipid fraction is mainly responsible for skin impermeability. As an illustration, skin becomes 20-50 times more permeable when the lipid fraction is extracted with an organic solvent.[1] At this point, the origin of skin impermeability is mainly associated with the presence of lipid crystalline phases. At physiological temperature, SC lipids are mainly in a crystalline state, forming solid orthorhombic structures, which is proposed to be highly impermeable.[2-4]

SC lipid composition is rather unique for biological membranes: an equimolar mixture of ceramides (Cer), free fatty acids (FFA), and cholesterol (Chol). There are at least 15 subclasses of ceramides in human SC, including ceramides bearing a non-hydroxylated chain (Cer NS).[5] Cer NS present different acyl chain lengths, usually from 16 to 30 carbon (C) atoms, the most abundant being the C24 chain.[6, 7] Ceramide EOS (Cer EOS) is constituted by a sphingosine base bearing a very-long omega-hydroxy fatty acid with a chain length distribution between 26 C and 36 C atoms to which an unsaturated C18 fatty acid chain is esterified. There is also a chain length distribution of the free fatty acid component, the most abundant being saturated with 22 C, 24 C, and 26 C atoms.[8]

X-ray and neutron diffraction studies have shown that SC lipids form two co-existing lamellar phases with different spacing: the short periodicity phase (SPP) with a repeat distance of approximately 6 nm, and the long periodicity phase (LPP) with a periodicity of around 13

nm.[9] The LPP plays an important role for skin barrier; for example, the diffusion rate of aminobenzoic acid derivatives in model membranes lacking Cer EOS, which only form the SPP, was increased compared to that in the presence of the LPP.[10] Furthermore, Cer EOS seems to play a crucial role in the formation of the LPP. Previous studies show that the presence of Cer EOS is a requirement to prepare SC model membranes with both SPP and LPP and that replacing the unsaturated C18 chain of Cer EOS by a saturated C18 chain is detrimental for the formation of the LPP.[11, 12] Furthermore, some skin diseases like atopic dermatitis and dry skin are characterised by a low content of Cer EOS,[13] which is thought to influence the formation of the LPP and, which may contribute to the reduction in skin barrier.

Several models for the organization of SC lipids into the SPP and LPP have been proposed.[14-18] Recently, a model based on neutron diffraction analyses showed that Cer NS could dictate the length of the unit cell in the SPP, sharing the unit cell space with Chol and FFA. The LPP, on the other hand, could be formed of Cer EOS and Cer NS, and surrounded by Chol and very-long chain FFAs.[18]

In this work, we have characterized the chain order of different components in mirror SC model lipid mixtures forming the LPP. The mixtures included 33.3 (mol)% ceramide (13.3 (mol)% of Cer EOS with an oleate chain, and 20.0 (mol)% of Cer NS), 33.3 (mol)% cholesterol, and 33.3 (mol)% FFA (0.8 (mol)% FFA16, 1.5 (mol)% FFA18, 2.9 (mol)% FFA20, and 28.2 (mol)% FFA24) (Fig. 3.1).

For the spectroscopic analysis, mirror mixtures with the same composition but containing one deuterated species were prepared: deuterated Cer NS-d_{47}, deuterated Cer EOS-d_{33}, or deuterated FFA24-d_{47}. SC FFAs actually include FFA22; however, we used a

proportion of deuterated FFA24 (~85 (mol)% of the total FFA) that represents the combined amount of FFA22 and FFA24 in order to probe the behavior of the very-long FFA chains with a single deuterated species representative of this class of molecules. The mirror mixture with FFA24-d_{47} included hydrogenated FFA16, FFA18, and FFA20.

The chain order has been characterized using three independent complementary techniques. ^{2}H-NMR is a powerful technique in the study of stratum corneum model membranes since it provides valuable information about the chain orientational order and phase behavior of the deuterated lipid constituent.[19, 20] The methylene stretching vibrations, observed in the infrared (IR), and Raman spectra, allow the characterization of the lipid chain conformational order.[21-23] These approaches exploit the isotopic shift effect to provide a simultaneous and independent characterization of different components in a mixture when a species with a deuterated chain is used: the C-D symmetric stretching mode ($\nu_s CD_2$) is an intrinsic probe of the deuterated chain order while the methylene symmetric stretching band ($\nu_s CH_2$) describes the chain order of the hydrogenated components.

3.3 Materials and Methods

3.3.1 Materials

Two Ceramides, the protiated Cer EOS and Cer NS, were generously provided by Evonik (Essen Germany). Partly deuterated Cer EOS and NS (Fig. 3.1), were custom synthesized by Evonik (Essen, Germany). Palmitic acid (C16:0), stearic acid (C18:0), arachidic acid (C20:0), lignoceric acid (C24:0) and Chol were obtained from Sigma- Aldrich Chemie GmbH (Schnelldorf, Germany). Deuterated lignoceric acid was obtained from ARC laboratories (Apeldoorn, Netherlands). Silicon wafers were obtained from Okmetic (Vantaa,

Finland). The solvents that were used were supplied by Labscan (Dublin, Ireland) and were of analytical grade.

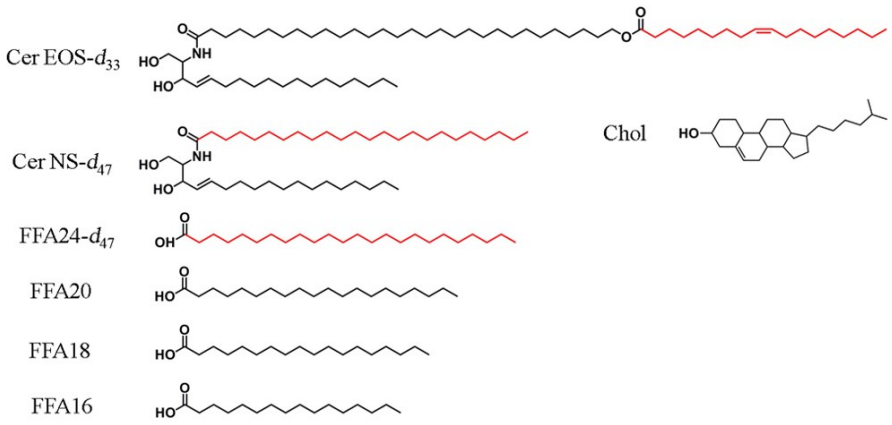

Figure 3.1. The molecular structure of the lipids investigated in the present study. The deuterium-labeled portions are represented in red color.

3.3.2 Sample preparation

The synthetic Cers, Chol and FFA were used in an equimolar ratio. The molar ratio between Cer EOS and Cer NS was 0.4:0.6, while the fatty acids were used in a molar ratio of FFA24:FFA20:FFA18:FFA16 84.6:8.75:4.57:2.05. To prepare the mixtures, the appropriate amount of lipids (~20 mg) was dissolved in chloroform/methanol (2:1 v/v) mixture at a concentration of 5 mg/ml. Subsequently the lipids were sprayed on a silicon substrate on an area of 1.5×4.0 cm^2 using a Camag Linomat IV sample applicator (Muttenz, Switzerland). Spraying was performed at a rate of 5 µl/min, under a gentle stream of nitrogen gas. Subsequently, the lipid mixture was equilibrated for 10 min at 70 °C, close to the melting temperature of the lipid mixture. After equilibration, the sample was slowly cooling down and carefully scraped from the support and inserted into a NMR tube. The NMR tube was air tight closed under a flow of Argon gas to prevent oxidation.

3.3.3 Small angle X-ray diffraction

Small angle X-ray diffraction was used to determine the lamellar organization. The small angle X-ray diffraction measurements were carried out at the European Synchrotron Radiation Facility (Grenoble, France) at station BM26B. The pattern was collected on a Pilatus 1M detector for two times 60 s. The sample-to-detector distance was approximately 2 m. The scattering intensity I (arbitrary units) was measured as a function of the scattering vector q (in nm 1), defined as $q = 4\pi\sin\theta/\lambda$, in which θ is the scattering angle and λ is the wavelength. From the positions of the peaks, the repeat distance was calculated $d = n2\pi/q_n$, in which n is the order of the diffraction peak and q_n the peak position of the n^{th} order.

3.3.4 ^{2}H-NMR analysis

Solid-state NMR measurements were performed on a Bruker Avance II 400 WB spectrometer at a ^{2}H-frequency of 61.4 MHz, using a Bruker static probe with a 5 mm coil. The spectra were acquired using a quadrupolar echo pulse sequence with a 1.80-µs 90° pulse, separated by an interpulse delay of 40 µs, and a recycle time of 50 s for slow-relaxing solid phase and 0.3 s for gel and disordered phases. Samples were placed into a Teflon holder, hydrated with an acetate buffer (50 mM, pH 5), and incubated at 37 °C. After 24 h of incubation, a first spectrum was recorded. Then, samples were left at 37 °C for 7 days. A spectrum was collected after the week. In all cases, there was no difference between this spectrum and the one collected after one-day incubation, suggesting that the sample was at thermodynamic equilibrium. A minimum of 1000 scans was collected for each spectrum.

3.3.5 IR analysis

Infrared spectroscopy analyses were carried out using a Thermo Nicolet 4700 spectrometer. A portion of hydrated lipid mixture was put between two CaF_2 windows separated by a 5 μm-thick Teflon spacer. An additional 25-μL aliquot of acetate buffer was added to the sample to maintain hydration during the measurements. This assembly was inserted in a temperature-controlled brass sample holder and placed into the spectrometer. The spectra were acquired as a function of increasing temperature, varying from 25 to 70 °C with a temperature step of 2 °C and an equilibration period of 5 minutes for each temperature. Spectra were recorded co-adding 32 scans with a nominal spectral resolution of 1 cm^{-1}. The reported band positions correspond to the band maximum.

3.3.6 Raman analysis

Raman measurements were performed using a Witec confocal Raman system, with an immersion 63X objective (NA = 1.0). A small portion of the sample was placed on a CaF_2 window and gently squeezed in order to obtain a relatively flat surface. The sample was immersed in the acetate buffer to ensure complete hydration during the measurements. The sample temperature was adjusted to 33 °C. A 532-nm laser was used as excitation source with a 10-mW power at the sample surface. Spectra were recorded between 1000 and 3200 cm^{-1} with a spectral resolution of 1 cm^{-1}, the acquisition time for each spectrum was 3 s.

3.4 Results

The X-ray diffraction curve of the protiated sample is provided in Supplemental information, Fig. 3.S1. The position of the peaks revealed a single lamellar phase spacing with a repeat distance of 13 nm, corresponding to the LPP. In addition, phase separated

crystalline Chol is present.

^{2}H-NMR spectra of Cer EOS/Cer NS/FFAs/Chol mixtures were recorded from mirror mixtures made with FFA24-d_{47}, Cer NS-d_{47}, or Cer EOS-d_{33}. Figure 3.2 shows the spectra evolution of the deuterium-labeled mixtures as a function of temperature.

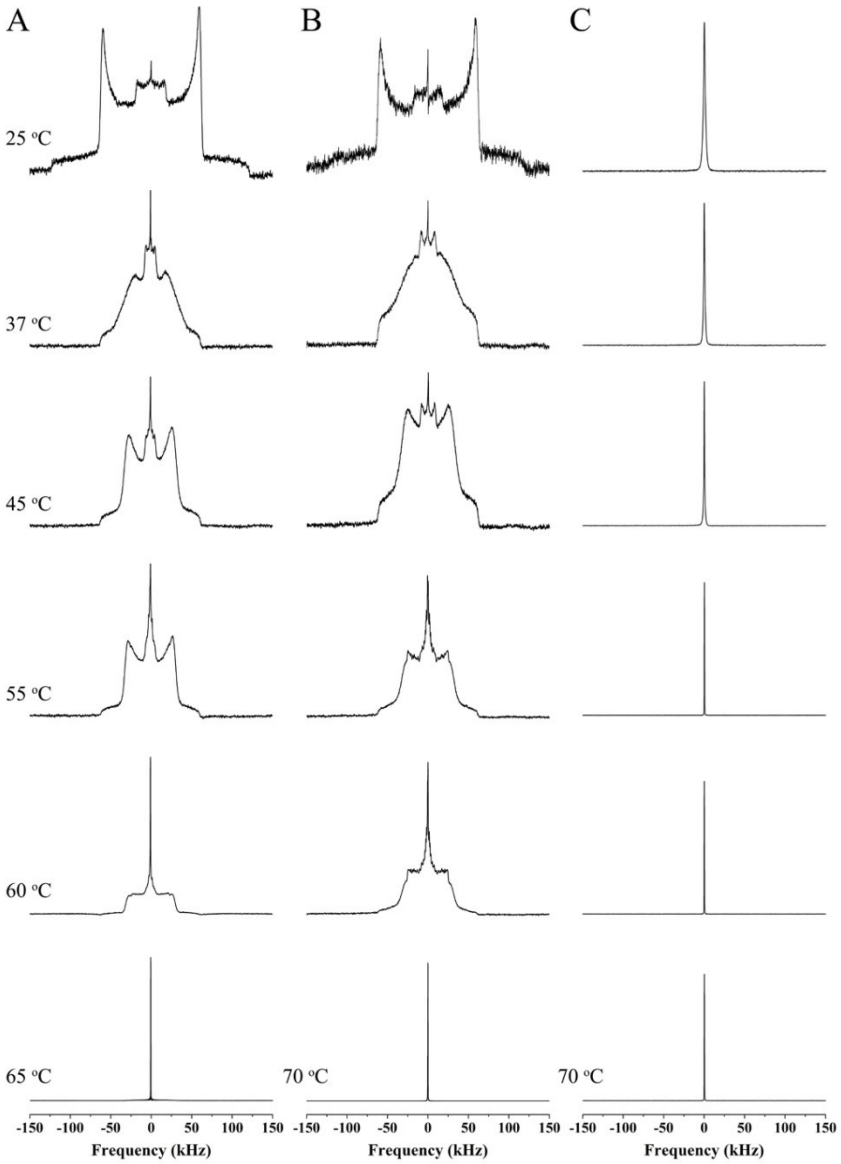

Figure 3.2. Thermal evolution of the ^{2}H-NMR spectra of the Cer EOS/Cer NS/FFAs/Chol mirror mixtures; column A: FFA24-*d*, column B: Cer NS-*d*, and column C: Cer EOS-*d*.

Fig. 3.2A shows the behavior of deuterated lignoceric acid in the Cer EOS/Cer NS/FFAs/Chol mixture. At low temperatures, the spectrum was typical of lipids in a solid phase, *i.e.* composed of two patterns: a broad signal with a quadrupolar splitting of ~120 kHz, which corresponds to the equivalent methylene groups along the FFA24 all-*trans* immobile (on the NMR timescale) acyl chain, and a second powder pattern, with a quadrupolar splitting of ~35 kHz, due to the terminal methyl groups. FFA24 spectrum at ~37 °C, with a width at the base of ~ 128 kHz, indicated a transition of the fatty acid towards a gel phase. Upon heating up to 60 °C, the evolution of the spectrum showed an increase of chain rotational diffusion while remaining in an almost all-*trans* configuration.[2, 24] Heating above 60 °C caused a transition toward a liquid-ordered phase (l_o). In this phase, FFA24 molecules underwent fast rotational motion along the lipid long axis while orientational order of lipid chains remained high. The spectrum shape was associated to the overlapping powder patterns due to the order gradient along the chain. Heating above 65 °C caused a transition to an isotropic phase, characterized by a narrow central peak corresponding to FFA24 molecules that re-oriented randomly on the NMR time scale.

The behavior of deuterated ceramide NS in the mixture is described in Fig. 3.2B. Cer NS experienced phase transitions analogous to those of FFA24 in the mixture, *i.e.* solid phase at the physiological temperature of the skin, a solid-to-gel phase transition at ~37 °C, a gel-to-l_o phase transition at around 60 °C, and finally a transition towards an isotropic phase starting at 70 °C.

The mixture containing Cer EOS with a deuterated oleate chain (Fig. 3.2C) showed a completely different behavior. This sample exhibited a narrow signal over all the investigated temperature range. This ^{2}H-NMR signature is typical of molecules undergoing

isotropic motions, an observation suggesting that the oleate chains were highly disordered, as in a liquid phase. Four additional experiments were carried out in order to discard micelle formation and/or extended lipid separation. First, the sample was suspended in a large excess of buffer (1 mL) and centrifuged at 3500 rpm for 30 min. The supernatant was discarded and the spectrum of the pellet was recorded: it showed only the narrow line. This result indicated that Cer EOS was not forming small aggregates that would have remained in the supernatant, but this lipid was included in the lipid matrix. Furthermore, mass spectrometry showed that Cer EOS was intact after the measurements. Second, the spectrum of the sample that was dehydrated by freeze-drying was recorded and it showed only the narrow line (see Supplemental Information, Fig. 3.S2). This finding indicated that the driving force for the formation of a solid matrix with liquid-phase domains organization is not primarily hydrophobic interactions as it is observed in absence of water. Third, the dry sample was cooled down and the spectrum remained essentially a narrow line down to -20 °C (Fig. 3.S2). Fourth, a Cer EOS/Cer NS/FFAs/Chol mixture sample containing both Cer EOS-d_{33} and FFA24-d_{47} was prepared. The spectrum showed the wide powder pattern of immobile deuterated chains coexisting with the narrow line (see Supplemental Information, Fig. 3.S3), indicating the coexistence of solid and liquid-like lipids in the sample. The relative areas of these spectral components agreed with the proportion and number of deuterium nuclei of FFA24-d_{47} and Cer EOS-d_{33}, considering the former contributing only to the solid-phase signal and the latter to the narrow signal. The intensity of the narrow line remained constant up to -10 °C. Upon further cooling, a pattern associated with solid phase grew and the spectrum displayed only this solid powder pattern at -50 °C.

Infrared spectroscopy was used to probe changes in conformational order of lipid

chains since the positions of the methylene stretching vibrations are sensitive to *trans/gauche* isomerization of acyl chains.[25-27] The position of the deuterated methylene symmetric stretching band ($\nu_s CD_2$) was associated with deuterated chain order while the position of the hydrogenated methylene symmetric stretching band ($\nu_s CH_2$) described the overall conformational order of all the hydrogenated lipid chains in the mixture. Figure 3.3 shows the evolution of these spectral parameters as a function of temperature for the Cer EOS/Cer NS/FFAs/Chol mixtures.

In the sample containing FFA24-d_{47} (Fig. 3.3A), the position of the $\nu_s CD_2$ band remained at ~2088.5 cm^{-1} between 25 and 60 °C, indicating highly ordered FFA24-d_{47} acyl chain.[25, 26] Upon heating above 60 °C, the band position abruptly shifted toward high wavenumbers, reaching 2095.6 cm^{-1} at 70 °C. This value is characteristic of a disordered acyl chain[28, 29] and the band shift was associated with the disordering of FFA24-d_{47} chains, as previously observed for analogous mixtures.[2, 30] At low temperatures, the $\nu_s CH_2$ band was found at around 2850 cm^{-1}, a value indicative of high chain order.[25, 26] The band position slightly increased by ~1 cm^{-1} between 30 and 40 °C, presumably due to a solid-to-gel transition as reported previously for analogous mixtures.[2, 30] Its value increased abruptly at 60 °C, reaching 2853.5 cm^{-1} at 70 °C. This upshift was indicative of an increase of the conformational chain disorder.[31, 32]

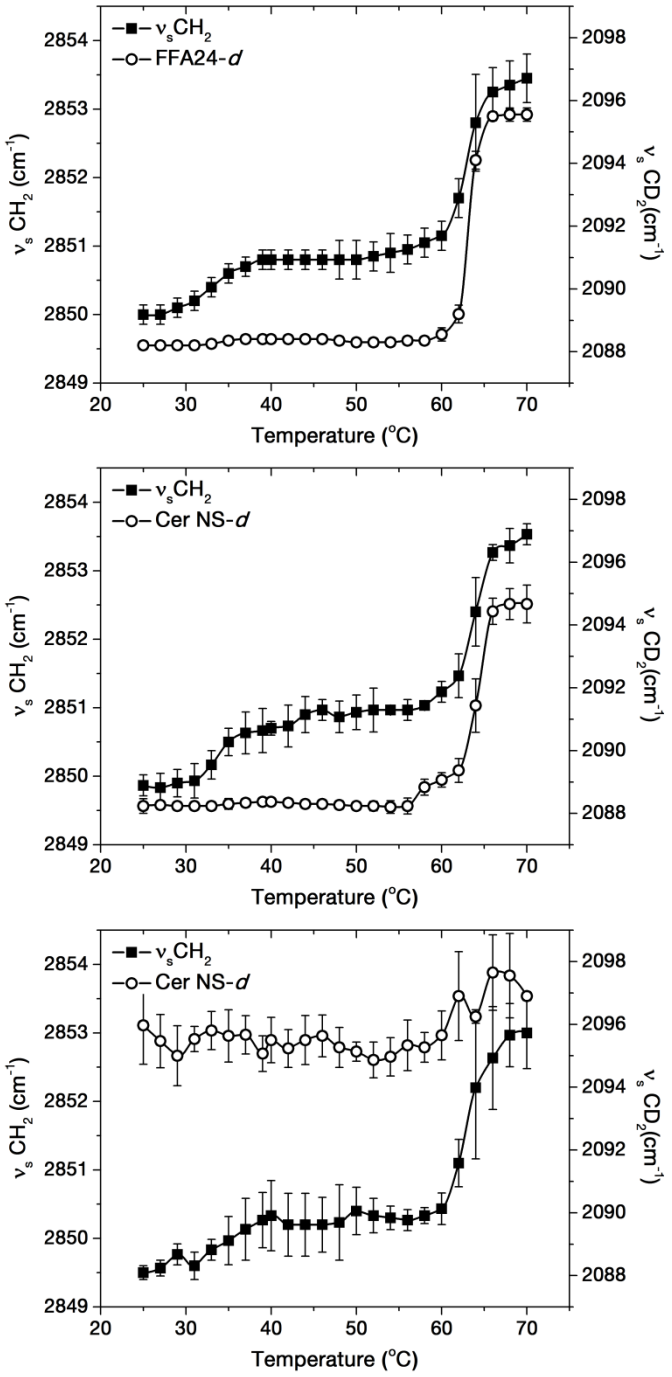

Figure 3.3. Thermotropic behavior of Cer EOS/Cer NS/FFAs/Chol mixtures containing A: FFA24-d_{47}, B: Cer NS-d_{47}, and C: Cer EOS-d_{33}. The data points represent the average and the standard deviation for n=3.

A similar behavior was observed for the sample containing deuterated Cer NS (Fig. 3.3B). The $\nu_s CD_2$ band was observed at ~2088.5 cm^{-1}, from 25 to about 60 °C, indicating that Cer NS-d_{47} chain was highly ordered. Upon further heating, the band position upshifted and reached 2094.7 cm^{-1} at 70 °C, reporting the increase of conformational chain disorder of the Cer NS chain. The thermal profile obtained for the $\nu_s CH_2$ band position was similar to that of the sample containing FFA24-d_{47}.

The mixture containing Cer EOS-d_{33} (Fig. 3.3C) showed high values for the position of the $\nu_s CD_2$ band, with a mean value of 2095.7 ± 0.8 cm^{-1} over the entire temperature range. The band position was actually very similar to those obtained for FFA24-d_{47} and Cer NS-d_{47} molecules at 70 °C. These results indicate that the oleate chain of Cer EOS was highly disordered, even at low temperatures. The hydrogenated lipid acyl chains, however, followed a behavior analogous to the previous samples. The $\nu_s CH_2$ position was ~2849.5 cm^{-1} at 25 °C, increased slightly between 32 to 40 °C, was constant from 40 °C to 60 °C, and rapidly increased to ~2853 cm^{-1} at 70 °C. It should be noted that the $\nu_s CH_2$ position was systematically slightly lower (by about 0.5 cm^{-1}) than those recorded for the mixtures with FFA24-d_{47} or Cer NS-d_{47}. In these mixtures, Cer EOS contributed to the C-H stretching region (as the hydrogenated form was present) and its high conformational disorder was likely responsible for the small upshift of the $\nu_s CH_2$ position, which described the overall order of all the hydrogenated chain species.

In order to further characterize the chain order, the C-D stretching region of the Raman spectra of the mirror mixtures was analyzed (Fig. 3.4).

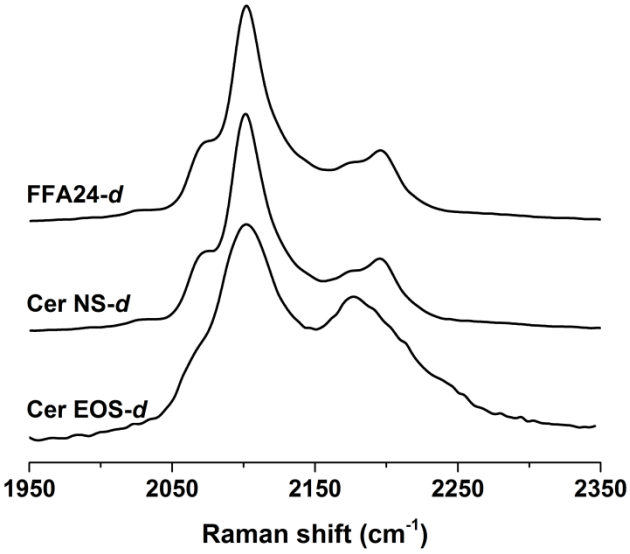

Figure 3.4. The C-D stretching region of the Raman spectra for the Cer EOS/Cer NS/FFAs/Chol mirror mixtures.

This region is dominated by a band at ~2100 cm^{-1}, assigned to the symmetric C-D stretching of the CD_2 groups.[29] Its width is related to the conformational order of the deuterated acyl chain.[31] The band width at the 65% of the height was 21.6 cm^{-1} for the mixture including FFA24-d_{47} and Cer NS-d_{47}, and 42.4 cm^{-1} for that with CerEOS-d_{33}. These observations also indicated that the acyl chains of FFA24 and Cer NS are both ordered while the oleate chain in CerEOS is highly disordered, as inferred from the ^2H NMR and IR spectroscopy results.

3.5 Discussion

The present work reveals a novel feature of SC lipid organization: this lipid structure is formed by solid lipids in which highly disordered liquid domains, formed by the oleate chain of CerEOS, are embedded. The existence of a large solid/crystalline component in SC lipid fraction is a well-established aspect: for example, wide-angle X-ray diffraction patterns

reported crystalline structures in human SC.[32] IR spectra of SC model mixtures, as well as real SC, showed highly ordered chains with orthorhombic packing.[28, 33] Solid-state NMR of several model mixtures mimicking SC lipid phase gave mainly rise to the pattern characteristic of immobile acyl chains.[20, 34] The presence of a fluid lipid fraction has been proposed for the first time more than 20 years ago by Bo Forslind.[16] Under this hypothesis, the presence of crystalline domains forming mosaic-like structures were bound by lipids in a fluid phase. This model rationalized the low permeability of SC as well as its flexibility.[16] Recently, an organization of SC lipids reproducing the SPP and LPP structure based on neutron diffraction results was proposed.[18] In this model, the lipid packing left a limited space for the linoleate chain of Cer EOS and it was proposed that the chain, in contrast to the fully extended acyl chains of the other lipid species, would be highly disordered. These disordered chains could indeed not be observed in the diffraction experiments. It was shown, however, by IR spectroscopy, that the deuterated linoleate chain of Cer EOS in a model mixture similar the one used in the present work and forming exclusively LPP, was fluid.[35] The present results reveal that the unsaturated chain of Cer EOS experiences a liquid-like dynamics, proposing the existence of hydrocarbon droplets in the SC solid lipid matrix. It has been shown[36] that the model mixtures including oleate or linoleate as the unsaturated chain of Cer EOS behaved similarly as they both form the LPP, and their unsaturated chains were proposed to be disordered by IR spectroscopy. The unexpected presence of liquid domains is proposed to be associated with the steric confinement of the oleate chains. The crystallization process leads to the ordering all the methylene segments into an all-*trans* configuration to maximize interchain van der Waals interactions. According to the proposed lipid organization, the dimension of the space available to the oleate chain is too short for a

fully extended oleate chain (~19 Å).[37] This confinement would prevent chain stretching, and lipid solidification. The fact that the oleate chain of Cer EOS remained in the liquid state at a temperature as low as -20 °C, as observed by ^{2}H NMR, is an exceptional behavior as compounds bearing an oleate chain have a melting point considerably higher than this value. The melting point of oleic acid is 16.3 °C (38). The melting point of cis-9- octadecen-1-ol is between 0-3 °C (38), that of cis-9-octadecenylamine is 25 °C,[38] that of cis-9-octadecenoamide is 76 °C,[38] and that of cis-9-octadecene is 0-2 °C.[39] The depression of this melting point is reminiscent of the decrease in the crystallization temperature of molecules trapped in nanopores (for reviews, see: [40-41]). Such phenomenon is even observed with water when the geometrical constraints associated with the pore size hinder the formation of the tetrahedral ice structure by the water molecules.[42]

Despite this spatial confinement, the dynamics of the oleate chain remained, even at -20 °C, fast on the NMR time scale (10^{-5} s) as the quadrupolar interactions were completely averaged out. The liquid-like behavior of the oleate chains suggests that they are not isolated from each other but a certain number of them are grouped together, forming local hydrocarbon nanodroplets (Fig. 3.5).

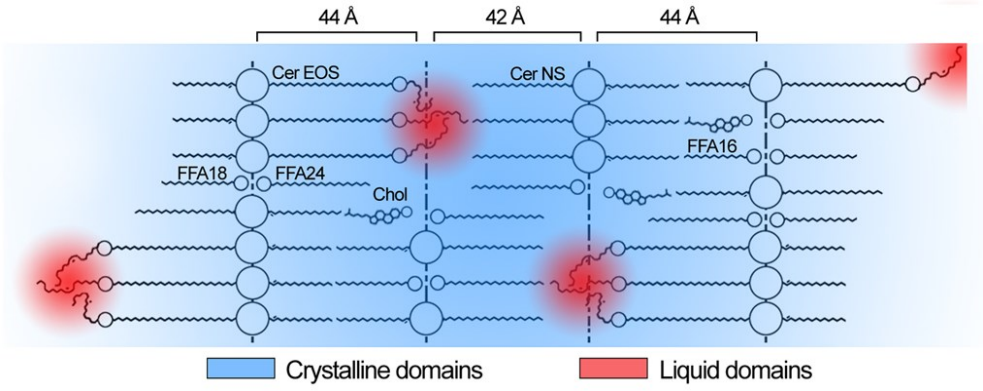

Figure 3.5. Suggested locations of the liquid domains into the crystalline lipid matrix.

The presence of an unsaturation in the chain is a structural element favoring the formation of a liquid phase and increasing chain disorder;[43] for example, the melting points of oleic acid and octadecanoic acid are 14 °C and 69 °C, respectively.[38] Interestingly, the presence of an unsaturation in the ester-linked acyl chain of Cer EOS appears to be essential for the formation of the LPP: small angle X-ray observations of mixtures made with human ceramide/Cer EOS/FFAs/Chol showed the formation of the LPP when Cer EOS bore an unsaturated linoleate or oleate chain but not a stearate (saturated) chain.[12, 36] In these mixtures, the hydrocarbon chain of Cer EOS was more disordered when it was a linoleate or oleate chain than when it was a saturated stearate chain, reinforcing the conclusion that a distinct structure that includes liquid domains is formed with Cer EOS bearing an unsaturated chain.

The existence of liquid domains in the SC matrix could lead to revising the understanding of skin barrier property. It has been proposed that the presence of small solid/crystalline domains in the SC lipid fraction would make the diffusion path extremely tortuous, leading to a very limited permeability.[44] The presence of liquid hydrocarbon droplets in the matrix could be actually a key element contributing to the SC impermeability. These apolar domains located in the head group regions would act as obstacles for the diffusion of hydrophilic compounds through the SC. Moreover they could act as traps for the apolar species, which would strongly partition in these hydrocarbon liquid droplets. The migration of the SC matrix towards the surface and the subsequent shedding would be an efficient way to prevent the penetration of apolar compounds in the body. This hypothesis is supported by the permeability measurements showing that a SC model mixture lacking Cer EOS, and therefore not forming the characteristic long periodicity phase, displayed a 2-fold increased permeability

compared to the corresponding model mixture that included Cer EOS, which forms the long periodicity phase.[10] The putative role of these liquid domains in SC impermeability provides a structural rationale for the phenomenological link between the presence of the LPP and the skin barrier impermeability.

3.6 Supporting Information

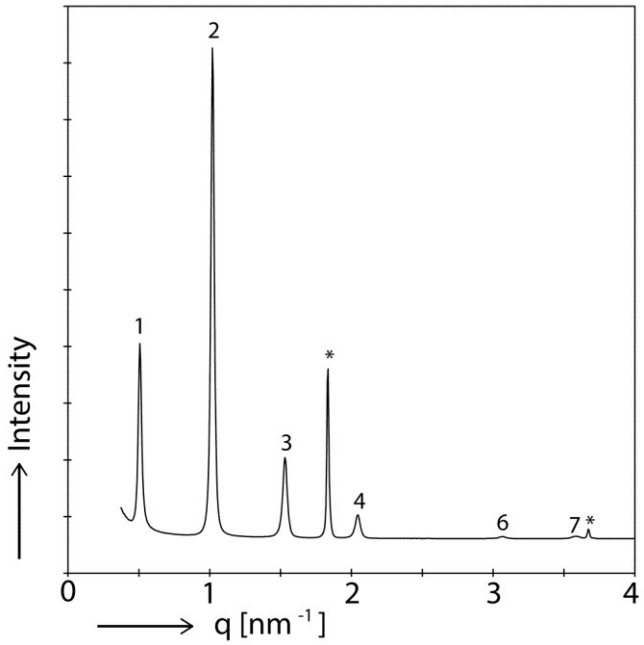

Figure 3.S1. SAXD patterns of the Cer EOS/Cer NS/FFAs/Chol mixture, showing the LPP formation. The * indicate the peaks associated with crystalline cholesterol.

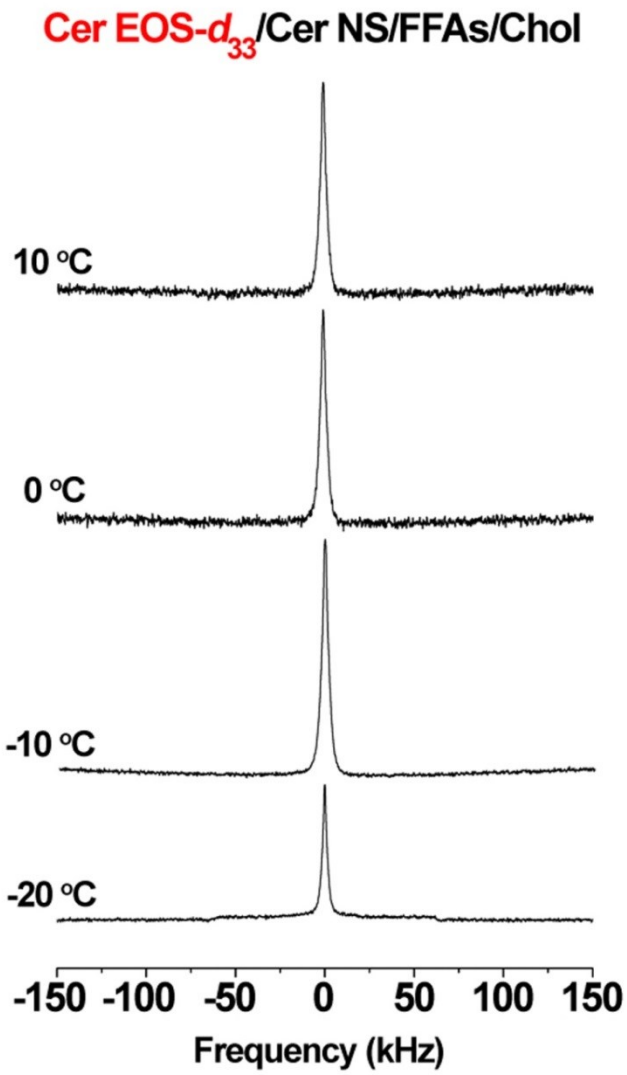

Figure 3.S2. ^{2}H-NMR spectra of the Cer EOS-d_{33}/Cer NS/FFAs/Chol mixture measured at different temperatures.

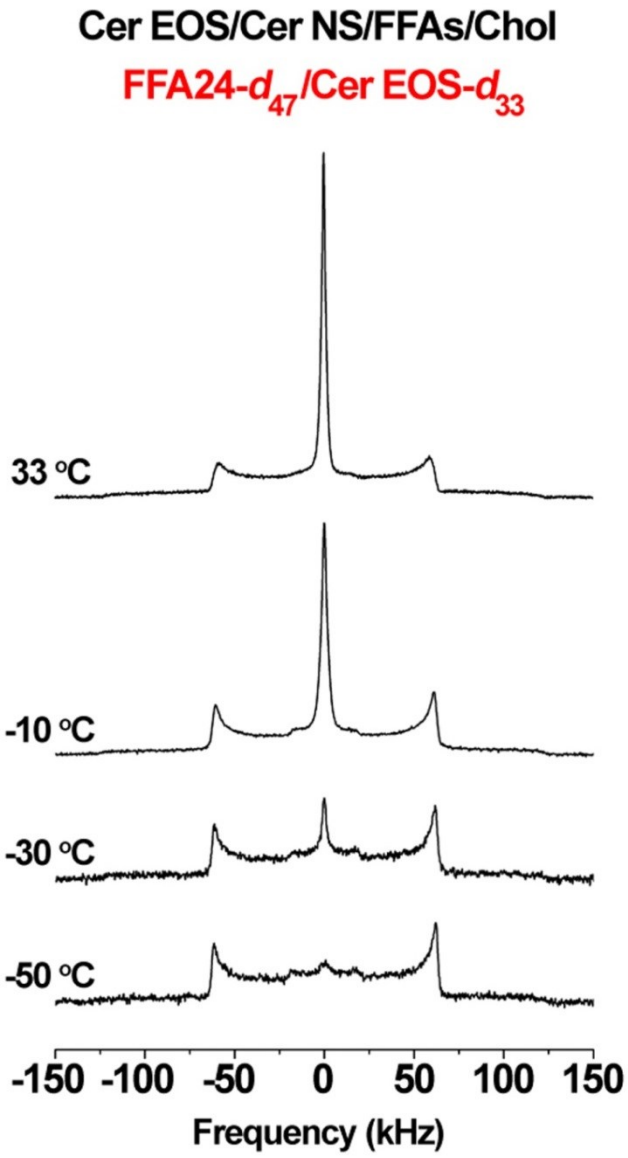

Figure 3.S3. ^{2}H-NMR spectra of the Cer EOS/Cer NS/FFAs/Chol mixture with both deuterated FFA24-d_{47} and Cer EOS-d_{33} measured at different temperatures.

3.7 Acknowledgments

We like to thank the company Evonik (Essen, Germany) for their generous provision of CERs and the personnel at the DUBBLE beam line 26b at the ESRF located at Grenoble, France, for their assistance during the X-ray diffraction measurements. M.L. thanks the Natural Sciences and Engineering Research Council (NSERC) of Canada for the financial support. A.P.R. thanks the Fonds Québécois de la Recherche sur la Nature et les Technologies (FQRNT) for his Doctoral Research Scholarship for Foreign Students. This work was also funded by the FQRNT through its financial support to the Center for Self-Assembled Chemical Structures (CSACS).

3.8 References

(1) Blank, I. H. Factors which influence the water content of the stratum corneum. *J. Invest. Dermatol.* **1952**, *18*, 433-440.

(2) Paz Ramos, A.; Lafleur, M. Chain Length of Free Fatty Acids Influences the Phase Behavior of Stratum Corneum Model Membranes. *Langmuir* **2015**, *31*, 11621-11629.

(3) Stahlberg, S.; Školová, B.; Madhu, P. K.; Vogel, A.; Vávrová, K.; Huster, D. Probing the Role of the Ceramide Acyl Chain Length and Sphingosine Unsaturation in Model Skin Barrier Lipid Mixtures by ^{2}H Solid-State NMR Spectroscopy. *Langmuir* **2015**, *31*, 4906-4915.

(4) Pham, Q. D.; Topgaard, D.; Sparr, E. Tracking solvents in the skin through atomically resolved measurements of molecular mobility in intact stratum corneum. *Proc. Natl. Acad. Sci. USA* **2017**, *114*, E112-E121.

(5) van Smeden, J.; Boiten, W. A.; Hankemeier, T.; Rissmann, R.; Bouwstra, J. A.; Vreeken, R. J. Combined LC/MS-platform for analysis of all major stratum corneum lipids, and the profiling of skin substitutes. *Biochim. Biophys. Acta* **2014**, *1841*, 70-79.

(6) Bouwstra, J. A.; Gooris, G. S.; Cheng, K.; Weerheim, A.; Bras, W.; Ponec, M. Phase behavior of isolated skin lipids. *J. Lipid Res.* **1996**, *37*, 999-1011.

(7) t'Kindt, R.; Jorge, L.; Dumont, E.; Couturon, P.; David, F.; Sandra, P.; Sandra, K. Profiling and Characterizing Skin Ceramides Using Reversed-Phase Liquid Chromatography–Quadrupole Time-of-Flight Mass Spectrometry. *Anal. Chem.* **2012**, *84*, 403-411.

(8) Norlén, L.; Nicander, I.; Lundsjö, A.; Cronholm, T.; Forslind, B. A new HPLC-based method for the quantitative analysis of inner stratum corneum lipids with special reference to the free fatty acid fraction. *Arch. Dermatol. Res.* **1998**, *290*, 508-516.

(9) Mojumdar, Enamul H.; Gooris, Gert S.; Barlow, David J.; Lawrence, M. J.; Deme, B.; Bouwstra, Joke A. Skin Lipids: Localization of Ceramide and Fatty Acid in the Unit Cell of the Long Periodicity Phase. *Biophys. J.* **2015**, *108*, 2670-2679.

(10) de Jager, M.; Groenink, W.; Bielsa i Guivernau, R.; Andersson, E.; Angelova, N.; Ponec, M.; Bouwstra, J. A Novel in Vitro Percutaneous Penetration Model: Evaluation of Barrier Properties with P-Aminobenzoic Acid and Two of Its Derivatives. *Pharm. Res.* **2006**, *23*, 951-960.

(11) de Jager, M. W.; Gooris, G. S.; Dolbnya, I. P.; Bras, W.; Ponec, M.; Bouwstra, J. A. Novel lipid mixtures based on synthetic ceramides reproduce the unique stratum corneum lipid organization. *J. Lipid Res.* **2004**, *45*, 923-932.

(12) Bouwstra, J. A.; Gooris, G. S.; Dubbelaar, F. E. R.; Ponec, M. Phase Behavior of Stratum Corneum Lipid Mixtures Based on Human Ceramides: The Role of Natural and Synthetic Ceramide 1. *J. Invest. Dermatol.* **2002**, *118*, 606-617.

(13) Imokawa, G.; Abe, A.; Jin, K.; Higaki, Y.; Kawashima, M.; Hidano, A. Decreased Level of Ceramides in Stratum Corneum of Atopic Dermatitis: An Etiologic Factor in Atopic Dry Skin? *J. Invest. Dermatol.* **1991**, *96*, 523-526.

(14) Boncheva, M. The physical chemistry of the stratum corneum lipids. *Int. J. Cosmetic Sci.* **2014**, *36*, 505-515.

(15) Kessner, D.; Kiselev, M.; Dante, S.; Hauß, T.; Lersch, P.; Wartewig, S.; Neubert, R. H. H. Arrangement of ceramide [EOS] in a stratum corneum lipid model matrix: new aspects revealed by neutron diffraction studies. *Eur. Biophys. J.* **2008**, *37*, 989-999.

(16) Forslind, B. O. A domain mosaic model of the skin barrier. *Acta Derm-Venereol.* **1994**, *74*, 1-6.

(17) Norlén, L. Skin Barrier Structure and Function: The Single Gel Phase Model. *J. Invest. Dermatol.* **2001**, *117*, 830-836.

(18) Mojumdar, E. H.; Gooris, G. S.; Groen, D.; Barlow, D. J.; Lawrence, M. J.; Demé, B.; Bouwstra, J. A. Stratum corneum lipid matrix: Location of acyl ceramide and cholesterol in the unit cell of the long periodicity phase. *Biochim. Biophys. Acta* **2016**, *1858*, 1926-1934.

(19) Davis, J. H. The description of membrane lipid conformation, order and dynamics by 2H-NMR. *Biochim. Biophys. Acta* **1983**, *737*, 117-171.

(20) Fenske, D. B.; Thewalt, J. L.; Bloom, M.; Kitson, N. Models of stratum corneum intercellular membranes: ^{2}H NMR of macroscopically oriented multilayers. *Biophys. J.* **1994**, *67*, 1562-1573.

(21) Wunder, S. L.; Merajver, S. D. Raman spectroscopic study of the conformational order in hexadecane solutions. *J. Chem. Phys.* **1981**, *74*, 5341-5346.

(22) Moore, D. J.; Rerek, M. E.; Mendelsohn, R. FTIR Spectroscopy Studies of the Conformational Order and Phase Behavior of Ceramides. *J. Phys. Chem. B* **1997**, *101*, 8933-8940.

(23) Snyder, R. G.; Hsu, S. L.; Krimm, S. Vibrational spectra in the C-H stretching region and the structure of the polymethylene chain. *Spectrochim. Acta Mol. Biomol. Spectrosc.* **1978**, *34*, 395-406.

(24) Jansson, M.; Thurmond, R. L.; Barry, J. A.; Brown, M. F. Deuterium NMR study of intermolecular interactions in lamellar phases containing palmitoyllysophosphatidylcholine. *J. Phys. Chem.* **1992**, *96*, 9532-9544.

(25) Mendelsohn, R.; Flach, C. R.; Moore, D. J. Determination of molecular conformation and permeation in skin via IR spectroscopy, microscopy, and imaging. *Biochim. Biophys. Acta* **2006**, *1758*, 923-933.

(26) Mendelsohn, R.; Moore, D. J. Vibrational spectroscopic studies of lipid domains in biomembranes and model systems. *Chem. Phys. Lipids* **1998**, *96*, 141-157.

(27) Gooris, G. S.; Bouwstra, J. A. Infrared Spectroscopic Study of Stratum Corneum Model Membranes Prepared from Human Ceramides, Cholesterol, and Fatty Acids. *Biophys. J.* **2007**, *92*, 2785-2795.

(28) Moore, D. J.; Rerek, M. E.; Mendelsohn, R. Lipid Domains and Orthorhombic Phases in Model Stratum Corneum: Evidence from Fourier Transform Infrared Spectroscopy Studies. *Biochem. Biophys. Res. Commun.* **1997**, *231*, 797-801.

(29) Mendelsohn, R.; Sunder, S.; Bernstein, H. J. Deuterated fatty acids as Raman spectroscopic probes of membrane structure. *Biochim. Biophys. Acta* **1976**, *443*, 613-617.

(30) Oguri, M.; Gooris, G. S.; Bito, K.; Bouwstra, J. A. The effect of the chain length distribution of free fatty acids on the mixing properties of stratum corneum model membranes. *Biochim. Biophys. Acta* **2014**, *1838*, 1851-1861.

(31) Mendelsohn, R.; Koch, C. C. Deuterated phospholipids as raman spectroscopic probes of membrane structure. *Biochim. Biophys. Acta* **1980**, *598*, 260-271.

(32) Bouwstra, J. A.; Gooris, G. S.; van der Spek, J. A.; Bras, W. Structural Investigations of Human Stratum Corneum by Small-Angle X-Ray Scattering. *J. Invest. Dermatol.* **1991**, *97*, 1005-1012.

(33) Moore, D. J.; Snyder, R. G.; Rerek, M. E.; Mendelsohn, R. Kinetics of Membrane Raft Formation: Fatty Acid Domains in Stratum Corneum Lipid Models. *J. Phys. Chem. B* **2006**, *110*, 2378-2386.

(34) Brief, E.; Kwak, S.; Cheng, J. T. J.; Kitson, N.; Thewalt, J.; Lafleur, M. Phase Behavior of an Equimolar Mixture of N-Palmitoyl-D-*erythro*-sphingosine, Cholesterol, and Palmitic Acid, a Mixture with Optimized Hydrophobic Matching. *Langmuir* **2009**, *25*, 7523-7532.

(35) Janssens, M.; Gooris, G. S.; Bouwstra, J. A. Infrared spectroscopy studies of mixtures prepared with synthetic ceramides varying in head group architecture: Coexistence of liquid and crystalline phases. *Biochim. Biophys. Acta* **2009**, *1788*, 732-742.

(36) de Sousa Neto, D.; Gooris, G.; Bouwstra, J. Effect of the ω-acylceramides on the lipid organization of stratum corneum model membranes evaluated by X-ray diffraction and FTIR studies (Part I). *Chem. Phys. Lipids* **2011**, *164*, 184-195.

(37) Abrahamsson, S.; Ryderstedt-Nahringbauer, I. The crystal structure of the low-melting form of oleic acid. *Acta Cryst.* **1962**, *15*, 1261-1268.

(38) CRC Handbook of Chemistry and Physics. 97th ed.; CRC Press: Boca Raton, FL, **2016-2017**.

(39) Deatherage, F. E.; Olcott, H. S. Synthesis of cis-9-Octadecene, 9-Octadecyne and 9,10-Octadecane-diol. *J. Am. Chem. Soc.* **1939**, *61*, 630-631.

(40) Mataz, A.; Gregory, B. M. Effects of confinement on material behaviour at the nanometre size scale. *J. Phys. Condens. Matter* **2005**, *17*, R461.

(41) Jiang, Q.; Ward, M. D. Crystallization under nanoscale confinement. *Chem. Soc. Rev.* **2014**, *43*, 2066-2079.

(42) Cerveny, S.; Mallamace, F.; Swenson, J.; Vogel, M.; Xu, L. Confined Water as Model of Supercooled Water. *Chem. Rev.* **2016**, *116*, 7608-7625.

(43) Seelig, A.; Seelig, J. Effect of a single cis double bond on the structure of a phospholipid bilayer. *Biochemistry* **1977**, *16*, 45-50.

(44) Menon, G. K.; Cleary, G. W.; Lane, M. E. The structure and function of the stratum corneum. *Int. J. Pharm.* **2012**, *435*, 3-9.

Chapitre 4: Effect of saturated very long-chain fatty acids on the organization of lipid membranes: a study combining ^{2}H NMR spectroscopy and molecular dynamics simulations

Adrian Paz Ramos, Patrick Lagüe, Guillaume Lamoureux, Michel Lafleur.

The Journal of Physical Chemistry B, **2016**, 120, 6951–6960.

4.1 Abstract

Little is known about the interaction of very long-chain saturated fatty acids (VLCFAs) with biological membranes. However, this could play an important role on interleaflet interactions and signal transduction mechanisms in cells. The aim of this work is to determine how VLCFA structurally adapts in fluid phospholipid bilayers, since both species must exhibit a significant hydrophobic mismatch. The membrane organization has been described by means of ^{2}H NMR and molecular dynamics simulations. Our results show that the protonation state affects the position and order of free fatty acids (FFAs) in phospholipid membranes. It was shown that the protonated FFA-C24 carboxyl group is located slightly under the POPC head group and therefore its acyl chain can interact with the lipids of the opposite leaflet. This interdigitation of the end of the acyl chain causes a second plateau observed in S_{C-D} profiles, a very unusual feature in lipid systems.

4.2 Introduction

Hydrophobic matching is an essential contribution to the energetics in biological membranes: the length of the hydrophobic segments of the various membrane components should match to create a consistent apolar core. The hydrophobic matching between the lipid bilayer thickness and the length of protein transmembrane segments has been shown to impact the configuration of biological membranes.[1,2] It was proposed, for example, that this matching played a basic role in the evolution selection of membrane proteins,[3] and in protein sorting at the level of the Golgi complex.[4] In an analogous manner, hydrophobic matching of membrane lipids, including the modulation of bilayer thickness by cholesterol, is a central contribution in the organization of membranes; it has been shown to dictate the formation of domains in biological membranes, and to influence many physiological processes.[5,6]

In the present work, we examine how very long-chain saturated fatty acids (VLCFAs), with chains longer than 18 carbons (>C18), adapt in fluid membranes. These species must exhibit a significant hydrophobic mismatch considering that typical human plasma membranes contain lipids with shorter chains for example, palmitoyl (C16:0) and oleoyl (C18:1) are the most abundant lipid chains in red blood cell membranes.[7] VLCFAs are present as minor component in membranes. However, some severe neurodegenerative diseases, such as X-linked adrenoleukodystrophy (X-ALD), cerebro-hepato-renal (Zellweger) syndrome, and type 2 diabetes, are characterized by an accumulation of VLCFAs at abnormally high concentrations.[7–10] Type 2 diabetes patients accumulate about 47% more nonesterified VLCFAs compared to healthy persons.[7] Similarly, the amount of saturated VLCFAs in plasma (esterified and nonesterified) constitutes about 3.1% of total fatty acids for healthy persons and

4.8% of the total for X-ALD patients.[11] This accumulation of VLCFAs appears to translate into the increase in microviscosity of erythrocyte membranes observed in those patients.[12]

Such long species should experience a distinct behavior as they should adapt to the hydrophobic mismatch with the apolar interior of membranes. Current knowledge indicates that their dynamic is different from that of usual long free fatty acids (FFAs). For example, the rate of spontaneous desorption of VLCFAs from phospholipid membranes was found to be 10^5-10^6 times slower than that of common FFA (C16 and C18).[13,14] These findings reflected the exponential decrease of the rate of desorption with increased chain length. It was also found that hexacosanoic acid (FFA-C26) displayed a reduced affinity for bovine serum albumin (BSA) compared to oleic acid, a phenomenon that can contribute to the accumulation of VLCFAs in membranes. Not only was the number of BSA binding sites more limited for FFA-C26 compared to LCFA (C12-18) but high-affinity sites appeared to be incompetent to bind FFA-C26. The flip-flop of saturated VLCFAs (C20:0-C24:0) was also shown to be considerably slower ($t_{1/2}$ < 1 s) than that observed for long chain (C14:0-C18:0) FAs ($t_{1/2}$ <10 ms).[14] This difference may also contribute to the accumulation of VLCFAs in membranes in the above-mentioned diseases.[14,15]

The structure adopted by VLCFAs in biological membranes is not clearly determined. Ho *et al.*[13] proposed that the long VLCFA acyl chain could bend at the center of the phospholipid bilayer or penetrate (interdigitate) into the opposite leaflet. An analogous hydrophobic mismatch exists for lipids with highly asymmetric acyl chains even though, in these systems, the two chains are linked in a covalent manner. Highly asymmetric acyl chain phosphatidylcholines (PC) have been shown to form interdigitated bilayers in the gel phase.[16,17] In the fluid phase, the structure is not as clearly defined but it appears that the lipid

chains remained partially interdigitated. X-ray diffraction measurements indicated that the bilayers became thicker during the gel-to-fluid phase transition, despite the fact that the effective length of disordered acyl chains should be reduced. This variation was proposed to be associated with a reduction of the chain interdigitation in the fluid phase.[17] A deuterium nuclear magnetic resonance spectroscopy (^{2}H NMR) study of bilayers prepared with PC bearing highly asymmetric acyl chains (C20;C12, and C10;C22) revealed that the longer hydrocarbon chain exhibited unusual orientational order distributions where there was a greater proportion of methylene groups with small order parameters than expected for typical fluid bilayers.[18] These groups were proposed to be located at the end of the long acyl chains and would interact with the acyl chains of lipids from the opposite leaflets.[18] Recently,[19] a molecular dynamics (MD) simulations study of bilayers that included sphingomyelin (SM) bearing highly asymmetric acyl chains (C18:1;C24:0) indicated that these lipids led to partial interdigitation of the leaflets, the C24 acyl chains protruding into the opposite leaflet much deeper than any other chain in the studied systems. Such phenomenon presents an interesting mechanism for the transmembrane coupling between leaflets in biological membranes.

In this study, we combined ^{2}H NMR spectroscopy and MD simulations to determine how VLCFA structurally adapts in fluid bilayers with hydrophobic thickness that present hydrophobic mismatch. We characterized model membranes composed of a binary mixture of a phospholipid, 1-palmitoyl-2-oleoyl-*sn*-glycero-3-phosphocholine (POPC), and a free fatty acid with different chain lengths (C16, C20, and C24). The proportion of FFA in the POPC matrix was 7.5 mol%. Mirror mixtures of equivalent composition and containing POPC-d_{31} or deuterated FFA were prepared. ^{2}H NMR allowed the characterization of the orientational order gradient along the labeled chain as the recorded quadrupolar splittings are measurements

of the local averaged orientation of the C-D bonds relative to the bilayer normal.[20–22] MD simulations provided a detailed molecular description of these bilayers. The good agreement between the experimental and theoretical results allowed us to solidly detail the conformational adaptation of the acyl chains in the bilayers containing VLCFA.

4.3 Materials and Methods

4.3.1 Materials

1-Palmitoyl-2-oleoyl-*sn*-glycero-3-phosphocholine (POPC, >99%) and POPC-d_{31} (>99%) were obtained from Avanti Polar Lipids (Birmingham, AL, USA). Palmitic acid (FFA-C16, >99%), arachidic acid (FFA-C20, >99%), lignoceric acid (FFA-C24, >99%), 4-(2-hydroxyethyl)-1-piperazineethanesulfonic acid (HEPES, > 99%), ethylenediaminetetraacetic acid (EDTA, 99%), and deuterium-depleted water (>99%) were purchased from Sigma Chemical Co. (St. Louis, MO, USA). Perdeuterated FFA-C16d_{31} (99.3%), FFA-C20d_{39} (98.9%), and FFA-C24d_{47} (98.8%) were obtained from CDN Isotopes (Pointe-Claire, QC, Canada). NaCl (>99%) was purchased from Amresco (Solon, OH, USA). Methanol (spectrograde) and benzene (high purity) were obtained from American Chemicals Ltd. (Montreal, QC, Canada) and BDH Inc. (Toronto, ON, Canada), respectively.

4.3.2 Membranes Preparation

Mixtures of POPC and FFA were prepared by dissolving weighed amounts of the solids in a solution of benzene/methanol 9:1 (v/v); POPC-d_{31} or deuterated FFAs were used. Lipids were hydrated with 1 mL of HEPES buffer (25 mM) containing NaCl (120 mM) and EDTA (0.1 mM), that was prepared in deuterium-depleted water. The desired pH was adjusted with diluted NaOH or HCl solutions. All samples contained about 5 mg of the deuterated

species in order to get a similar signal. As the proportion of FFA in the mixtures was 7.5 mol%, the total lipid amount varied from 168 mg (POPC/FFA-C16d_{31}) to 5 mg (POPC-d_{31}/FFA-C16); under these conditions, all the samples were fully hydrated.

4.3.3 ^{2}H NMR Spectroscopy

^{2}H NMR measurements were performed on a Bruker Avance II 400 WB spectrometer operating at 9.4 T (^{2}H-frequency 61.4 MHz), using a Bruker static probe equipped with a 5 mm coil. Each spectrum resulted from 10 000 scans using the quadrupolar echo technique, with a 1.80-μs 90° pulse, an interpulse delay of 40 μs, and a recycle time of 300 ms. ^{2}H NMR spectra were collected from 25 to 70 °C.

The powder-type ^{2}H NMR spectra were dePaked to provide spectra characteristic of samples oriented at 90°, *i.e.*, with bilayer normal perpendicular with respect to the direction of the external magnetic field.[23] The quadrupolar splitting (Δν) of the terminal methyl was measured directly from the well-resolved innermost doublet of the dePaked spectra. The remaining of a dePaked spectrum was then divided into a number of areas corresponding to the number of CD_2 groups and a mean order parameter was calculated for each slice.[24] The local order parameters (S_{C-D}) were then inferred using:[24]

$$\Delta\nu_Q = \frac{3}{2} A_Q \left(\frac{3\cos^2\beta - 1}{2}\right) |S_{C-D}| \qquad \text{Eq. 4.1}$$

where A_Q denotes the static quadrupolar constant (167 kHz for a C-D bond) while β is the angle between the bilayer normal and the magnetic field orientation. In smoothed order profiles, a monotonous decrease of orientational order was assumed from C2, the methylene

group close to the lipid head group (C1 corresponded to the carbon of the ester link), to the end of the acyl chain.

4.3.4 MD Simulations

4.3.4.1 Systems Setup

CHARMM-GUI25 was used to build two bilayer systems: one composed of 200 POPC molecules, and another composed of 185 POPC molecules (93 for the lower leaflet and 92 for the upper) and 15 1,2-dinervonyl-*sn*-glycero-3-phosphocholine (DNPC) molecules (7 for the lower leaflet and 8 for the upper). A water thickness of 22.5 Å on top and bottom of each system was used, with a NaCl concentration of 120 mM. Then, 15 POPC molecules of the pure POPC bilayer were randomly replaced by palmitic acid molecules (FFA-C16) chain (7 for the lower leaflet and 8 for the upper), while the DNPC molecules of the POPC/DNPC bilayer were replaced with lignoceric acid molecules (FFA-C24), leading to a concentration of 7.5 mol % of FFA for each system, respectively. Finally, two additional systems were built from these systems by protonating the FFAs. The FFA24 topology was built from the FFA16 topology and the protonated carboxyl head group parameters were transferred from the aspartate side-chain parameters. The deprotonated systems were neutralized by deletion of 15 Cl^- atoms.

4.3.4.2 Simulation Details

All-atom simulations were done with the NAMD 2.9 software[26] and the CHARMM36 force field,[27,28] TIP3P waters,[29,30] and periodic boundary conditions. All bonds involving a hydrogen atom were kept rigid. Nonbonded interactions were truncated at 12 Å with a smooth switching of the forces over the range of 10-12 Å. Long-range electrostatics were calculated

via the particle mesh Ewald (PME) method,[31] using a fourth-order interpolation required for GPU acceleration in NAMD and a grid spacing of ~1 Å. Constant temperature and pressure conditions were simulated using Langevin dynamics with a damping coefficient of 1/ps at a temperature of 25 °C. Isotropic pressure was controlled by a Nosé-Hoover Langevin piston at ~227 atm to account for long-range Lennard-Jones terms following the long-range correction method.[32] Pressure for the long-range correction method was updated every 2 ns with a long cutoff at 30 Å. The simulations used a 1 fs time step with the multiple time steps r-RESPA integrator updating nonbonded and long-range electrostatics every 2 steps. Nonbonded pair lists were updated every 10 steps and coordinates were saved every 1 ps for analysis. Each system was run for 400 ns. The first 100 ns, considered as equilibrium time (this equilibration period is more than 10 times the required period to achieve the steady state for lipid properties investigated in the present work[33]), were discarded from analysis.

4.3.4.3 Trajectory Analysis

The average structure of the lipids was characterized by the magnitude of the deuterium order parameter, $|S_{CD}|$, and was calculated as:[34]

$$|S_{CD}| = \left|\frac{1}{2}\langle 3\ cos^2\theta - 1\rangle\right| \qquad \text{Eq. 4.2}$$

where θ is the angle between the C−H bond vector and the bilayer normal and the brackets denote an average over time and over lipids of the same composition.

4.4 Results and Discussion

Figure 4.1 shows the ^{2}H NMR spectra and the corresponding deconvoluted (dePaked) spectra obtained from binary mixtures of POPC with one investigated deuterated FFA, at 25 °C.

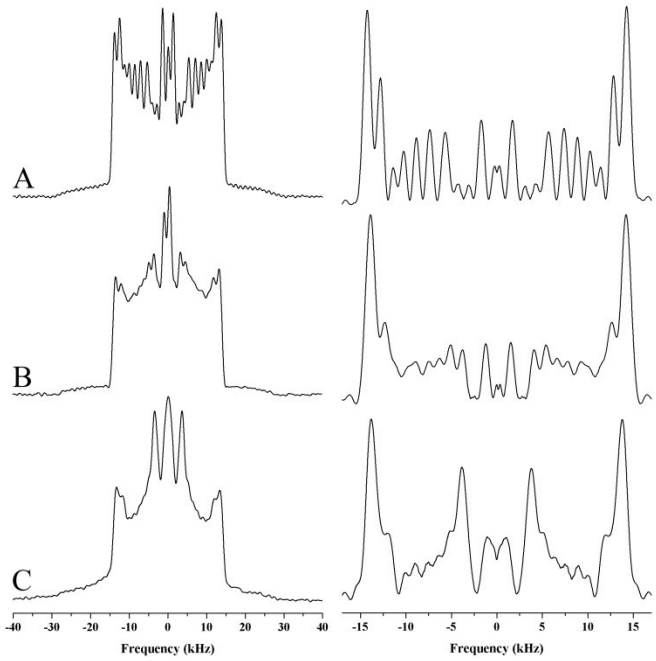

Figure 4.1. ^{2}H NMR (left) and corresponding dePaked spectra (right) recorded at 25 °C from binary mixtures of (A) POPC/FFA-C16d_{31}, (B) POPC/FFA-C20d_{39}, and (C) POPC/FFA-C24d_{47}.

The three spectra exhibited a quadrupolar splitting of approximately 30 kHz for the outermost doublet, a value characteristic of acyl chains in the fluid lamellar phase.[35,36] The quadrupolar splittings of the terminal CD_3 group could be easily assigned to the innermost doublet as these methyl experienced fast rotation along the last C-C bond of the chain. These well resolved doublets displayed a quadrupolar splitting of ~2.5 kHz. The remaining of the spectra corresponded to overlapping doublets resulting from the different methylene (CD2)

groups experiencing different dynamics along the acyl chain. The dePaked spectra of POPC/FFA-C16d_{31} mixture showed several well-resolved peaks. The outermost signal, that has the highest intensity, included several overlapping peaks with similar quadrupolar splittings. This signal corresponds to the plateau region of the order parameter profiles.[37]

Two features should be highlighted for the spectra recorded from the samples containing FFA-C20d_{39} and FFA-C24d_{47}. First, the resolution of the peaks was lower. Second, an intense doublet signal, between +2.5/+6 kHz and -2.5/-6 kHz, grew as a function of FFA chain length. This contribution was associated with methylene groups with low orientational order, a first indication of the response of VLCFA adapting to POPC bilayers.

The ^{2}H NMR spectra and the corresponding dePaked spectra of the mirror samples containing deuterated POPC-d_{31} are shown in Figure 4.2.

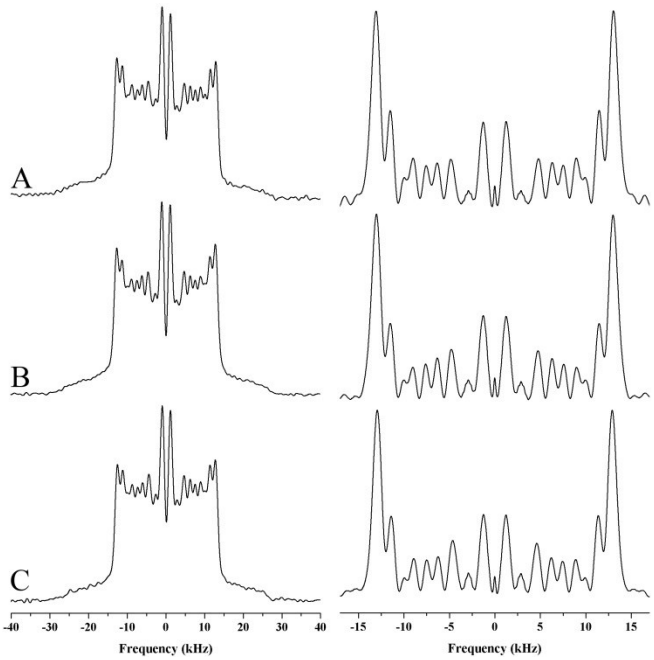

Figure 4.2. ^{2}H NMR (left) and corresponding dePaked spectra (right) recorded at 25 °C from binary mixtures of (A) POPC-d_{31}/FFA-C16, (B) POPC-d_{31}/FFA-C20, and (C) POPC-d_{31}/FFA-C24.

The spectra were almost identical for the three samples and, in fact, were very similar to those previously reported for pure POPC.[24,38] The outermost doublets showed a quadrupolar splitting value of 28 kHz whereas the more mobile CD_3 group gave rise to the central doublet with a quadrupolar splitting of about 2.5 kHz. The dePaked spectra showed several resolved doublets, typical of the orientational order gradient along the deuterated palmitoyl chain.[20,36] The similarity between the three spectra suggested that the addition of FFA with different chain length, at a concentration of 7.5 mol%, did not significantly perturb POPC bilayers.

The smoothed order profiles could be derived from the ^2H NMR spectra; their evolution as a function of temperature is presented in Figure 4.3. All the profiles displayed a plateau region near the lipid head group. In the cases of POPC-d_{31}/FFA-C24 and POPC/FFA-C16d_{31} samples (Figures 4.3A and B, respectively), the plateau was followed by a rapid decrease of S_{C-D} going toward the end of the chain, a profile typical of fluid phase bilayers.[35,36] The smoothed order profiles obtained previously[37] for the palmitoyl chain of FFA-C16 and of 1,2-dipalmitoyl-*sn*-glycero-3-phosphocholine (DPPC) in an equimolar mixture of these species in the fluid phase were also similar, showing their shared environment and dynamics. A temperature increase led to a decrease in orientational order as the thermal energy promotes the *trans/gauche* isomerization along the saturated alkyl chain.

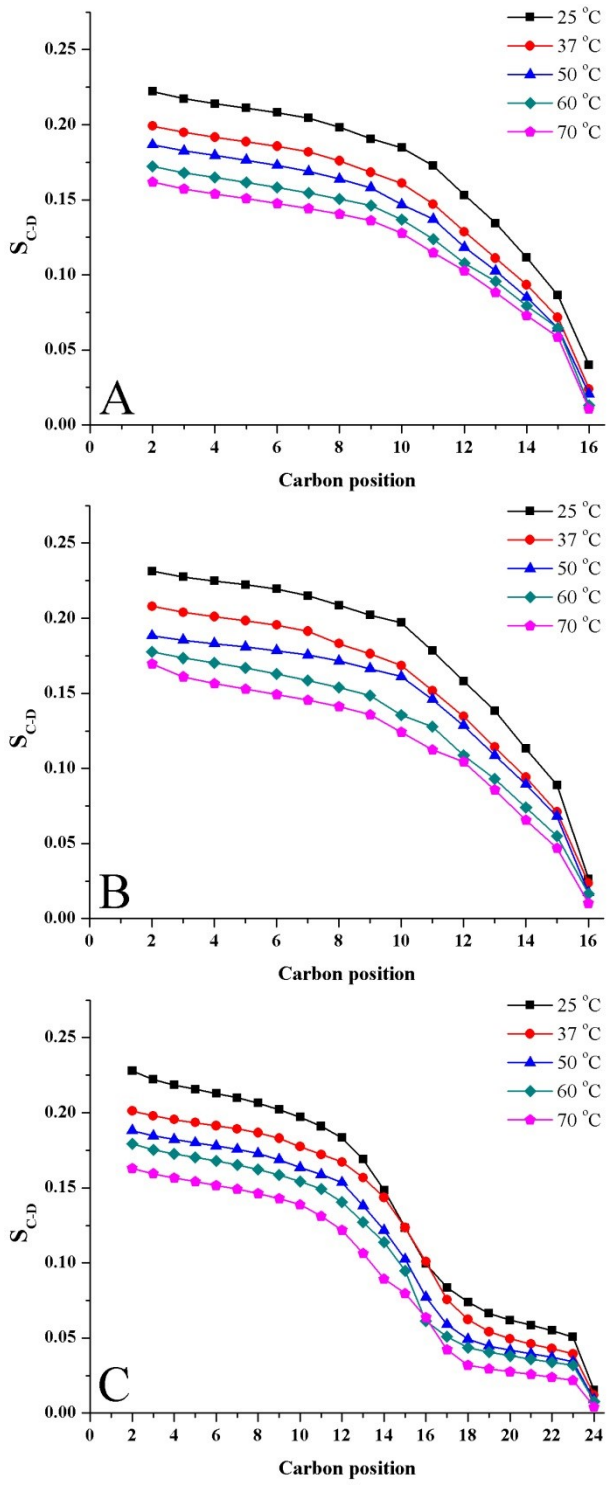

Figure 4.3. Smoothed orientational order profile for (A) POPC-d_{31}/FFA-C24, (B) POPC/FFA-C16d_{31}, and (C) POPC/FFA-C24d_{47} samples.

Table 4.1 reports the decrease of the overall orientational order along the chain associated with a temperature increase.

Table 4.1 Variation of the overall orientational order when increasing temperature.

	POPC-d_{31}/ FFA-C16	POPC-d_{31}/ FFA-C20	POPC-d_{31}/ FFA-C24	POPC/ FFA-C16d_{31}	POPC/ FFA-C20d_{39}	POPC/ FFA-C24d_{47}
$d\langle S_{C-D}\rangle/dT$ ($\times 10^3$)	-1.15 ± 0.08	-1.10 ± 0.10	-1.05 ± 0.07	-1.29 ± 0.09	-1.16 ± 0.06	-1.06 ± 0.04
R^2	0.981	0.955	0.984	0.981	0.990	0.993

The smoothed order profiles obtained for POPC/FFA-C24d_{47} mixture also displayed a plateau with relatively high orientational order, a region associated with the segment of the chain close to the head group (Figure 4.3C). The S_{C-D} values in this region were similar to those obtained for the free fatty acids and the palmitoyl chain of POPC of the other mixtures. It should be noted that, for a given temperature, this plateau region involved a longer segment with increasing FFA chain length, a phenomenon previously observed with a homologous series of phosphatidylcholines with saturated acyl lengths varying from C12 to C18.[39] The profiles also included, as a distinct feature, a second plateau in the region with low orientational order, formed by six methylene groups (Figure 4.3C). In the smoothed profiles, these low S_{C-D} values were assigned to the end of the chain as a monotonous decrease in order was hypothesized. The presence of this second plateau persisted upon heating to 70 °C. The effect of heating on the overall order of POPC/FFA-C24d_{47} is reported in Table 4.1.

All the systems displayed a similar decrease in overall orientational order as a function of temperature. However, there was a small decrease of $d\langle S_{C-D}\rangle/dT$ as a function of chain

length (Table 4.1). This observation was associated with the fact that several positions already showed reduced order parameters for the very long chains.

MD simulations were carried out for the POPC/FFA-C16 and POPC/FFA-C24 mixtures. The order parameters for each methylene group along the acyl chains were extracted from the simulations and compared with the experimental values (Figure 4.4). The experimental S_{C-D} values were assigned to the carbon positions in order to optimize the match with the order profile obtained from the simulations. These theoretical order profiles were obtained assuming a complete protonation of FFAs.

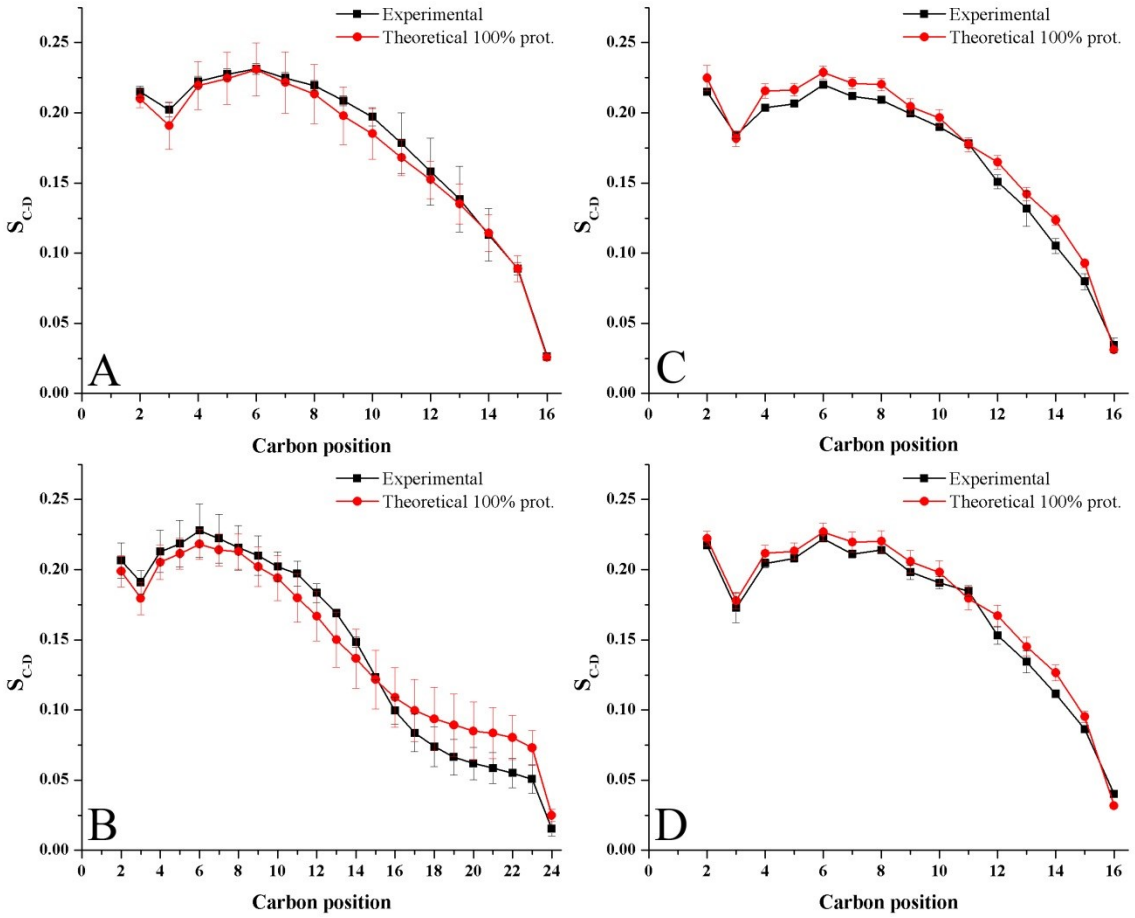

Figure 4.4. MD simulations and experimental order profiles of: A) POPC/FFA-C16d_{31}, B) POPC/FFA-C24d_{47}, C) POPC-d_{31}/FFA-C16 and D) POPC-d_{31}/FFA-C24.

The theoretical and experimental order profiles of both the FFA and POPC palmitoyl chain of POPC/FFA-C16 mixtures exhibited a very good agreement (Figure 4.4A and C, respectively). As expected,[24] the smoothed profiles reproduced the main features of the orientational order profiles; however, a significant difference was observed for the position of carbon 3 where a discontinuity was observed as a result of a kink of the C2-C3-C4 segment of the acyl chain.[35]

POPC/FFA-C24d_{47} sample showed also a good agreement between experimental and MD order profiles (Figure 4.4B). The MD results indicated that the unusual number of carbon positions with small order parameters were located at the end of the FFA-C24 chain, creating a second plateau. The discontinuity at the position 3 was also observed for the VLCFA. The experimental and theoretical results of palmitoyl chain in deuterated POPC samples (Figure 4.4D) showed a very good agreement; the profiles were nearly identical to those obtained for POPC-d_{31}/FFA-C16 mixture.

Figure 4.5 displays the electron density profiles, calculated from the MD trajectories, for the protonated FFA-C16 and FFA-C24 in POPC bilayers.

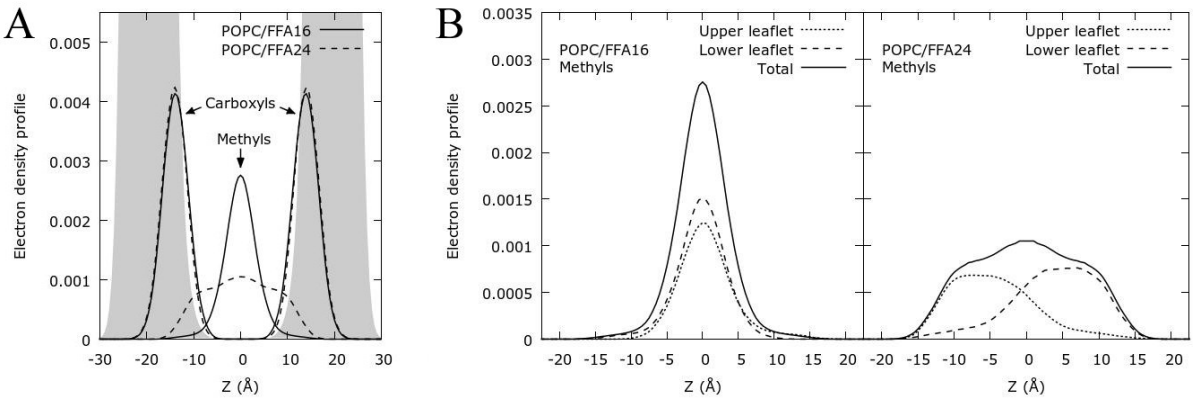

Figure 4.5. A) Average electron density profiles of the POPC phosphate group (in gray) and the fatty acid carboxyl and terminal methyl groups along the bilayers for the protonated FFA/POPC bilayers. B) Respective contribution of the terminal methyl of the fatty acids in each leaflet, the upper leaflet referring to the positive z values.

The carboxyl groups of either FFA were located at the same level of the interface, close to the bilayer interior, at ±14.0 Å from the bilayer center (Figure 4.5A). The results however reveal a drastic difference for the FFA terminal methyl group distribution. On one hand, FFA-C16 methyl location could be described by a Gaussian distribution centered at the middle of the bilayer; the distribution was similar for both upper and lower leaflets. FFA-C24 methyl groups, on the other hand, displayed a broader distribution. In fact the FFA-C24 chains protrude into the opposite leaflet of the bilayer and their methyl groups extend up to 15 Å into the opposite leaflet. Furthermore, the FFA-C24 methyl group distributions show a plateau over the range of 2-11 Å each side of the bilayer's center. Such distribution of the FFA-C24 methyl groups would lead to the second plateau with the small order parameters at the end of the FFA-C24 chain (Figure 4.4B). The distribution of the protonated FFAs in a POPC bilayer is noticeable from the representations of the final trajectory frames, presented in Figure 4.6.

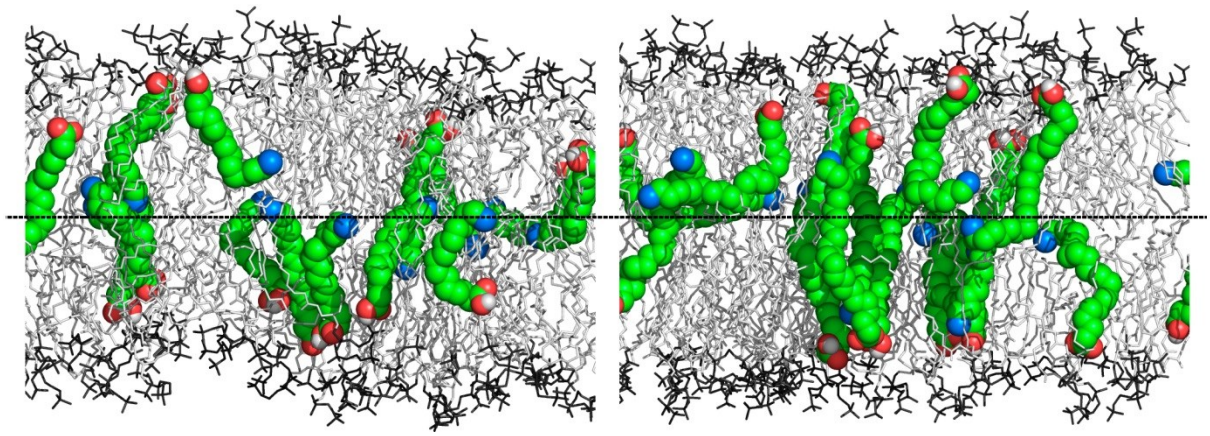

Figure 4.6. Representations of the final frame from the protonated FFA-C16 (left) and FFA-C24 (right) systems, from MD simulations. POPC molecules are shown as light gray sticks with polar heads in dark gray. FFA molecules are represented using a space-filling model where carbons are green, oxygens of the carboxylic groups are red, and terminal methyls are blue. The middle of the bilayer is indicated by a horizontal dashed line. Water molecules, hydrogens and some lipids were omitted for clarity.

The graphical snapshots of the POPC/FFA systems showed that the lipid organization was very similar to those of typical fluid membranes.[34] As predicted by the average electron density profiles, FFA polar heads were mainly located at the aqueous phase/hydrophobic core interface. The interdigitation of FFA-C24 into the opposite leaflet has been highlighted by adding a black line to indicate the middle of the bilayer. It is observed that the methyl group of several FFA-C24 molecules end up in the leaflet opposite to the one in which its polar head group is located. It also can be noticed that some FFA-C24 molecules have bent near the bilayer center. This interdigitation and higher concentration of FFA-C24 tails resulting from the bending near the bilayer center caused the second plateau observed in S_{C-D} profiles (Figure 4.4B).

All the above MD results were obtained assuming that FFA molecules were protonated. The apparent pKa of FFA inserted into fluid bilayers is considerably higher than the values for fatty acids in the monomeric form (estimated to be around 4.8).[40,41] The apparent pKa of hexacosanoic acid (FFA-C26) in an egg PC matrix (2 mol% of FFA) was estimated to 7.5.[13] This value is similar to the apparent pKa of oleic acid (FFA-C18:1) at a concentration of 5 mol% in egg PC vesicles, determined to be 7.6,[42] while the pKa of FFA-C16 in an equimolar mixture with cholesterol was estimated to be 8.2.[43] Therefore, the measurements carried out at pH 7.4 are in conditions near the apparent pKa and the protonation state of FFA in the investigated mixtures could influence the reported behavior. In order to assess the influence of the protonation of FFA on the behavior of POPC/FFA bilayers, ^{2}H NMR spectroscopy was carried out on samples at different pH and MD simulations were performed on the mixtures including completely deprotonated FFA. From an experimental point of view, we carried out ^{2}H NMR on samples at pH 5 (where it was assumed that FFAs were fully protonated) and 11 (where it was assumed that FFAs were fully deprotonated).

Figure 4.7 shows the spectra of POPC/FFA-C16d_{31} and POPC/FFA-C24d_{47} mixtures at pH 11; the spectra at pH 7.4 are included for comparison purposes the spectrum of POPC/FFA-C24d_{47} mixtures at pH 5 was also recorded (Supporting Information) and was found identical to that at pH 7.4.

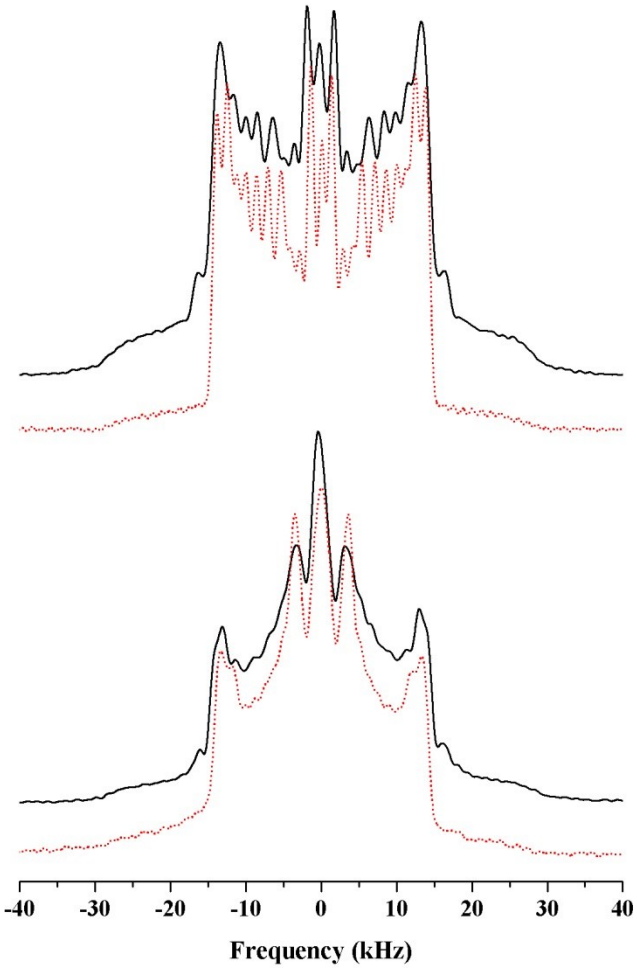

Figure 4.7. ^{2}H NMR spectra from POPC/FFA-C16d_{31} (top) and POPC/FFA-C24d_{47} (bottom) mixtures at pH 11 (black full) and pH 7.4 (red dotted); T = 25 ^{o}C.

Both deprotonated samples (*i.e.*, at pH 11) revealed the presence of a new small doublet at ±16.3 kHz. Furthermore, the mixture containing FFA-C24d_{47} showed a reduction on the signal at +2.5/+6 kHz and −2.5/−6 kHz, which was previously assigned to the CD_2 groups at the end of the acyl chain (Figure 4.7, bottom). For the POPC/FFA-C16d_{31} mixture, except for the aforementioned signal at high frequency, no other difference was found between the spectra at pH 7.4 and 11 (Figure 4.7, top).

MD simulations were carried out for the POPC/FFA systems assuming deprotonated FFAs. The resulting order profiles were compared with those obtained experimentally by ^{2}H NMR at pH 11 (Figure 4.8).

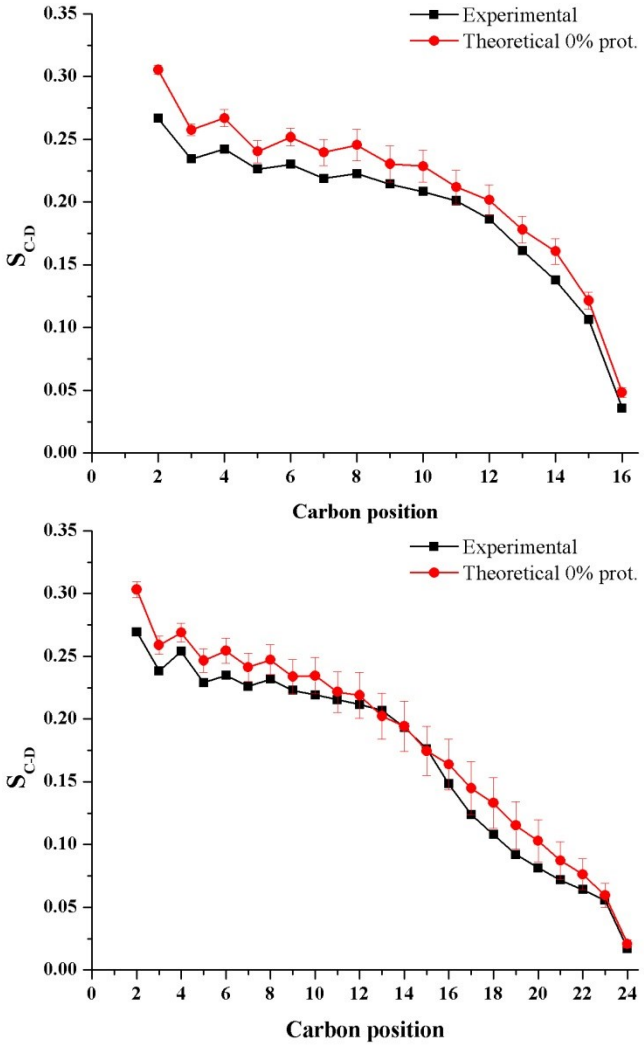

Figure 4.8. MD simulations (at 0% protonation) and experimental order profile (pH = 11) of FFAC16d_{31} (up) and FFA-C24d_{47} (bottom) in POPC/FFA mixtures.

The agreement between experimental and MD simulation values was good for both samples. MD simulations revealed that C2 methylene group has a relatively high order parameter of 0.30, in agreement with simulation results of deprotonated FFA obtained by

Yazdi *et al*.[44] This higher order parameter for C2 is due to a location closer to the lipid-water interface than for the protonated FFA (more on this below). Therefore, this group corresponded to the large quadrupolar splitting of 32.6 kHz observed on the spectra. The sample containing FFA-C16 displayed a typical order profile with a plateau region followed by a rapid decrease of S_{C-D} toward the end of the acyl chain. In conditions where the FFA-C24 was deprotonated, the plateau corresponding to low orientational order essentially disappeared and it was replaced by a quasi linear reduction of the S_{C-D} values.

The MD simulations allowed comparing the order profiles of the FFA and of the palmitoyl chain of POPC in the POPC/ FFA-C24 mixture; this comparison for the protonated and deprotonated FFA24 is presented in Figure 4.9.

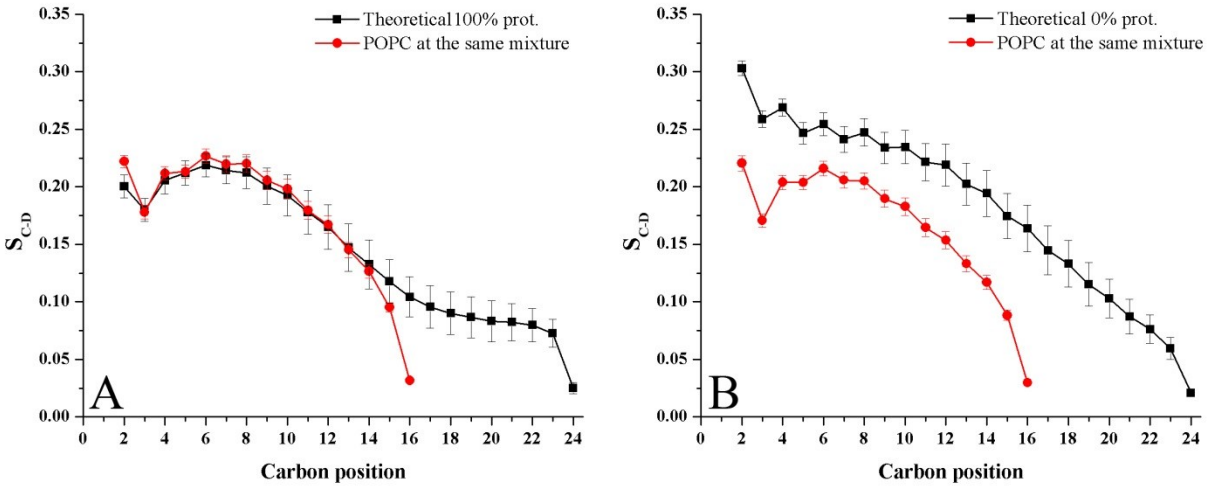

Figure 4.9. MD simulations order profiles of POPC/FFA-C24 mixture with (A) fully protonated, and (B) fully deprotonated FFA-C24. ■ : orientational order of FFA-C24, and ● : orientational order of POPC palmitoyl chain.

On one hand, the plateau region of protonated FFA-C24 and POPC showed very similar values of S_{C-D} (Figure 4.9A). In addition, the S_{C-D} values at the second plateau of the

FFA-C24 chain (from C15 to C23) were between 0.1 and 0.07, which is very similar to the value of C15 in the palmitoyl chain of POPC (0.08). This result indicates that the ends of both acyl chains experience a similar disorder. On the other hand, the deprotonated FFA-C24 showed S_{C-D} values higher than the protonated form (with an average increase of about 0.04), suggesting that the FFA-C24 molecules in POPC mixtures were more ordered in their ionized form (Figure 4.9B). POPC acyl chains were not significantly affected by the ionization of the FFA-C24, as both profiles remain nearly identical. A similar analysis for the POPC/FFA-C16 system was made (Supporting Information). In this mixture, it was also noticed an average increase of about 0.05 in the S_{C-D} values, showing that the acyl chain of FFA-C16, analogous to FFA-C24, was more ordered when deprotonated.

Figure 4.10 shows the electron density profiles obtained from the MD trajectories, for the POPC phosphate, the carboxyl and methyl groups of the deprotonated FFA-C16d_{31}, and FFA-C24d_{47} in POPC bilayers.

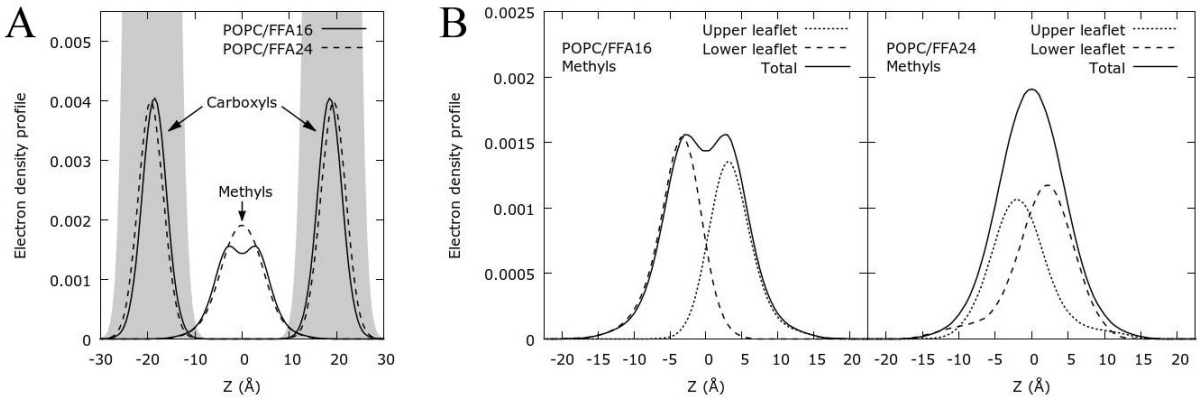

Figure 4.10. A) Average electron density profiles of the POPC phosphate (in gray), the fatty acid carboxyl and terminal methyl groups along the bilayers for the deprotonated FFA/POPC bilayers. B) Respective contribution of the terminal methyl of the fatty acid in each leaflet, the upper leaflet referring to the positive z values.

In contrast to the protonated FFAs, the carboxyl groups of ionized FFAs were located at the water-lipid interface, at ±19.5 Å from the middle of the bilayer (Figure 4.10A and Figure 4.5A). The presence of a charged carboxylate group drove the FFA molecules to be more exposed to the aqueous environment. The shift hindered the motion of the FFA acyl chain that became more ordered, as noticed from the FFA-C24 order parameters (Figure 4.8A). Moreover, it modifies the distribution of the terminal methyl groups. For the deprotonated acid, FFA-C16 methyl groups were located in the middle of the bilayers but they remained mainly in their respective leaflet, causing a small dip at the bilayer center. In contrast, FFA-C24 methyl groups led to a slight interdigitation, penetrating in the opposite leaflet by about 2 to 3 Å (Figure 4.10B). As a result, a Gaussian-like overall distribution centered at the middle of the bilayers was obtained. In this mixture, the deprotonation of the acid caused a considerable reduction in chain interdigitation; this finding is at the origin of the disappearance of the second plateau observed in the order profiles (Figure 4.8). These differences between the deprotonated- and protonated-FFA-C24 locations in POPC bilayers are also noticeable from the representations of the trajectory frames (Figure 4.11).

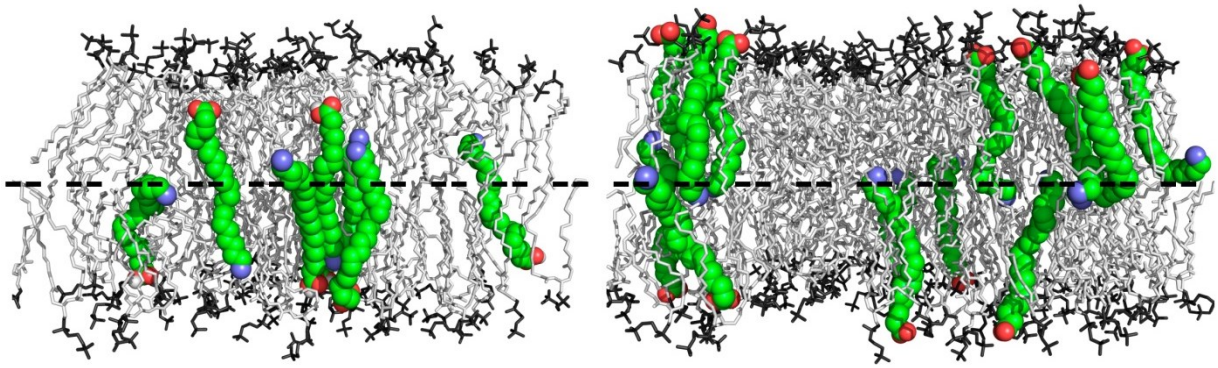

Figure 4.11. Representations of the final frame from the protonated (left) and deprotonated (right) FFA-C24 systems from MD simulations.

While protonated FFA-C24 head groups were found slightly inside the bilayer and the methyl groups mainly in the opposite leaflet, the deprotonated FFA-C24 head groups were located in the aqueous interphase at the same level of phosphate groups, and the alkyl chains showed very limited interdigitation.

The present study reveals that the order of the POPC molecules in the liquid-crystalline (L_α) phase is not significantly affected by the presence of long-chain fatty acid (FFA-C16) or VLCFA (FFA-C20 and FFA-C24), when its concentration is 7.5 mol%. It has been shown that the addition of 20% of FFA-C16 into fluid DPPC membranes increased the phospholipid order; the S_{C-D} values of DPPC-d_{62} in the presence of FFA-C16 are approximately 10% higher than those observed for pure DPPC bilayer.[37] Moreover, the presence of FFA-C16 increased the temperature of the gel-to-L_α phase transition by 2 °C.[37] This stabilization of DPPC membranes by FFA-C16 molecules has been associated with their ability to fill the voids in the apolar region of the bilayers, which are created by the crowding of the DPPC head groups. The incorporation of FFA-C16 would not only decrease the destabilizing effect of head group crowding but also increase the van der Waals interactions in the hydrocarbon core, leading to a more stable system.[37] However, our results show that the incorporation of FFA of various chain lengths between C16 and C24 does not perturb significantly the surrounding phospholipids when its proportion is limited to 7.5 mol%.

We show that the degree of protonation affects the position and the order of the FFAs in phospholipid membranes. MD simulations showed that the protonated FFA carboxyl groups are located at around 14 Å from the bilayer center, at the interface of the phospholipid polar head groups and their alkyl chains (Figures 4.5A and 4.6A). The S_{C-D} values of the plateau region for the investigated FFAs were nearly identical to that of the palmitoyl chain of POPC,

irrespective of their length (Figure 4.3). These similarities in S_{C-D} values at the plateau region of FFAs and palmitoyl chain of POPC corroborate the location of FFA molecules at the POPC head group level. The values of order parameters as well as the plateau length are affected, among other factors, by changes of bilayer lateral pressure.[36] Carbons located at the same level experience generally the same lateral pressure, and would display similar order parameters.

The location of protonated FFAs favors their interaction at the bilayer center and with the opposite leaflet, depending of their chain length. FFA-C24 shows an important interdigitation toward the opposite leaflet, which causes a second plateau observed at low S_{C-D} values in the orientational order profiles. The reduction of the signal associated with methylene groups with low orientational order in FFA-C20d_{39} (Figure 4.1) suggests an interdigitation of the FFA chains that would be more limited. The length of FFA-C16 acyl chain does not lead to significant interaction with the lipids of the opposite leaflet.

There are three possibilities that could describe how VLCFA adapts in fluid phospholipid membranes: (i) protrusion, (ii) bending in the bilayer center, and (iii) interdigitation. The present results indicate that the first option is unfavorable and the adaptation is introduced by a combination of the last two possibilities; a very disordered terminal segment and chain interdigitation. The hydrophobic core of L_α-phase bilayers includes a considerable free volume at the bilayer center that allows the highly flexible linear and saturated alkyl chains to interdigitate. Interdigitation appears to be favored from a free energy point of view compared to the protrusion of FFA since the latter would imply a significant exposure of its apolar chain to the aqueous environment. A deep interdigitation of very long alkyl chain, as that observed in the system characterized in the present work, would

result in strengthened interchain interactions because of the better chain packing while keeping the conformational entropy.[47]

A similar behavior was inferred for highly asymmetric lipids bearing an acyl chain of 24 carbon atoms.[18,19] The smoothed orientational order profiles of PC with highly asymmetric acyl chains in L_α-phase bilayers showed the presence of a second plateau at low S_{C-D} values,[18] similar to the findings of the present work. Such second plateau was not found for the symmetric-chain analogues. A recent molecular dynamics simulation of lipid membranes that included highly asymmetric-chain SM molecules[19] reported that the very long chains of SM interdigitated deep into the opposing membrane leaflet. This feature is proposed to be characteristic of lipids bearing a very long acyl chain that exceeds the thickness of their leaflet. The extent of chain interdigitation in POPC fluid membranes is modulated by the FFA chain length and was found negligible when bilayer-matching FFA (FFA-C16) was selected.

When FFA molecules are deprotonated, their head groups are more exposed to the aqueous phase to ensure the proper hydration of the charged carboxylate group (Figures 4.10 and 4.11). This location increases the order of the acyl chains since they experience the high lateral pressure existing near the head group region; both MD simulations and ^{2}H NMR results show an increase in the average S_{C-D} values of about 0.04. Interestingly, the location of the molecule head group at the aqueous interphase causes the disappearance of the second plateau in FFA-C24 order profile and reduces considerably the interdigitation in the opposite leaflet. The protonation state of FFA is therefore a parameter that modulates the chain interdigitation and the coupling between the two leaflets of fluid bilayers.

Chain interdigitation is a phenomenon that could certainly affect the physicochemical properties of bilayers. For example, it could contribute to the increase in microviscosity of erythrocyte membranes observed in patients whose diseases led to an increased proportion of VLCFA.[12] The interdigitation of the VLCFA could cause an increased shear stress between both leaflets that would slow down lipid lateral diffusion. This hypothesis is supported by a previous MD study[48] that concluded that the intermonolayer friction in fluid bilayers would be increased by lipid interdigitation. Lipid interdigitation has been proposed to contribute to leaflet coupling in membranes. Such phenomenon could play a role in membrane events, such as signal transduction and lateral segregation of molecules. The extent of this contribution is modulated in a straightforward manner by the acyl chain mismatch−by the chain length *per se* or by the translation of the amphiphile as demonstrated by the protonation/deprotonation of FFA; this phenomenon could therefore be exploited to regulate some cellular processes.

4.5 Supporting Information

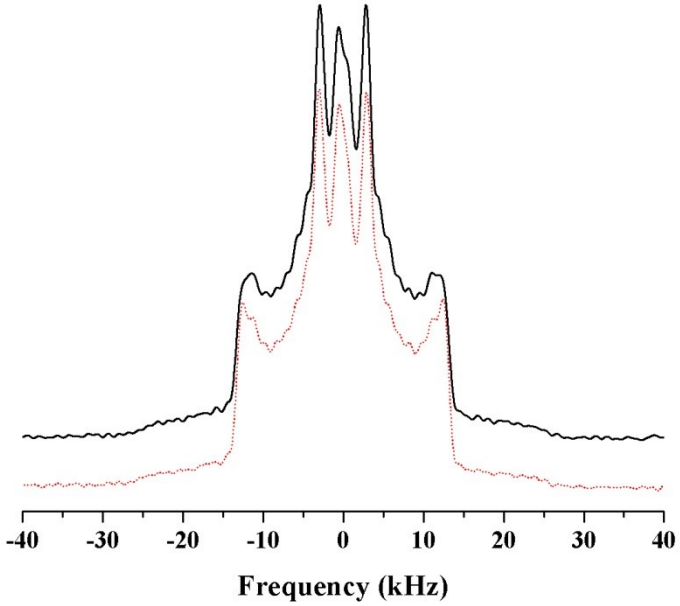

Figure 4.S1. ^{2}H NMR spectra from POPC/FFA-C24d_{47} mixtures at pH 5 (black full) and pH 7.4 (red dotted); T = 25 ^{o}C.

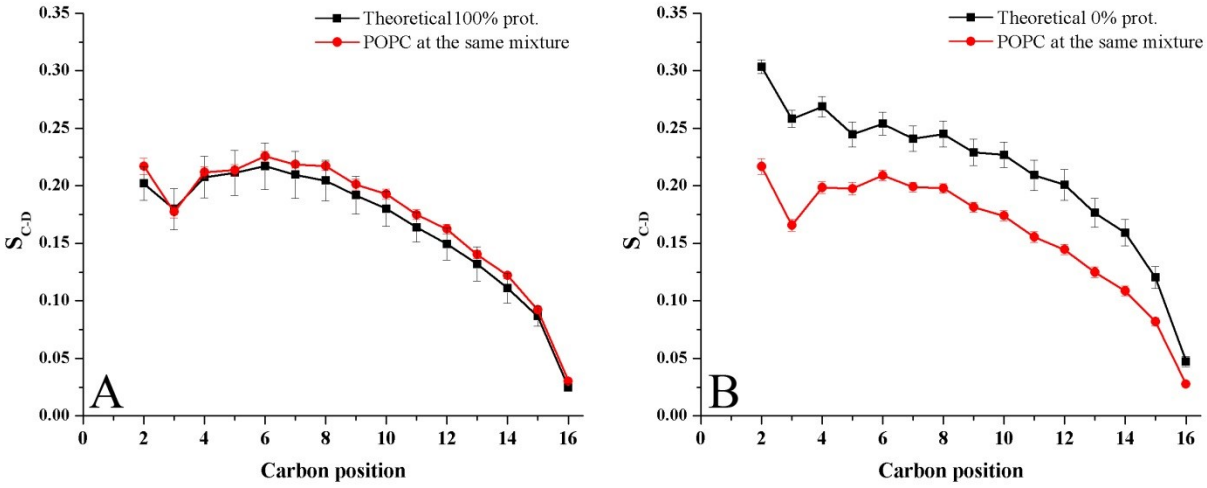

Figure 4.S2. Theoretical order profiles of POPC/FFA-C16 mixture with (A) fully protonated, and (B) fully unprotonated FFA-C24. ■ : orientational order of FFA-C24, and ● :orientational order of POPC palmitoyl chain.

4.6 Acknowledgments

We thank the Natural Sciences and Engineering Research Council (NSERC) of Canada for the financial support. A.P.R. thanks the Fonds Quebecoiś de la Recherche sur la Nature et les Technologies (FQRNT) for his Doctoral Research Scholarship for Foreign Students. This work was also funded by the FQRNT through its financial support of the Center for Self-Assembled Chemical Structures (CSACS). We thank Compute Canada and Calcul Quebeć for the provision of computer time on the Helios supercomputer.

4.7 References

(1) Mouritsen, O. G.; Bloom, M. Mattress model of lipid-protein interactions in membranes. *Biophys. J.* **1984**, *46*, 141-153.

(2) Killian, J. A. Hydrophobic mismatch between proteins and lipids in membranes. *Biochim. Biophys. Acta* **1998**, *1376*, 401-416.

(3) Bloom, M.; Mouritsen, O. G. The evolution of membranes. In *Handbook of Biological Physics*, **1995**; Vol. Structure and Dynamics of Membranes, 65-95.

(4) Bretscher, M. S.; Munro, S. Cholesterol and the Golgi apparatus. *Science* **1993**, *261*, 1280-1281.

(5) Sonnino, S.; Prinetti, A. Membrane domains and the “lipid raft” concept. *Curr. Med. Chem.* **2013**, *20*, 4-21.

(6) McIntosh, T. J. The 2004 Biophysical Society-Avanti Award in Lipids address: roles of bilayer structure and elastic properties in peptide localization in membranes. *Chem. Phys. Lipids* **2004**, *130*, 83-98.

(7) Hodson, L.; Skeaff, C. M.; Fielding, B. A. Fatty acid composition of adipose tissue and blood in humans and its use as a biomarker of dietary intake. *Prog. Lipid Res*. **2008**, *47*, 348-380.

(8) Baarine, M.; Ragot, K.; Athias, A.; Nury, T.; Kattan, Z.; Genin, E. C.; Andreoletti, P.; Ménétrier, F.; Riedinger, J.-M.; Bardou, M., *et al*. Incidence of Abcd1 level on the induction of cell death and organelle dysfunctions triggered by very long chain fatty acids and TNF-α on oligodendrocytes and astrocytes. *NeuroToxicology* **2012**, *33*, 212-228.

(9) Wanders, R. J. A.; van Roermund, C. W. T.; van Wijland, M. J. A.; Heikoop, J.; Schutgens, R. B. H.; Schram, A. W.; Tager, J. M.; van den Bosch, H.; Poll-Thé, B. T.; Saudubray, J. M., *et al*. Peroxisomal very long-chain fatty acid β-oxidation in human skin fibroblasts: activity in Zellweger syndrome and other peroxisomal disorders. *Clin. Chim. Acta* **1987**, *166*, 255-263.

(10) Marchetti, D. P.; Donida, B.; da Rosa, H. T.; Manini, P. R.; Moura, D. J.; Saffi, J.; Deon, M.; Mescka, C. P.; Coelho, D. M.; Jardim, L. B., *et al*. Protective effect of antioxidants on DNA damage in leukocytes from X-linked adrenoleukodystrophy patients. *Int. J. Dev. Neurosci*. **2015**, *43*, 8-15.

(11) Moser, H. W.; Moser, A. B.; Frayer, K. K.; Chen, W.; Schulman, J. D.; O'Neill, B. P.; Kishimoto, Y. Adrenoleukodystrophy: increased plasma content of saturated very long chain fatty acids. *Neurology* **1981**, *31*, 1241-1249.

(12) Knazek, R. A.; Rizzo, W. B.; Schulman, J. D.; Dave, J. R. Membrane microviscosity is increased in the erythrocytes of patients with adrenoleukodystrophy and adrenomyeloneuropathy. *J. Clin. Invest*. **1983**, *72*, 245-248.

(13) Ho, J. K.; Moser, H.; Kishimoto, Y.; Hamilton, J. A. Interactions of a very long chain fatty acid with model membranes and serum albumin. Implications for the pathogenesis of adrenoleukodystrophy. *J. Clin. Invest*. **1995**, *96*, 1455-1463.

(14) Zhang, F.; Kamp, F.; Hamilton, J. A. Dissociation of long and very long chain fatty acids from phospholipid bilayers. *Biochemistry* **1996**, *35*, 16055-16060.

(15) Pillai, B. K.; Jasuja, R.; Simard, J. R.; Hamilton, J. A. Fast diffusion of very long chain saturated fatty acids across a bilayer membrane and their rapid extraction by cyclodextrins: implications for Adrenoleukodystrophy. *J. Biol. Chem*. **2009**, *284*, 33296-33304.

(16) Lewis, R. N.; McElhaney, R. N. Studies of mixed-chain diacyl phosphatidylcholines with highly asymmetric acyl chains: a Fourier transform infrared spectroscopic study of interfacial hydration and hydrocarbon chain packing in the mixed interdigitated gel phase. *Biophys. J.* **1993**, *65*, 1866-1877.

(17) Zhu, T.; Caffrey, M. Thermodynamic, thermomechanical, and structural properties of a hydrated asymmetric phosphatidylcholine. *Biophys. J.* **1993**, *65*, 939-954.

(18) Lewis, R. N.; McElhaney, R. N.; Monck, M. A.; Cullis, P. R. Studies of highly asymmetric mixed-chain diacyl phosphatidylcholines that form mixed-interdigitated gel phases: Fourier transform infrared and ^{2}H NMR spectroscopic studies of hydrocarbon chain conformation and orientational order in the liquid-crystalline state. *Biophys. J.* **1994**, *67*, 197-207.

(19) Róg, T.; Orłowski, A.; Llorente, A.; Skotland, T.; Sylvänne, T.; Kauhanen, D.; Ekroos, K.; Sandvig, K.; Vattulainen, I. Interdigitation of long-chain sphingomyelin induces coupling of membrane leaflets in a cholesterol dependent manner. *Biochim. Biophys. Acta* **2016**, *1858*, 281-288.

(20) Davis, J. H. The description of membrane lipid conformation, order and dynamics by 2H-NMR. *Biochim. Biophys. Acta* **1983**, *737*, 117-171.

(21) Paré, C.; Lafleur, M. Formation of liquid ordered lamellar phases in the palmitic acid/cholesterol system. *Langmuir* **2001**, *17*, 5587-5594.

(22) Seeling, J.; Seeling, A. Lipid conformation in model membranes and biological membranes. *Q. Rev. Biophys*. **1980**, *13*, 19-61.

(23) Sternin, E.; Bloom, M.; Mackay, A. L. De-pake-ing of NMR spectra. *J. Magn. Reson*. **1983**, *55*, 274-282.

(24) Lafleur, M.; Fine, B.; Sternin, E.; Cullis, P. R.; Bloom, M. Smoothed orientational order profile of lipid bilayers by 2H-nuclear magnetic resonance. *Biophys. J.* **1989**, *56*, 1037-1041.

(25) Jo, S.; Kim, T.; Iyer, V. G.; Im, W. CHARMM-GUI: A web-based graphical user interface for CHARMM. *J. Comput. Chem*. **2008**, *29*, 1859-1865.

(26) Phillips, J. C.; Braun, R.; Wang, W.; Gumbart, J.; Tajkhorshid, E.; Villa, E.; Chipot, C.; Skeel, R. D.; Kalé, L.; Schulten, K. Scalable molecular dynamics with NAMD. *J. Comput. Chem*. **2005**, *26*, 1781-1802.

(27) Klauda, J. B.; Venable, R. M.; Freites, J. A.; O'Connor, J. W.; Tobias, D. J.; Mondragon-Ramirez, C.; Vorobyov, I.; MacKerell, A. D.; Pastor, R. W. Update of the CHARMM all-atom additive force field for lipids: validation on six lipid types. *J. Phys. Chem*. **2010**, *114*, 7830-7843.

(28) Best, R. B.; Zhu, X.; Shim, J.; Lopes, P. E. M.; Mittal, J.; Feig, M.; MacKerell, A. D. Optimization of the additive CHARMM all-atom protein force field targeting improved sampling of the backbone ϕ, ψ and side-chain $\chi 1$ and $\chi 2$ dihedral angles. *Chem. Theory Comput.* **2012**, *8*, 3257-3273.

(29) Jorgensen, W. L.; Chandrasekhar, J.; Madura, J. D.; Impey, R. W.; Klein, M. L. Comparison of simple potential functions for simulating liquid water. *J. Chem. Phys*. **1983**, *79*, 926-935.

(30) Durell, S. R.; Brooks, B. R.; Ben-Naim, A. Solvent-induced forces between two hydrophilic groups. *J. Phys. Chem*. **1994**, *98*, 2198-2202.

(31) Darden, T.; York, D.; Pedersen, L. Particle mesh Ewald: an N·log(N) method for Ewald sums in large systems. *J. Chem. Phys*. **1993**, *98*, 10089-10092.

(32) Lagüe, P.; Pastor, R. W.; Brooks, B. R. Pressure-based long-range correction for Lennard-Jones interactions in molecular dynamics simulations: application to alkanes and interfaces. *J. Phys. Chem*. **2004**, *108*, 363-368.

(33) Porasso, R. D.; López Cascales, J. J. A criterion to identify the equilibration time in lipid bilayer simulations. *Pap. Phys*. **2012**, *4*, 1-10.

(34) Pastor, R. W.; Venable, R. M.; Feller, S. E. Lipid bilayers, NMR relaxation, and computer simulations. *Acc. Chem. Res*. **2002**, *35*, 438-446.

(35) Seelig, A.; Seelig, J. Dynamic structure of fatty acyl chains in a phospholipid bilayer measured by deuterium magnetic resonance. *Biochemistry* **1974**, *13*, 4839-4845.

(36) Lafleur, M.; Cullis, P. R.; Bloom, M. Modulation of the orientational order profile of the lipid acyl chain in the L_α phase. *Eur. Biophys. J*. **1990**, *19*, 55-62.

(37) Pauls, K. P.; MacKay, A. L.; Bloom, M. Deuterium nuclear magnetic resonance study of the effects of palmitic acid on dipalmitoylphosphatidylcholine bilayers. *Biochemistry* **1983**, *22*, 6101-6109.

(38) Shaikh, S. R.; Kinnun, J. J.; Leng, X.; Williams, J. A.; Wassall, S. R. How polyunsaturated fatty acids modify molecular organization in membranes: insight from NMR studies of model systems. *Biochim. Biophys. Acta* **2015**, *1848*, 211-219.

(39) Petrache, H. I.; Dodd, S. W.; Brown, M. F. Area per lipid and acyl length distributions in fluid phosphatidylcholines determined by ^{2}H NMR spectroscopy. *Biophys. J.* **2000**, *79*, 3172-3192.

(40) Cistola, D. P.; Small, D. M.; Hamilton, J. A. Ionization behavior of aqueous short-chain carboxylic acids: a carbon-13 NMR study. *J. Lipid Res*. **1982**, *23*, 795-799.

(41) Spector, A. A. Fatty acid binding to plasma albumin. *J. Lipid Res*. **1975**, *16*, 165-179.

(42) Hamilton, J. A.; Cistola, D. P. Transfer of oleic acid between albumin and phospholipid vesicles. *Proc. Natl. Acad. Sci. USA* **1986**, *83*, 82-86.

(43) Ouimet, J.; Croft, S.; Paré, C.; Katsaras, J.; Lafleur, M. Modulation of the polymorphism of the palmitic acid/cholesterol system by the pH. *Langmuir* **2003**, *19*, 1089-1097.

(44) Yazdi, S.; Stein, M.; Elinder, F.; Andersson, M.; Lindahl, E. The molecular basis of polyunsaturated fatty acid interactions with the shaker voltage-gated potassium channel. *PLoS Comput. Biol*. **2016**, *12*, e1004704.

(45) Falck, E.; Patra, M.; Karttunen, M.; Hyvönen, M. T.; Vattulainen, I. Lessons of Slicing Membranes: Interplay of Packing, Free Area, and Lateral Diffusion in Phospholipid/Cholesterol Bilayers. *Biophys. J.* **2004**, *87*, 1076-1091.

(46) Marrink, S. J.; Sok, R. M.; Berendsen, H. J. C. Free volume properties of a simulated lipid membrane. *J. Chem. Phys.* **1996**, *104*, 9090-9099.

(47) Chiantia, S.; London, E. Acyl chain length and saturation modulate interleaflet coupling in asymmetric bilayers: effects on dynamics and structural order. *Biophys. J.* **2012**, *103*, 2311-2319.

(48) Niemelä, P. S.; Hyvönen, M. T.; Vattulainen, I. Influence of chain length and unsaturation on sphingomyelin bilayers. *Biophys. J.* **2006**, *90*, 851-863.

(49) Nickels, J. D.; Smith, J. C.; Cheng, X. Lateral organization, bilayer asymmetry, and inter-leaflet coupling of biological membranes. *Chem. Phys. Lipids* **2015**, *192*, 87-99.

Chapitre 5: Conclusion

5.1 Conclusions générales

Les travaux réalisés au cours de cette thèse ont permis d'approfondir la compréhension de la structure et le comportement de membranes modèles du SC. Premièrement, nous avons montré que la longueur de chaîne des acides gras formant des mélanges ternaires avec le céramide NS24 et le cholestérol, a un impact sur les propriétés physico-chimiques du mélange. En utilisant de l'acide lignocérique (FFA24), nous avons obtenu un échantillon homogène, résultat d'une meilleure interaction entre les différents composants du mélange. De plus, nous avons trouvé que le FFA24 subissait une transition de la phase solide à la phase gel. La combinaison de chaînes ordonnées et de membranes homogènes contribue probablement de manière fondamentale à l'imperméabilité du SC. En effet, certains travaux publiés à la suite de notre étude dans le Chapitre 2 ont montré qu'un mélange homogène montre une faible perméabilité de la membrane au passage des substances.[1-2] Par exemple, Uchiyama et coll.[1] ont montré qu'un mélange identique au nôtre (CerNS24/FFA24/Chol) était plus imperméable à l'acide éthyle-*p*-aminobenzoïque (E-PABA) (environ 7 fois plus imperméable après 5 h de contact avec le produit) qu'un mélange qui utilisait plusieurs acides gras entre 16 et 24 atomes de carbone (CerNS24/FFAs/Chol). Ils ont trouvé aussi que les acides à chaîne courte (FFA16 et FFA18) dans le mélange sont plus désordonnés, ce qui affecterait l'imperméabilité de cette membrane.

Plus récemment, Pullmannová et coll.[2] ont étudié l'influence de la longueur de chaîne de céramide NS (NS16 et NS24) dans un mélange de CerNS/FFAs/Chol/CholS. Dans cette étude, le céramide NS16 a provoqué la formation de domaines cristallins séparés, tandis que le

céramide NS24 favorisait la formation d'un mélange plutôt homogène. Comme résultat, le mélange moins homogène était jusqu'à 53 % plus perméable à l'eau, 55 % à la théophylline et 120 % plus perméable à l'indométacine.[2] Présentement, l'utilisation d'acides gras et de céramides à longue chaîne (C24), en plus du cholestérol, est devenue la norme pour l'élaboration de membranes modèles du SC.

Nous avons par la suite étudié des mélanges plus complexes, contenant les céramides EOS et NS, un mélange d'acides gras, ainsi que le cholestérol. Dans cette étude, nous avons montré des évidences spectroscopiques de la présence de domaines hautement désordonnés (liquides), constitués par les chaînes oléate du céramide EOS, au cœur de la phase solide cristalline du mélange. Jusqu'à présent, le céramide EOS était considéré une composante essentielle pour la formation de la phase de périodicité longue, mais la formation de nanodomaines liquides n'avait jamais été rapportée. La présence de domaines liquides dans la matrice lipidique du SC modifie l'idée générale que nous avons sur la barrière cutanée. Présentement, l'imperméabilité du SC est associée à la présence des cornéocytes et aux lipides à l'état solide cristallin dans la matrice lipidique. Sur la base des travaux de la thèse, il est proposé que les nanogouttelettes de nature hydrophobe peuvent agir comme des obstacles à la diffusion des molécules hydrophiles à travers le SC ou peuvent servir de pièges pour les espèces apolaires est un concept totalement nouveau.

La présence de nanogouttelettes pourrait aussi expliquer aussi le mécanisme d'action de certains agents transdermiques. Ces produits sont utilisés pour améliorer la diffusion de différents produits à travers la peau. Il est supposé que ces agents transdermiques agissent en fluidifiant la partie cristalline des membranes lipidiques. Cependant, la manière dont cela se produit n'est pas entièrement établie. De manière alternative, il est proposé que les agents

transdermiques s'accumulent dans les nanogouttelettes, augmentant progressivement leur taille. À cause de cela, ces structures pourraient entrer en contact, créant un passage continu à travers la matrice solide cristalline pour la libre diffusion des molécules par un mécanisme de percolation (Figure 5.1).

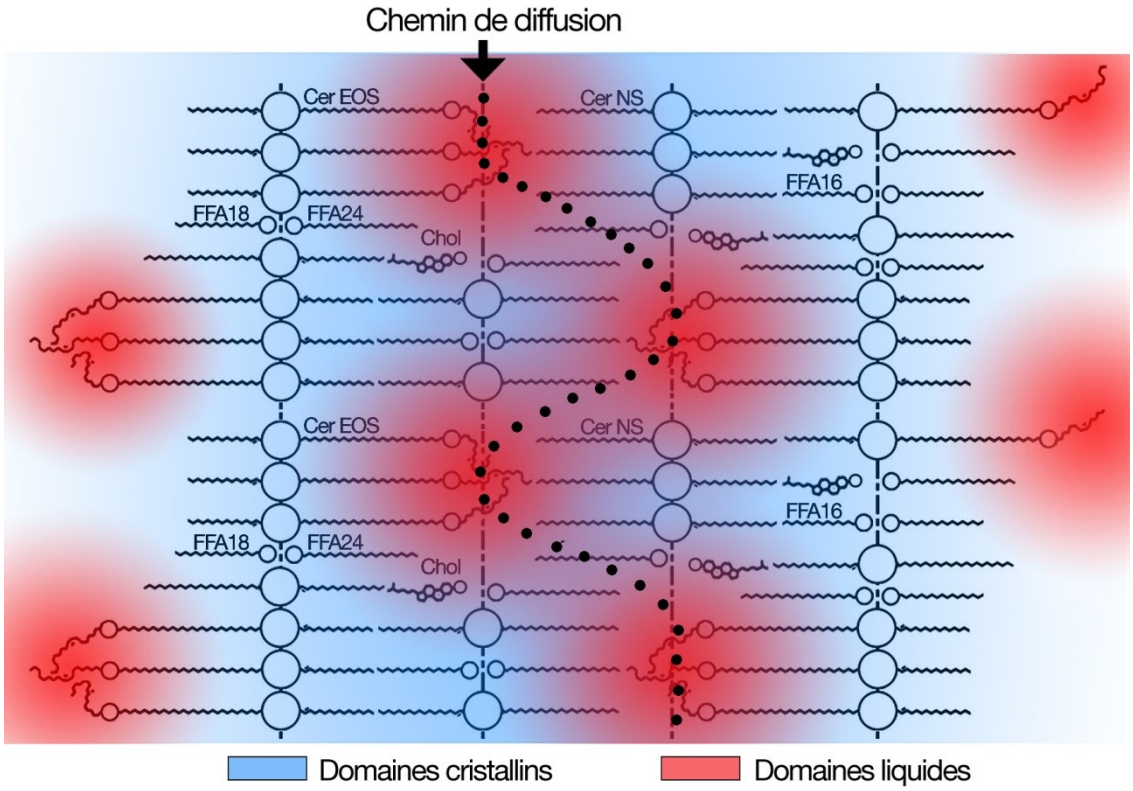

Figure 5.1. Représentation schématique de la section transversale de l'effet d'un agent transdermique menant à la percolation des nanogoutelettes.

Récemment, Eichner et coll.[3] ont étudié l'interaction du myristate d'isopropyle, un agent transdermique, avec une membrane modèle du SC composée de céramides AP et EOS, d'acide béhénique (FFA22) et de cholestérol. Les résultats obtenus par ^{2}H RMN ont montré que le myristate se trouve dans un état très désordonné (liquide) à l'intérieur du mélange lipidique, d'une façon très similaire aux chaînes oléates du céramide EOS de notre mélange.

Les auteurs concluent que le myristate d'isopropyle perturbe la structure lamellaire de la membrane et empêche la formation de la LPP. Par contre, ils n'ont pu dégager aucune information sur la localisation des molécules de myristate à l'intérieur de la structure. Ces résultats nous ont suggéré un possible mécanisme d'interaction entre les agents transdermiques et les nanogouttelettes.

Finalement, nous avons étudié l'interaction d'acides gras à très longue chaîne avec des membranes de POPC afin de déterminer l'effet des contraintes spatiales sur les chaînes acyles de lipides. Nos résultats de ^{2}H RMN et de simulations de dynamique moléculaire ont montré que la partie inférieure de la chaîne acyle de l'acide lignocérique (FFA24) protoné est très désordonnée, d'une façon similaire à ce qui a été observé pour la chaîne oléate du céramide EOS. Par contre, en opposition au comportement observé pour la chaîne oléate, qui formait des nanogouttelettes à cause des restrictions stériques, la chaîne de l'acide lignocérique s'insère dans la partie très désordonnée du feuillet opposé. Ce phénomène est possible car la membrane formée par des phospholipides est en phase fluide; il est facile pour l'acide lignocérique de sortir de son confinement stérique vers le feuillet opposé. Pour le SC, l'empilement des lipides est très compact et en phase solide, donc il est très difficile pour les chaînes oléate de sortir de l'espace restreint. Il est donc proposé que le confinement stérique associé à un empilement très particulier des lipides du SC joue un rôle fondamental dans la structure et la fonction du SC.

5.2 Perspectives

En premier lieu, nous considérons que des études supplémentaires devront être réalisées afin de valider la présence de nanogouttelettes dans les membranes modèles et le SC natif. Malheureusement, il est très difficile de visualiser ces structures par les techniques conventionnelles à cause de leur taille nanométrique. Une approche possible est l'utilisation d'un appareil IR-AFM. Cet instrument qui combine la spectroscopie infrarouge avec la microscopie à force atomique (AFM) permet de caractériser les régions plus désordonnées (domaines liquides) dans l'échantillon à partir de la position des bandes dans le spectre infrarouge, avec la résolution nanométrique de la pointe AFM (environ 10 nm). Cette technique a été récemment utilisée pour la caractérisation du SC.[4-5] Comme les lipides du SC natif sont tous hydrogénés, l'analyse devra se faire sur la bande d'élongation symétrique du lien C-H des méthylènes située autour de 2850 cm^{-1}. La présence d'une région très désordonnée dans la matrice cristalline déplacerait la position de la bande de 3 à 4 cm^{-1} vers les hautes fréquences.[6] Si cette petite variation est observable dans les spectres, il sera possible de localiser les nanogouttelettes et de les représenter sur une image chimique et sur une image de microscopie à force atomique.

Il serait également intéressant dans le futur de poursuivre la caractérisation de mélanges modèles en incluant d'autres lipides présents dans la matrice lipidique du SC natif. Les céramides NP et AP sont parmi les espèces de céramides les plus abondantes dans le SC humain, représentant, respectivement, environ 18 % et 6 % en poids du contenu des céramides dans le SC.[7] La présence de ces deux céramides est essentielle pour la formation de la phase de périodicité courte dans certaines membranes modèles du SC.[8-9] Il serait intéressant d'étudier le comportement de ces lipides dans un mélange contenant une série d'acides gras,

les céramides EOS et NS, ainsi que le cholestérol afin de déterminer l'impact de chacun sur la structure globale de cet arrangement lipidique. Ces travaux sont nécessaires pour faire progresser nos connaissances sur l'imperméabilité de la peau et nos approches pour améliorer l'administration transdermique de médicaments.

Finalement, il pourrait être intéressant de préparer des mélanges modèles où on fait varier la proportion de phase liquide et d'étudier l'influence de ce paramètre sur la perméabilité. La proportion de phase liquide/solide pourrait être déterminée par ^{2}H RMN.[10] De cette manière, il sera possible d'établir la relation structure/perméabilité dans ces mélanges.

5.3 Références

(1) Uchiyama, M.; Oguri, M.; Mojumdar, E. H.; Gooris, G. S.; Bouwstra, J. A. Free fatty acids chain length distribution affects the permeability of skin lipid model membranes. *Biochim. Biophys. Acta* **2016**, *1858*, 2050-2059.

(2) Pullmannová, P.; Pavlíková, L.; Kováčik, A.; Sochorová, M.; Školová, B.; Slepička, P.; Maixner, J.; Zbytovská, J.; Vávrová, K. Permeability and microstructure of model stratum corneum lipid membranes containing ceramides with long (C16) and very long (C24) acyl chains. *Biophys. Chem.* **2017**, *224*, 20-31.

(3) Eichner, A.; Stahlberg, S.; Sonnenberger, S.; Lange, S.; Dobner, B.; Ostermann, A.; Schrader, T. E.; Hauß, T.; Schroeter, A.; Huster, D., et al. Influence of the penetration enhancer isopropyl myristate on stratum corneum lipid model membranes revealed by neutron diffraction and 2H NMR experiments. *Biochim. Biophys. Acta* **2017**, *1859*, 745-755.

(4) Marcott, C.; Lo, M.; Kjoller, K.; Domanov, Y.; Balooch, G.; Luengo, G. S. Nanoscale infrared (IR) spectroscopy and imaging of structural lipids in human stratum corneum using an atomic force microscope to directly detect absorbed light from a tunable IR laser source. *Exp. Dermatol.* **2013**, *22*, 419-421.

(5) Goh, C. F.; Moffat, J. G.; Craig, D. Q. M.; Hadgraft, J.; Lane, M. E. Nano-thermal imaging of the stratum corneum and its potential use for understanding of the mechanism of skin penetration enhancer. *Thermochim. Acta* **2017**, *655*, 278-283.

(6) Moore, D. J.; Rerek, M. E.; Mendelsohn, R. Lipid domains and orthorhombic phases in model stratum corneum: evidence from Fourier transform infrared spectroscopy studies. *Biochem. Biophys. Res. Commun.* **1997**, *231*, 797-801.

(7) Bouwstra, J. A.; Gooris, G. S.; Cheng, K.; Weerheim, A.; Bras, W.; Ponec, M. Phase behavior of isolated skin lipids. *J. Lipid Res.* **1996**, *37*, 999-1011.

(8) de Jager, M. W.; Gooris, G. S.; Dolbnya, I. P.; Bras, W.; Ponec, M.; Bouwstra, J. A. The phase behaviour of skin lipid mixtures based on synthetic ceramides. *Chem. Phys. Lipids* **2003**, *124*, 123-134.

(9) Engelbrecht, T. N.; Schroeter, A.; Hau; Deme, B.; Scheidt, H. A.; Huster, D.; Neubert, R. H. H. The impact of ceramides NP and AP on the nanostructure of stratum corneum lipid bilayer. Part I: neutron diffraction and ^{2}H NMR studies on multilamellar models based on ceramides with symmetric alkyl chain length distribution. *Soft Matter* **2012**, *8*, 6599-6607.

(10) Kwak, S.; Brief, E.; Langlais, D.; Kitson, N.; Lafleur, M.; Thewalt, J. Ethanol perturbs lipid organization in models of stratum corneum membranes: An investigation combining differential scanning calorimetry, infrared and ^{2}H NMR spectroscopy. *Biochim. Biophys. Acta* **2012**, *1818*, 1410-1419.